THE REPUBLIC OF THE PHILIPPINES
DEPARTMENT OF PUBLIC WORKS AND HIGHWAYS (DPWH)

THE PROJECT FOR STUDY ON IMPROVEMENT OF BRIDGES THROUGH DISASTER MITIGATING MEASURES FOR LARGE SCALE EARTHQUAKES IN THE REPUBLIC OF THE PHILIPPINES

FINAL REPORT

APPENDIX 2-A

GENERALIZED ACCELERATION RESPONSE SPECTRA DEVELOPMENT BY PROBABILISTIC SEISMIC HAZARD ANALISIS (PSHA)

DECEMBER 2013

JAPAN INTERNATIONAL COOPERATION AGENCY (JICA)

CTI ENGINEERING INTERNATIONAL CO., LTD
CHODAI CO., LTD.
NIPPON KOEI CO., LTD.

APPENDIX 2-A

GENERALIZED ACCELERATION RESPONSE SPECTRA DEVELOPMENT BY PROBABILISTIC SEISMIC HAZARD ANALYSIS (PSHA)

Seismic acceleration spectral maps for the Philippines to be incorporated into the draft BSDS for the following return periods: (1) 1,000 years; (2) 500 years; (3) 100 years; and (4) 50 years are generated. At each return period, spectral maps are developed for three key spectral acceleration parameters: (1) peak ground acceleration (PGA); (2) spectral acceleration at 0.2 sec; and spectral acceleration at 1. sec. The maps are developed for AASHTO site class B (equivalent to V_{s30} = 760 m/s). The flow procedure is shown in Figure 2A-1.

Active faults as presently identified by Phivolcs (Philippine Institute of Volcanology and Seismology) are shown plotted in Figure 2A-2. Also shown plotted are instrumentally recorded earthquake events from 1907 to 2012 with magnitude greater than 4 and focal depth of less than 100 kms. which are compiled (consisting of about 26,000+ events) from Phivolcs and ISC (International Seismological Centre) websites into an earthquake catalog. The magnitude scale is homogenized in a common magnitude scale—moment magnitude scale in this study for the reasons that moment magnitude does not suffer from saturation during large earthquakes; and is now the most commonly adopted in most ground motion estimation models that are presently being proposed. Declustering algorithm based on Gardner and Knopoff (1974) is applied to retain only independent main shocks (into 7000+ events as shown plotted in Figure 2A-3), removing aftershocks and foreshocks. Completeness analysis based on the method of Stepp (1972) is applied to the catalog to remove possible biases towards bigger events in subsequent regression analysis for temporal characterization of earthquake occurrences for each defined seismic source model since it is known that lower magnitude earthquake events had been under-reported in the early part of the instrumental era; and become less so with progressively improved instruments.

Seismic source modeling consisting of fault models and background seismicity models are shown in Figure 2A-3. Background seismicity modeling is used to model seismic occurrences into areal zones where the observed seismicity exhibits a more or less diffused pattern that cannot be clearly identified with a specific fault. This may include earthquake occurrences in the future that could be attributable to blind thrusts or faults with no previous ground surface fault manifestations. Each earthquake event in the declustered set is identified to be associated with one of the fault models or background seismicity seismogenic areal zones. Bigger events are preferably made to be associated with the fault models.

For source-to-site distance uncertainty modeling, earthquakes in this study are assumed to be uniformly distributed within a particular source zone (i.e., earthquakes are considered equally likely to occur at any location within a source). Rupture may occur with equal likelihood anywhere in the fault plane in the fault zone and anywhere in the seismogenic areal zone. The spatial (source-tosite distance) uncertainty can be described by a probability density function P(R) which may be approximated by a normalized frequency distribution histogram.

For fault models characterizing crustal earthquakes, maximum potential earthquake size capable to be produced within the source is computed using the empirical method of Wells and Coppersmith (1994). On the other hand, the method of Papazachos et al (2004) is used to compute maximum potential earthquake size for sources due to trenches. For seismogenic areal zones modeling back-

ground seismicity, the highest recorded or documented magnitude plus 0.5 is used. List of historically documented earthquakes from 1589 to 1895 is based on the study by Bautista and Oike (2000).

Two types of earthquake recurrence models are used in this study: bounded Gutenberg-Richter recurrence model and characteristic earthquake recurrence model. The more commonly used bounded Gutenberg-Richter recurrence model in most PSHA implementation is expressed as:

$$\lambda_m = \nu \frac{\exp[-\beta(m - m_0)] - \exp[-\beta(m_{\text{max}} - m_0)]}{1 - \exp[-\beta(m_{\text{max}} - m_0)]} \qquad \text{for } m_0 \leq m \leq m_{\text{max}}$$

where m_0 is the lowest magnitude considered to be of engineering significance and m_{max} is the maximum magnitude based on seismological and geological considerations as discussed earlier. Characteristic earthquake recurrence model using data based on paleoseimological observation is preferred (but limited in use in this study due to the scarcity of data) due to the short history of instrumental recording in the world relative to geological period over which earthquakes recurred.

Probabilistic seismic hazard analysis (PSHA) provides a framework in which uncertainties in the size, location, and rate of recurrence of earthquakes and in the variation of ground motion characteristics with earthquake size and location can be identified, quantified, and combined in a rational manner (Thenhaus and Campbell, 2003).

The probability that an observed ground motion parameter X (spectral acceleration, in this study) will be greater than or equal to the value x in the next t years (the exposure period) given the annual exceedance rate $\lambda[X \geq x]$ is computed as:

$$P[X \geq x] = 1 - \exp(-t\, \lambda[X \geq x])$$

$$\lambda[X \geq x] \approx \sum_{\text{sources } i} v_i \int_{m_0}^{m_{\text{max}}} \int_{R|M} P[X \geq x|M, R]\, f_M(m)\, f_{R|M}(r|m)\, dr\, dm$$

where

$\lambda[X \geq x]$	the annual frequency that ground motion at a site exceeds the chosen level $X = x$;
v_i	the annual rate of occurrence of earthquakes on seismic source i having magnitudes between m_0 and m_{max};
m_0	the minimum magnitude of engineering significance (taken to be 5.0 in this study);
m_{max}	the maximum magnitude assumed to occur on the source;
$P[X \geq x\|M, R]$	the conditional probability that the chosen ground motion level is exceeded for a given magnitude M and distance R;
$f_M(m)$	probability density function of earthquake magnitude;
$f_{R\|M}(r\|m)$	probability density function of distance from the earthquake source to the site of interest.

Ground motion estimation models used in this study are based on Boore-Atkinson NGA (2007) applied to crustal earthquake sources, Young et al model (1997) applied to subduction sources; and Zhao et al (2006) applied to both crustal and subduction sources.

The iterative analysis is carried out for a grid interval of 10 kms covering the whole Philippines for a total of 16,471 points. Interpolation and smoothing of the contours are made using the nearest-neighbor algorithm. Results showing contours interposed with the source models and declustered earthquake events are shown in Figures 2A-4 to 2A-15.

Contour maps of seismic acceleration values which constitute four (corresponding to return periods of 1000 years, 500 years, 100 years, and 50 years) sets of maps at 3 key periods (0. sec, 0.2 sec, and 1. sec) are finally generated:

1. 1000-year return period
   (a) peak ground acceleration (PGA)
   — Fig. 2A-16 and 17 regional maps in Figs. 2A-17 to 2A-33
   (b) spectral acceleration at 0.2 sec (S_a at 0.2s)
   — Fig. 2A-34 and 17 regional maps in Figs. 2A-35 to 2A-51
   (c) spectral acceleration at 1. sec (S_a at 1.s)
   — Fig. 2A-52 and 17 regional maps in Figs. 2A-53 to 2A-69
2. 500-year return period
   (a) peak ground acceleration (PGA)
   — Fig. 2A-70 and 17 regional maps in Figs. 2A-71 to 2A-87
   (b) spectral acceleration at 0.2 sec (S_a at 0.2s)
   — Fig. 2A-88 and 17 regional maps in Figs. 2A-89 to 2A-105
   (c) spectral acceleration at 1. sec (S_a at 1.s)
   — Fig. 2A-106 and 17 regional maps in Figs. 2A-107 to 2A-123
3. 100-year return period
   (a) peak ground acceleration (PGA)
   — Fig. 2A-124 and 17 regional maps in Figs. 2A-125 to 2A-141
   (b) spectral acceleration at 0.2 sec (S_a at 0.2s)
   — Fig. 2A-142 and 17 regional maps in Figs. 2A-143 to 2A-159
   (c) spectral acceleration at 1. sec (S_a at 1.s)
   — Fig. 2A-160 and 17 regional maps in Figs. 2A-161 to 2A-177
4. 50-year return period
   (a) peak ground acceleration (PGA)
   — Fig. 2A-178 and 17 regional maps in Figs. 2A-179 to 2A-195
   (b) spectral acceleration at 0.2 sec (S_a at 0.2s)
   — Fig. 2A-196 and 17 regional maps in Figs. 2A-197 to 2A-213
   (c) spectral acceleration at 1. sec (S_a at 1.s)
   — Fig. 2A-214 and 17 regional maps in Figs. 2A-215 to 2A-231

The spectral acceleration contour maps by regions have been requested by DPWH for easier use of the bridge designers.

References:

D. M. Boore and G. M. Atkinson, "Boore-Atkinson NGA ground motion relations for the geometric mean horizontal component of peak and spectral ground motion parameters," Technical Report PEER 2007/01, Pacific Earthquake Engineering Research Center, 2007.

Maria Leonila P. Bautista and Kazuo Oike, "Estimation of the magnitudes and epicenters of Philippine historical earthquakes," *Tectonophysics,* 317(12):137-169, 2000.

Maria Leonila P. Bautista and Bartolome C. Bautista, "The Philippine historical earthquake catalog: its development, current state and future directions," *Annals of Geophysics,* 47(2/3), April/June 2004.

J. K. Gardner and L. Knopoff, "Is the sequence of earthquakes in Southern California, with aftershocks removed, poissonian?" *Bulletin of the Seismological Society of America,* 64(5), 1974.

Thomas H. Heaton, Fumiko Tajima, and Ann Wildenstein Mori, "Estimating ground motions using recorded accelerograms," *Surveys in Geophysics,* 8:2583, 1986.

A. R. Nelson, S. F. Personius, R. E. Rimando, R. S. Punongbayan, N. Tuñgol, H. Mirabueno, and A. Rasdas. "Multiple large earthquakes in the past 1500 years on a fault in Metropolitan Manila, the Philippines."*Bulletin of Seismological Society of America,* 90:7385, 2000.

B. C. Papazachos, E. M. Scordilis, D. G. Panagiotopoulos, C. B. Papazachos, and G. F. Karakaisis, "Global relations between seismic fault parameters and moment magnitude of earthquakes," *Bulletin of the Geological Society of Greece,* XXXVI, 2004.

L. Reiter. *Earthquake Hazard Analysis: Issues and Insights.* Columbia University Press, 1990.

Carl J. Stepp, "Analysis of completeness of the earthquake sample in the Puget Sound area and its effects on statistical estimates of earthquake hazard," In *Proceedings of the International Conference on Microzonation for Safer Construction Research and Application,* Seattle, Oct 30 to Nov 3, 1972, vol. 2, 1972.

P. C. Thenhaus and K. W. Campbell. "Seismic Hazard Analysis," in *Earthquake Engineering Handbook,* edited by W.-F. Chen and C. Scawthorn, CRC Press, 2003.

D. L. Wells and K. J. Coppersmith, "New empirical relationships among magnitude, rupture length, rupture width, rupture area, and surface displacement," *Bulletin of the Seismological Society of America,* 84(4):974–1002, August 1994.

R. R. Youngs, S.-J. Chiou, W. J. Silva, and J. R. Humphrey, “Strong ground motion attenuation relationships for subduction zone earthquakes,” *Seismological Research Letters,* 68(1), January/February 1997.

J. X. Zhao, J. Zhang, A. Asano, Y. Ohno, T. Oouchi, T. Takahashi, H. Ogawa, K. Irikura, H. K. Thio, P. G. Somerville, Y. Fukushima, and Y. Fukushima, “Attenuation relations of strong ground motion in Japan using site classification based on predominant period,” *Bulletin of the Seismological Society of America,* 96(3):898913, June 2006.

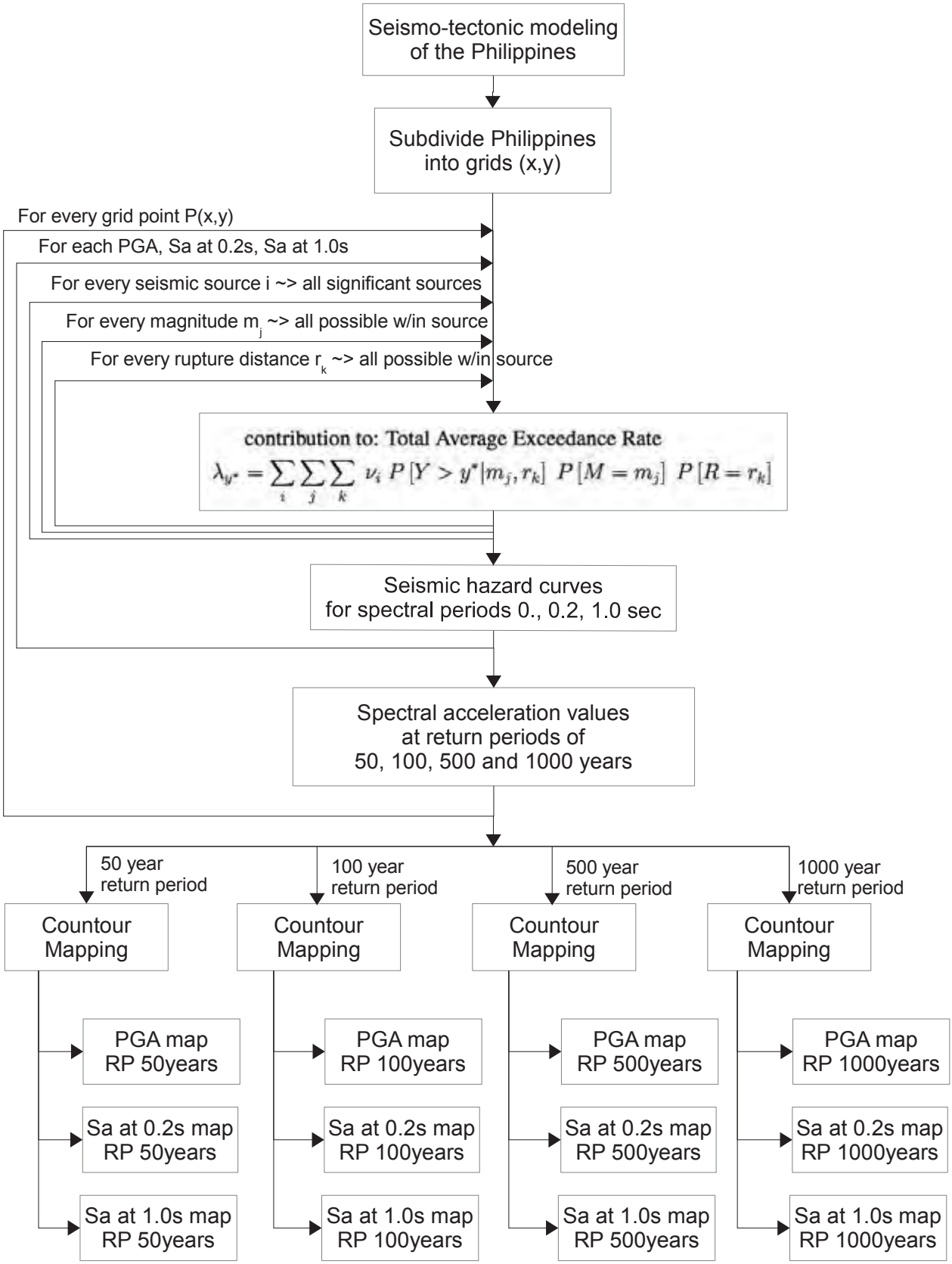

Figure 2A-1 Procedure of PSHA study for spectral mapping of PGA, S_a at 0.2 s and 1. s at base rock equivalent to AASHTO site class B ($V_{s30} = 760$ m/s) corresponding to return periods of 50, 100, 500, and 1000 years

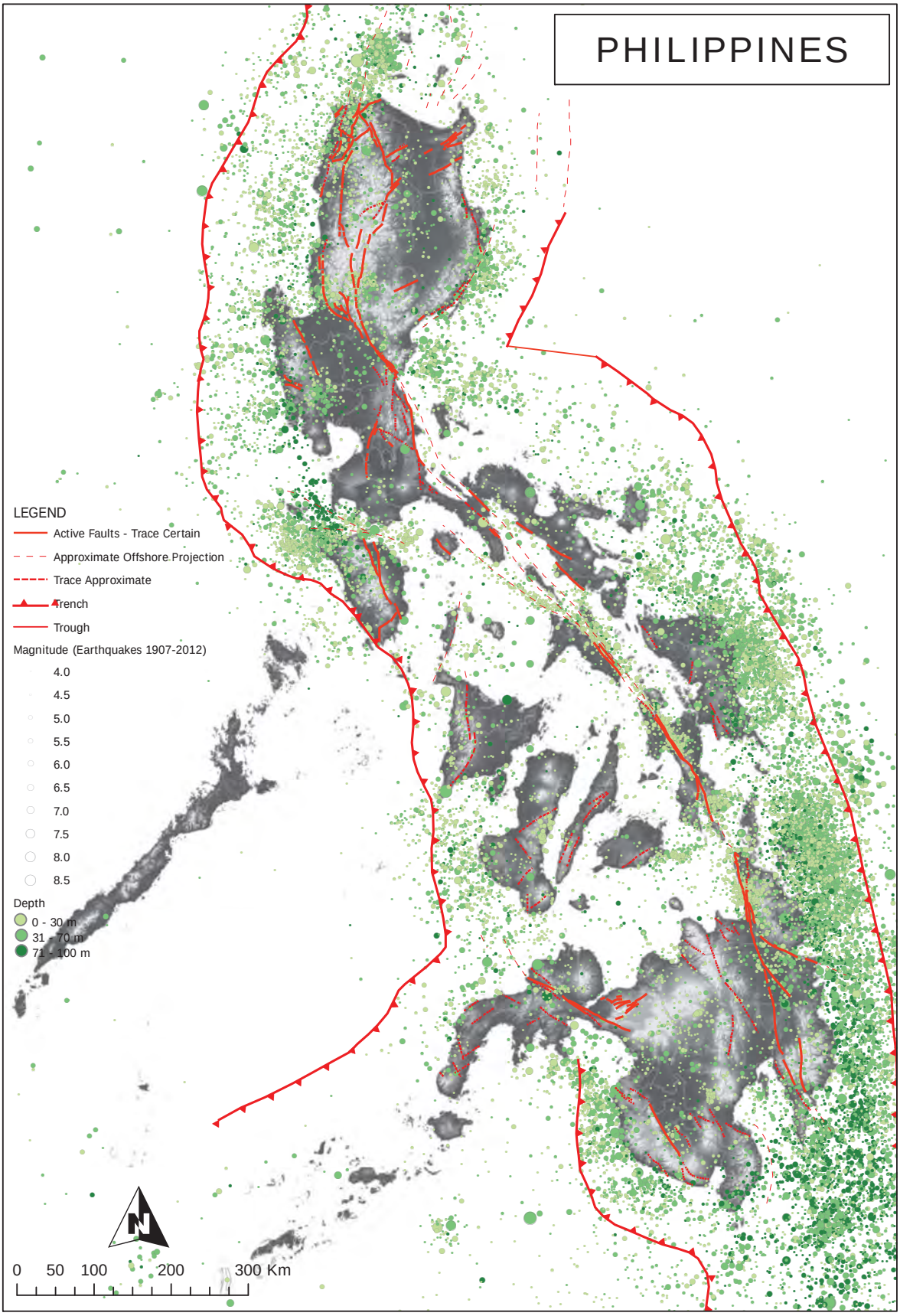

Figure 2A-2 Seismological and Tectonic Setting of the Philippines
(instrumentally recorded earthquake events 1907–2012; $M_w > 4$, $d < 100$ kms)

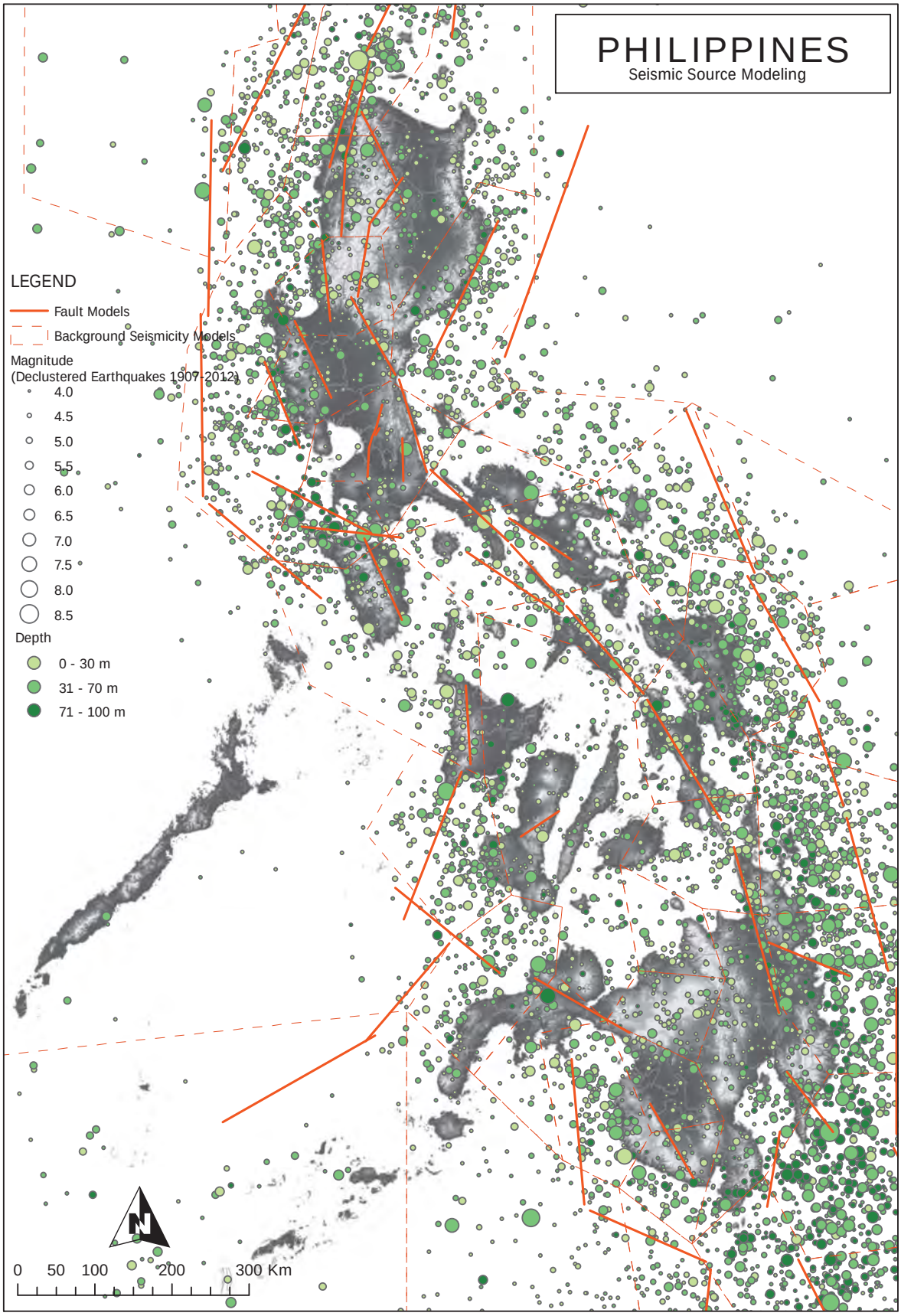

Figure 2A-3 Seismic source modeling (fault models and background seismicity models) for this PSHA study of the Philippines

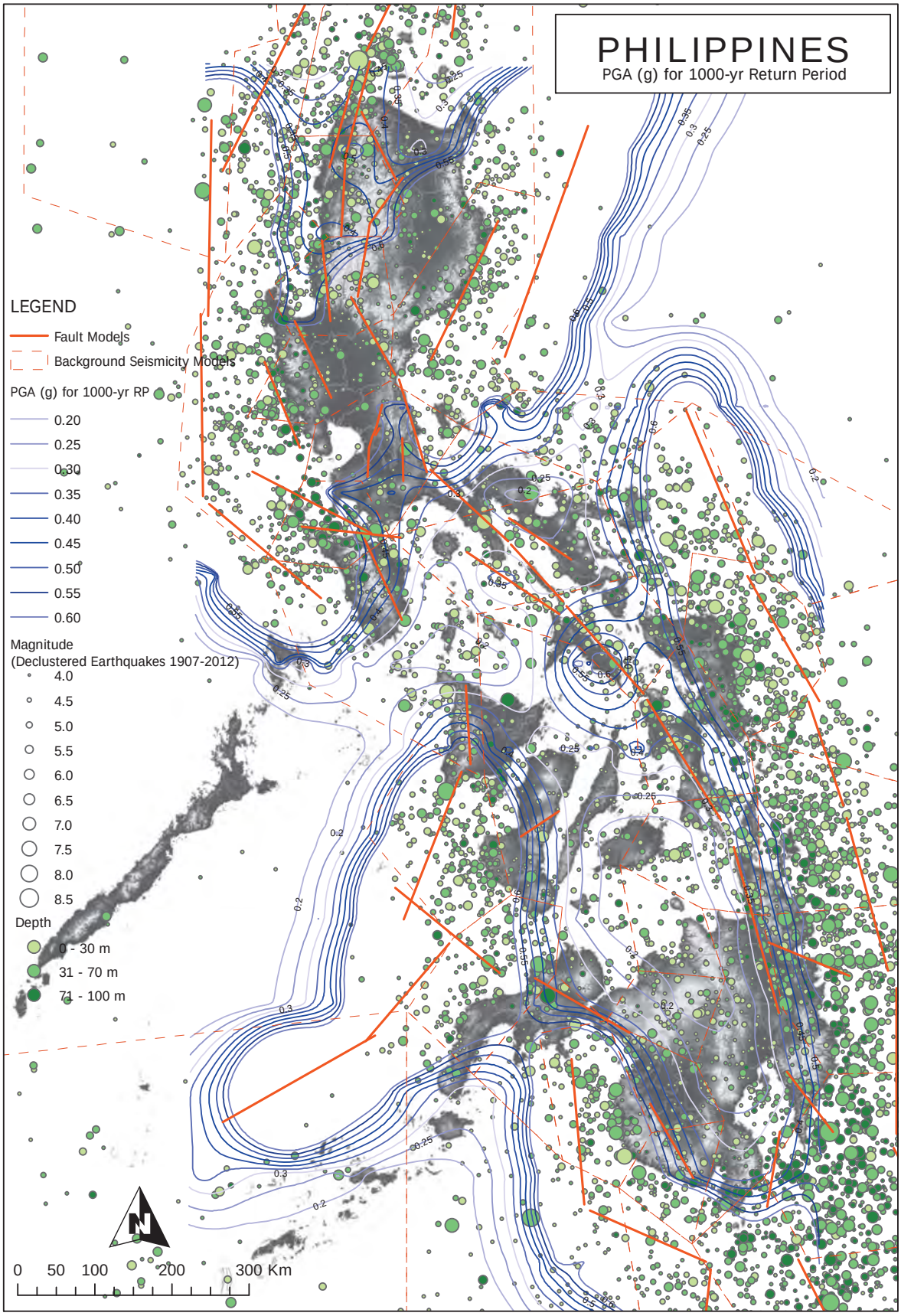

Figure 2A-4 Contoured result of PGA for 1,000-year return period superimposed on seismic source models and declustered earthquake plots used in analysis

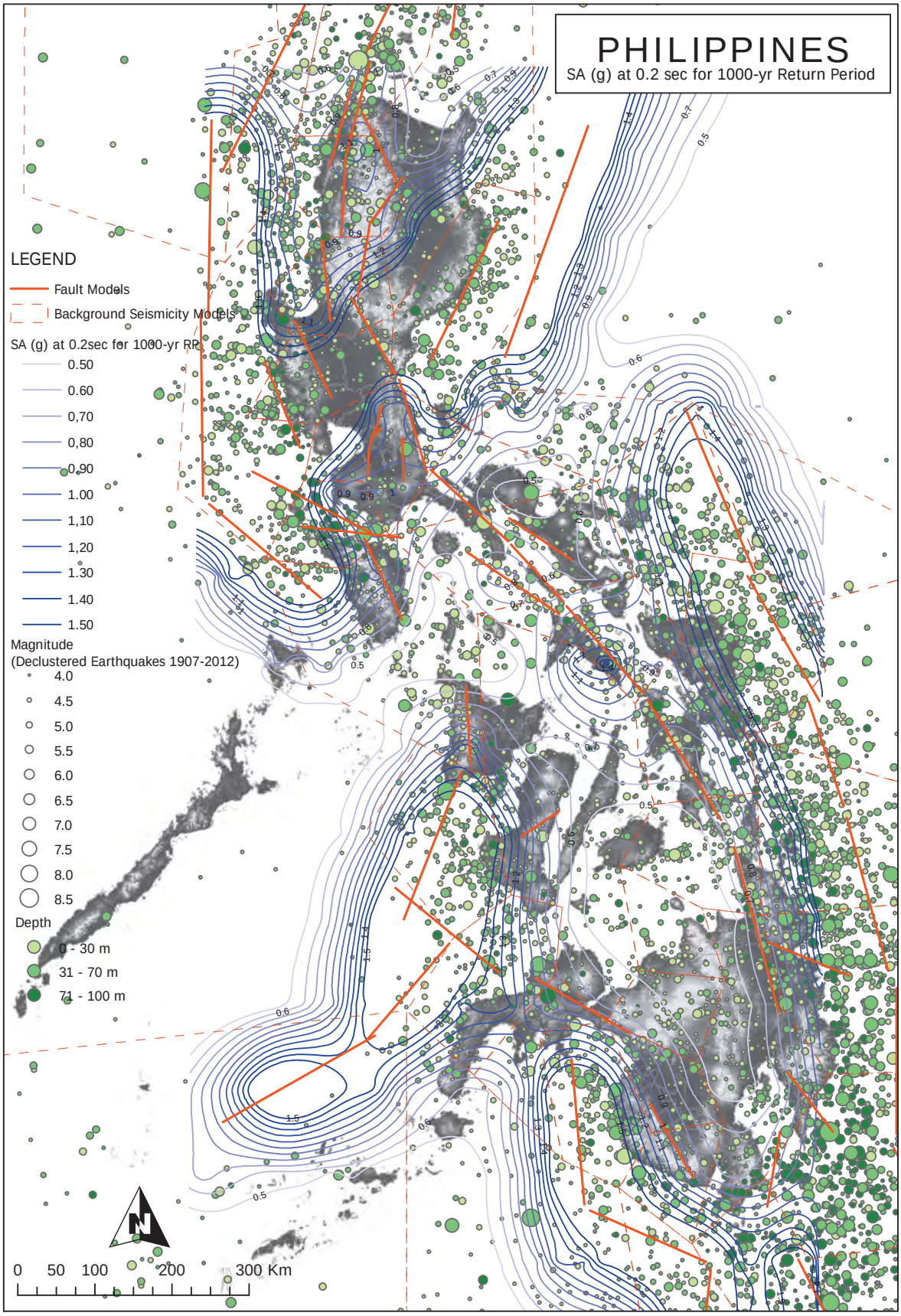

Figure 2A-5 Contoured result of S_a at 0.2 sec. for 1,000-year return period superimposed on seismic source models and declustered earthquake plots used in analysis

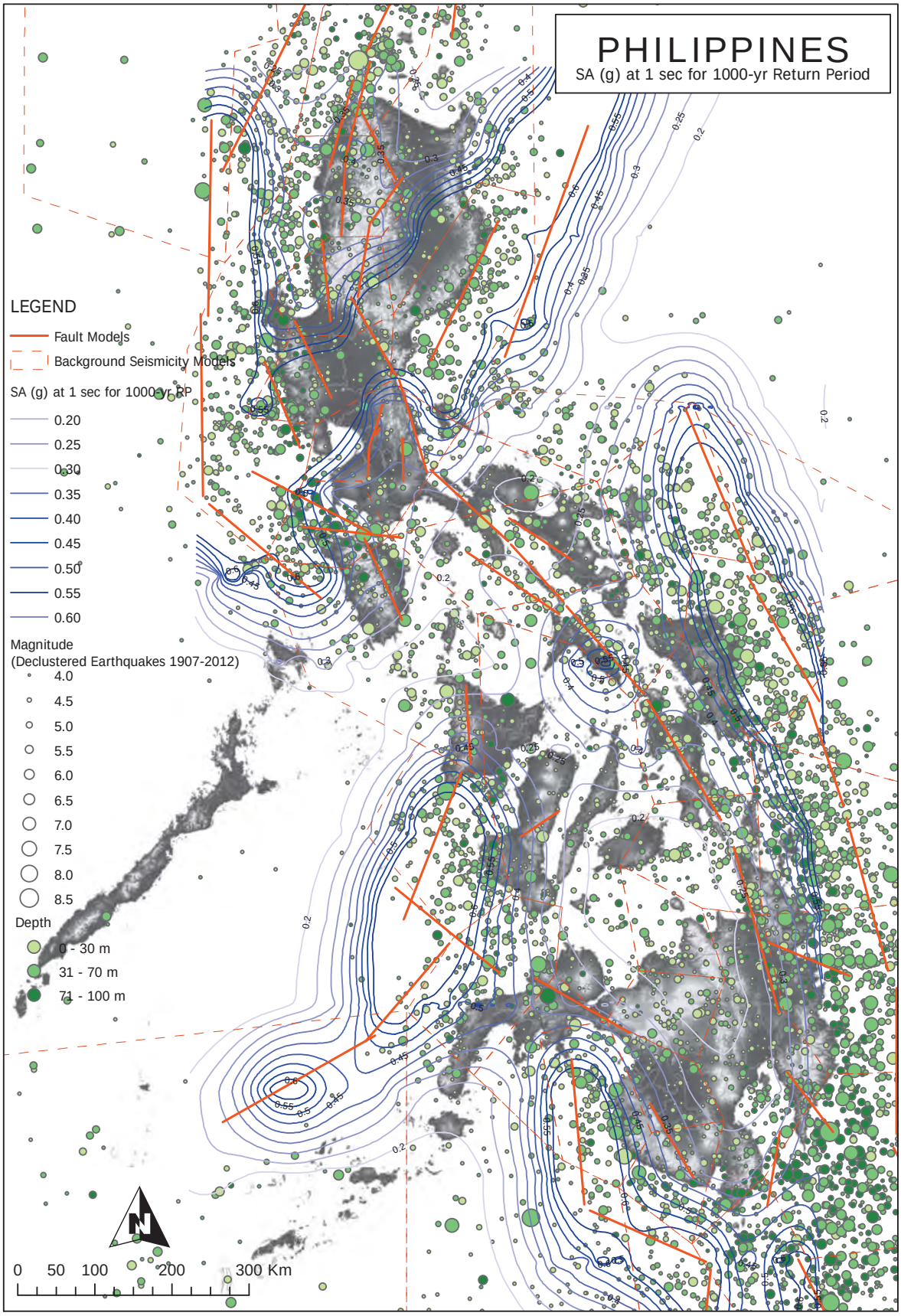

Figure 2A-6 Contoured result of S_a at 1. sec. for 1,000-year return period superimposed on seismic source models and declustered earthquake plots used in analysis

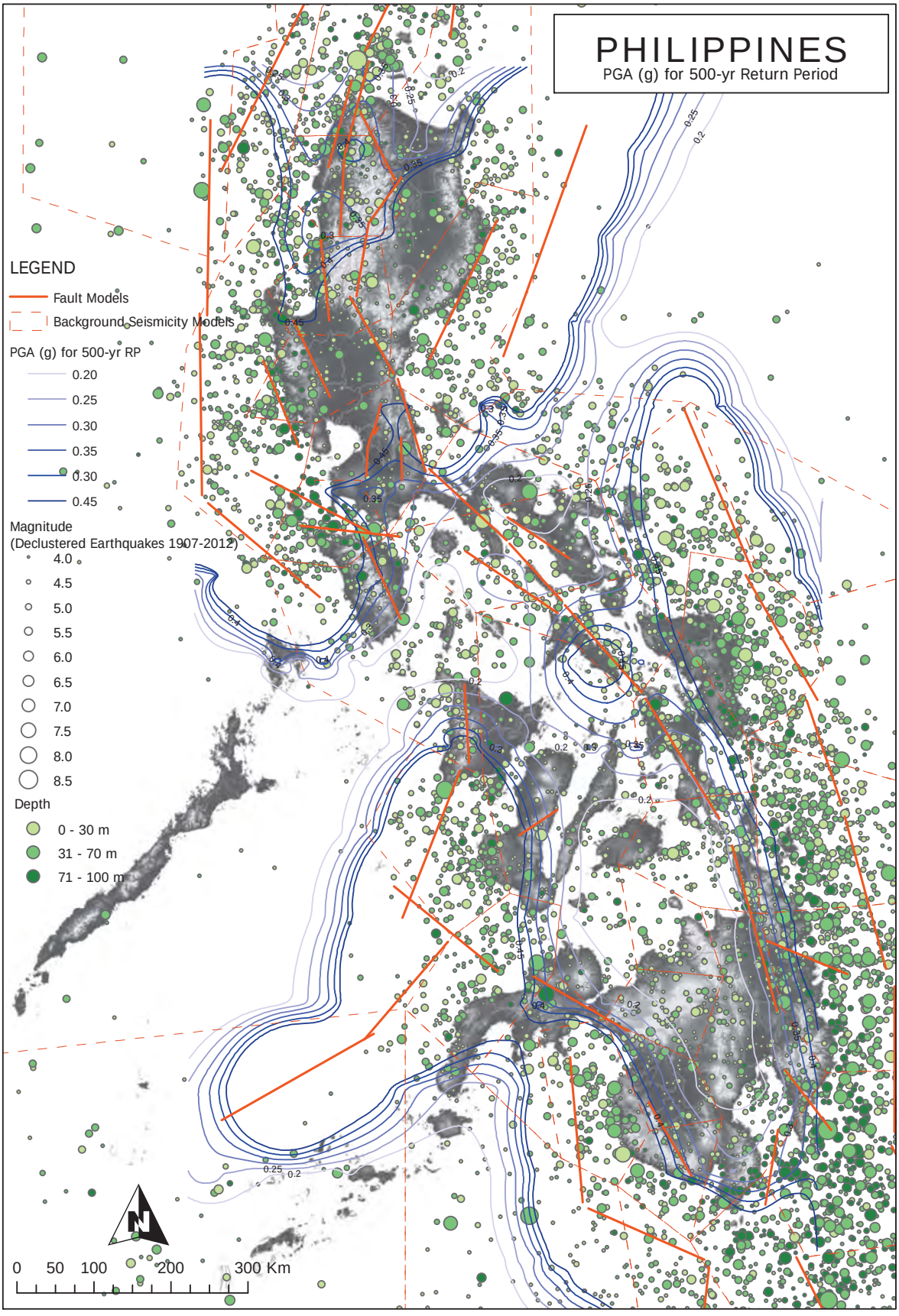

Figure 2A-7 Contoured result of PGA for 500-year return period superimposed on seismic source models and declustered earthquake plots used in analysis

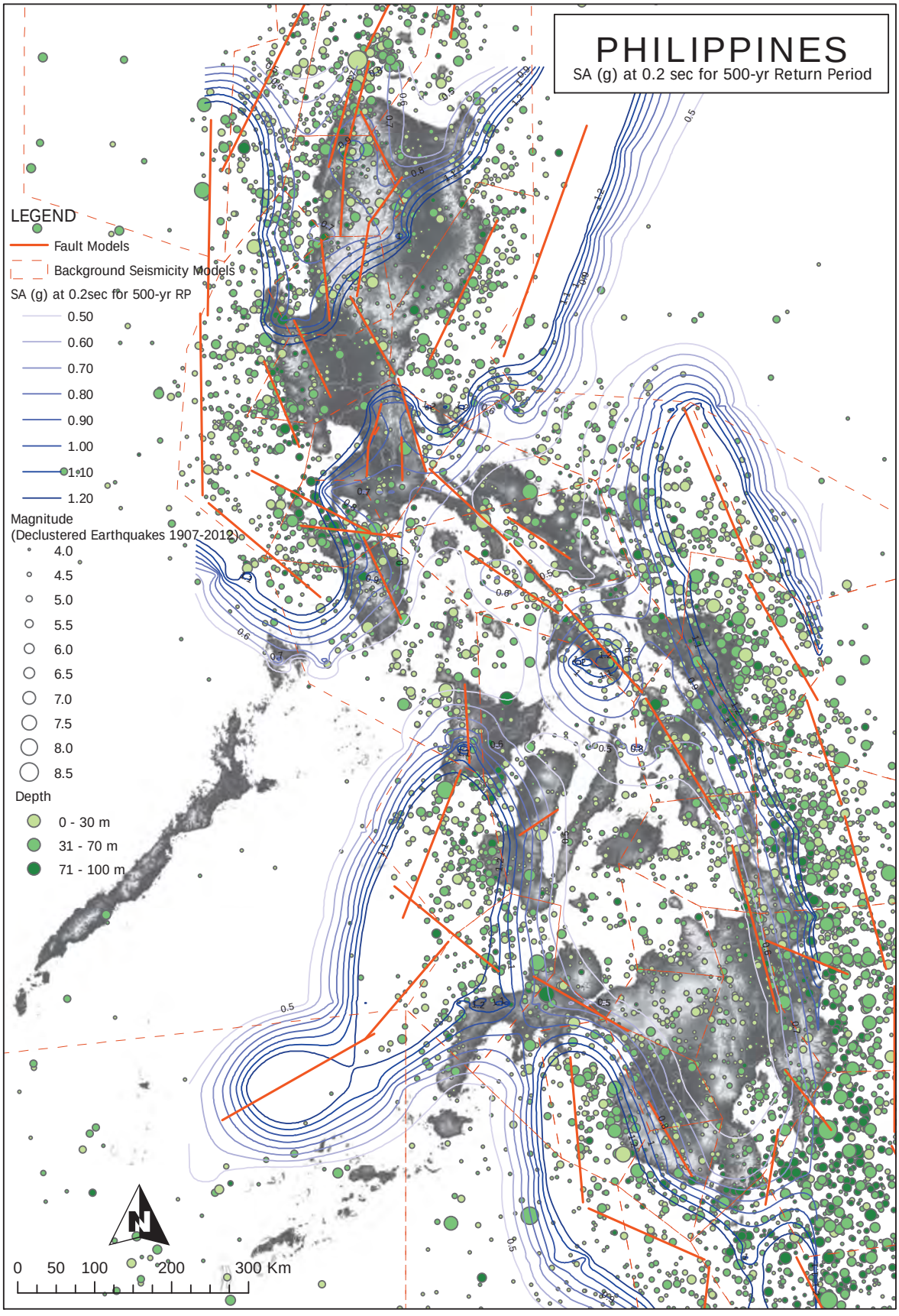

Figure 2A-8 Contoured result of S_a at 0.2 sec. for 500-year return period superimposed on seismic source models and declustered earthquake plots used in analysis

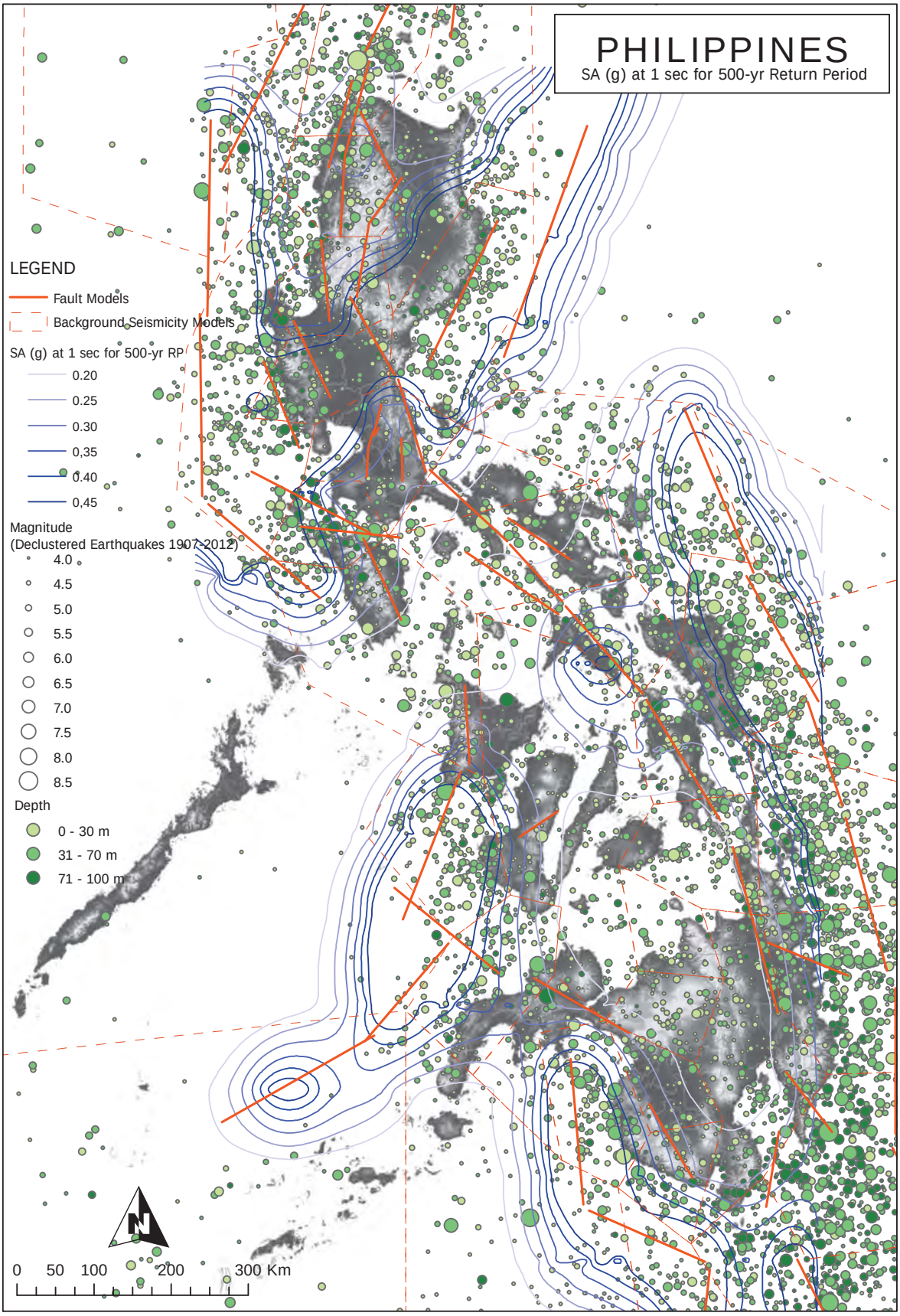

Figure 2A-9 Contoured result of S_a at 1. sec. for 500-year return period superimposed on seismic source models and declustered earthquake plots used in analysis

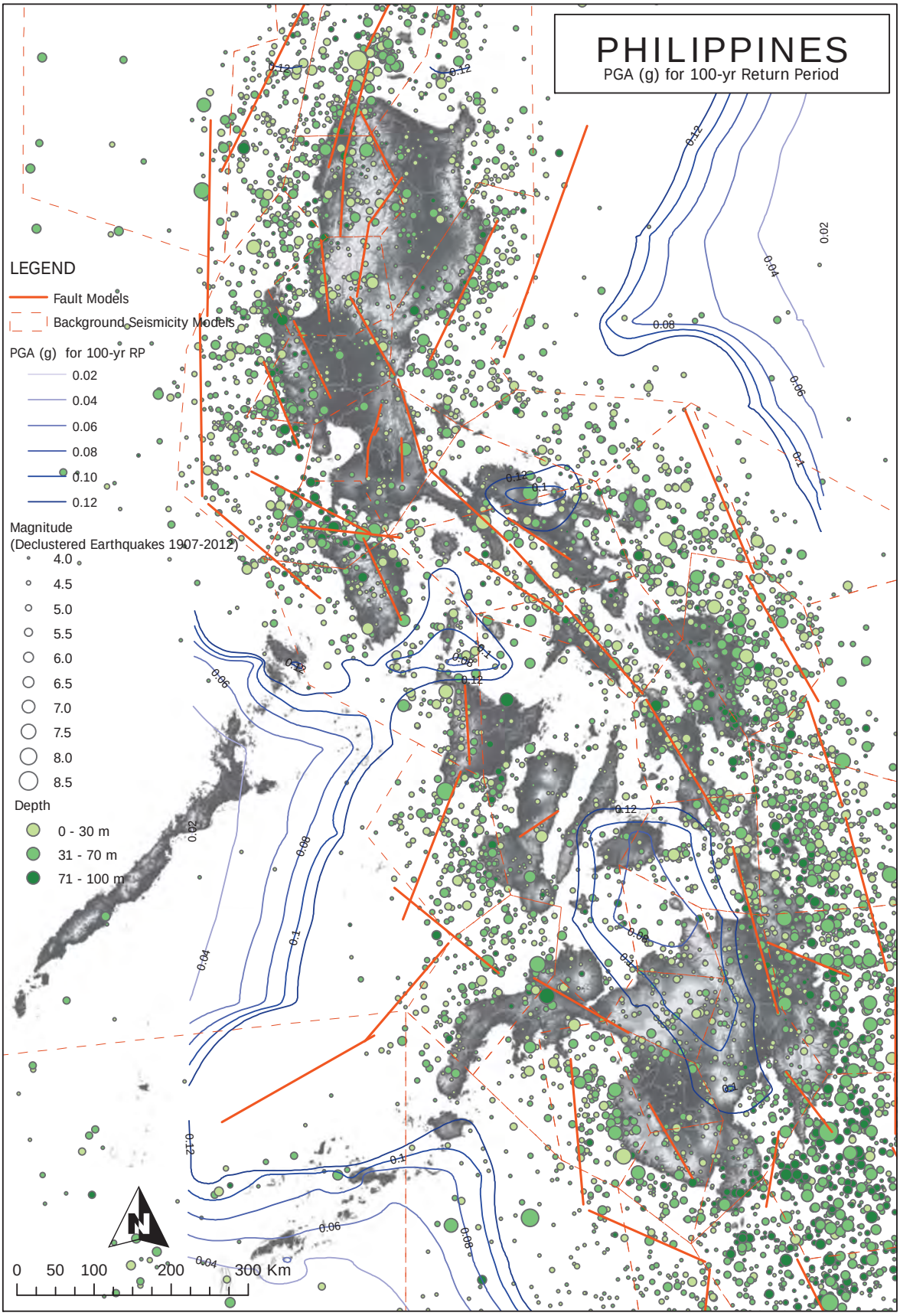

Figure 2A-10 Contoured result of PGA for 100-year return period superimposed on seismic source models and declustered earthquake plots used in analysis

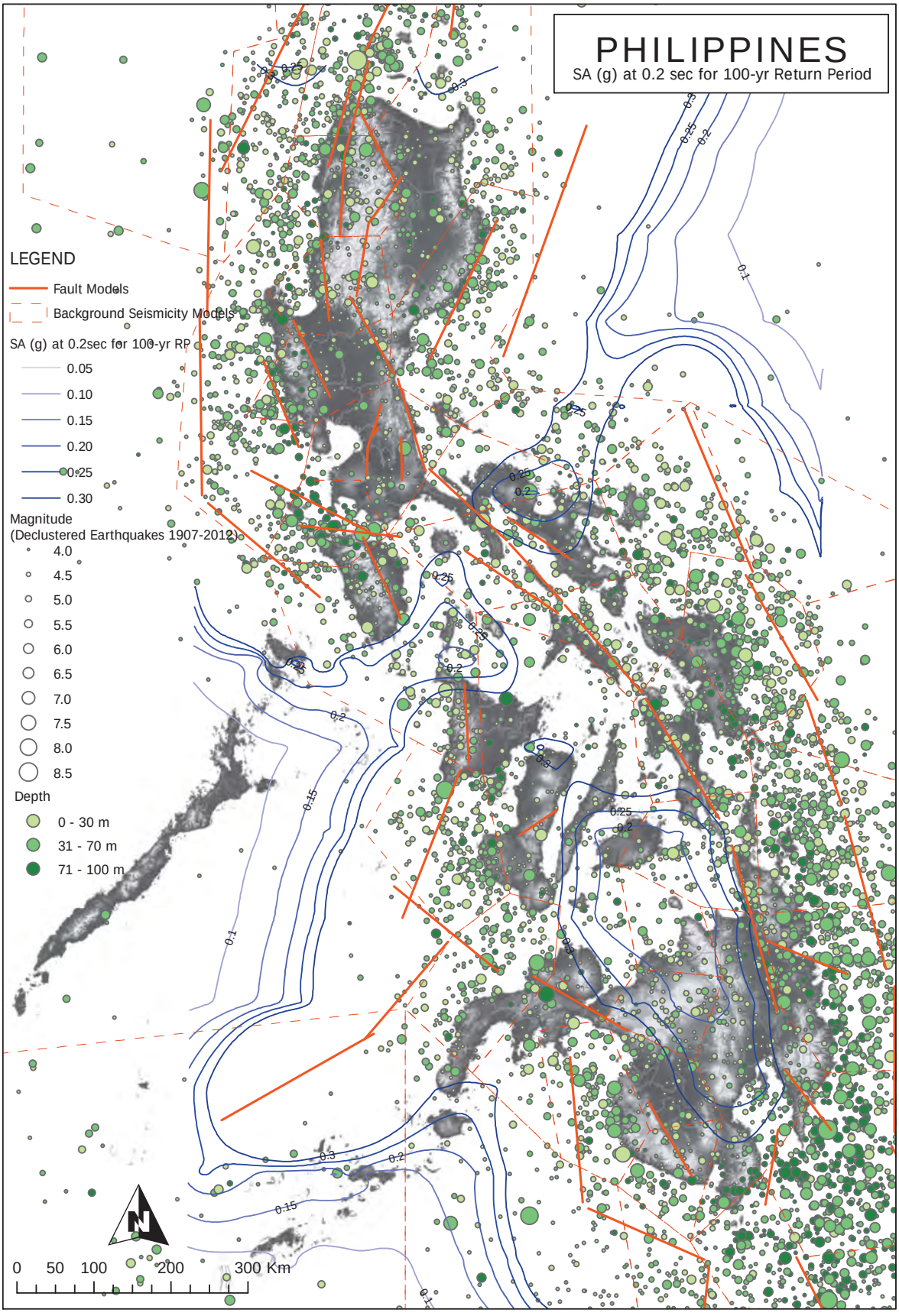

Figure 2A-11 Contoured result of S_a at 0.2 sec. for 100-year return period superimposed on seismic source models and declustered earthquake plots used in analysis

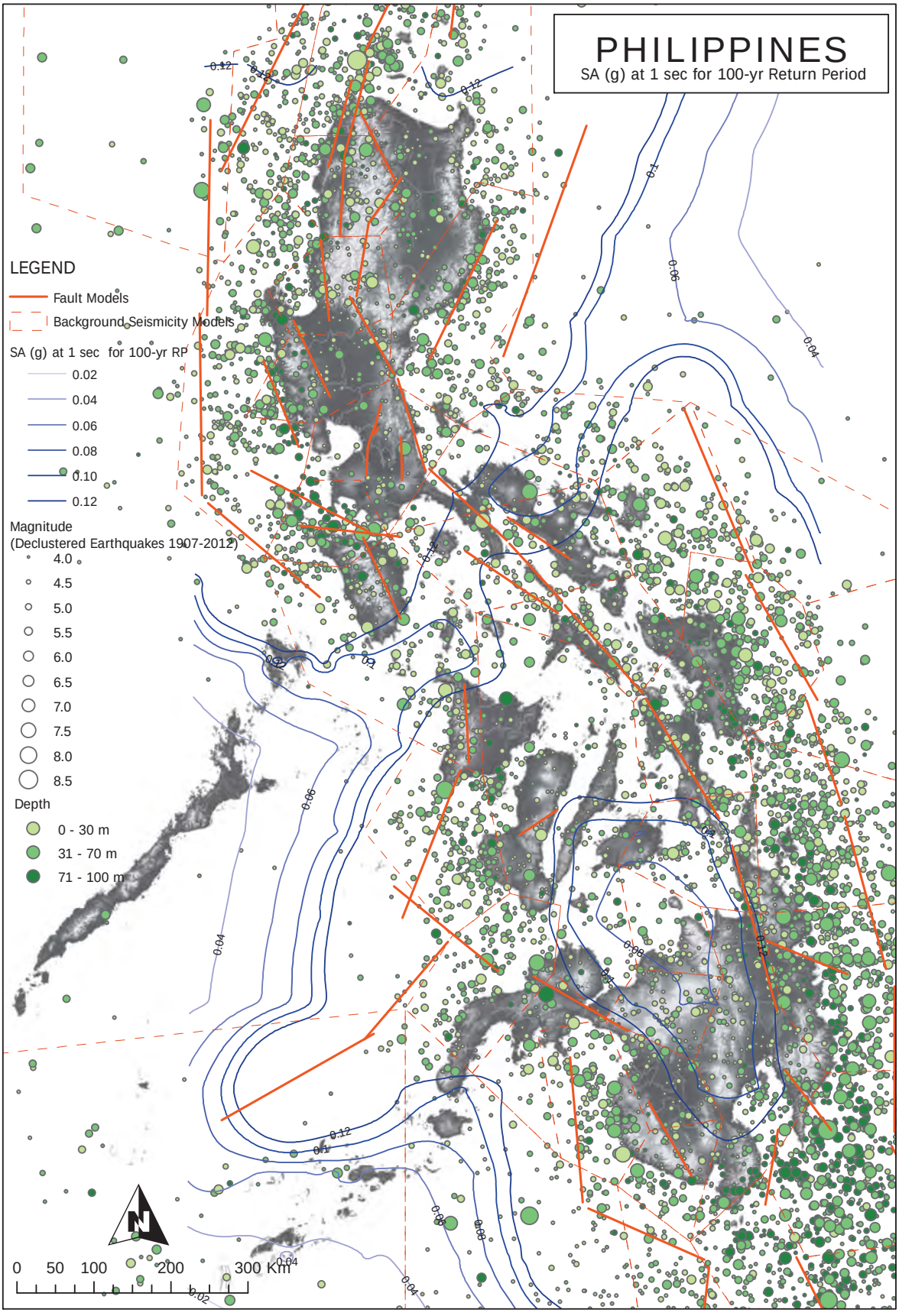

Figure 2A-12 Contoured result of S_a at 1. sec. for 100-year return period superimposed on seismic source models and declustered earthquake plots used in analysis

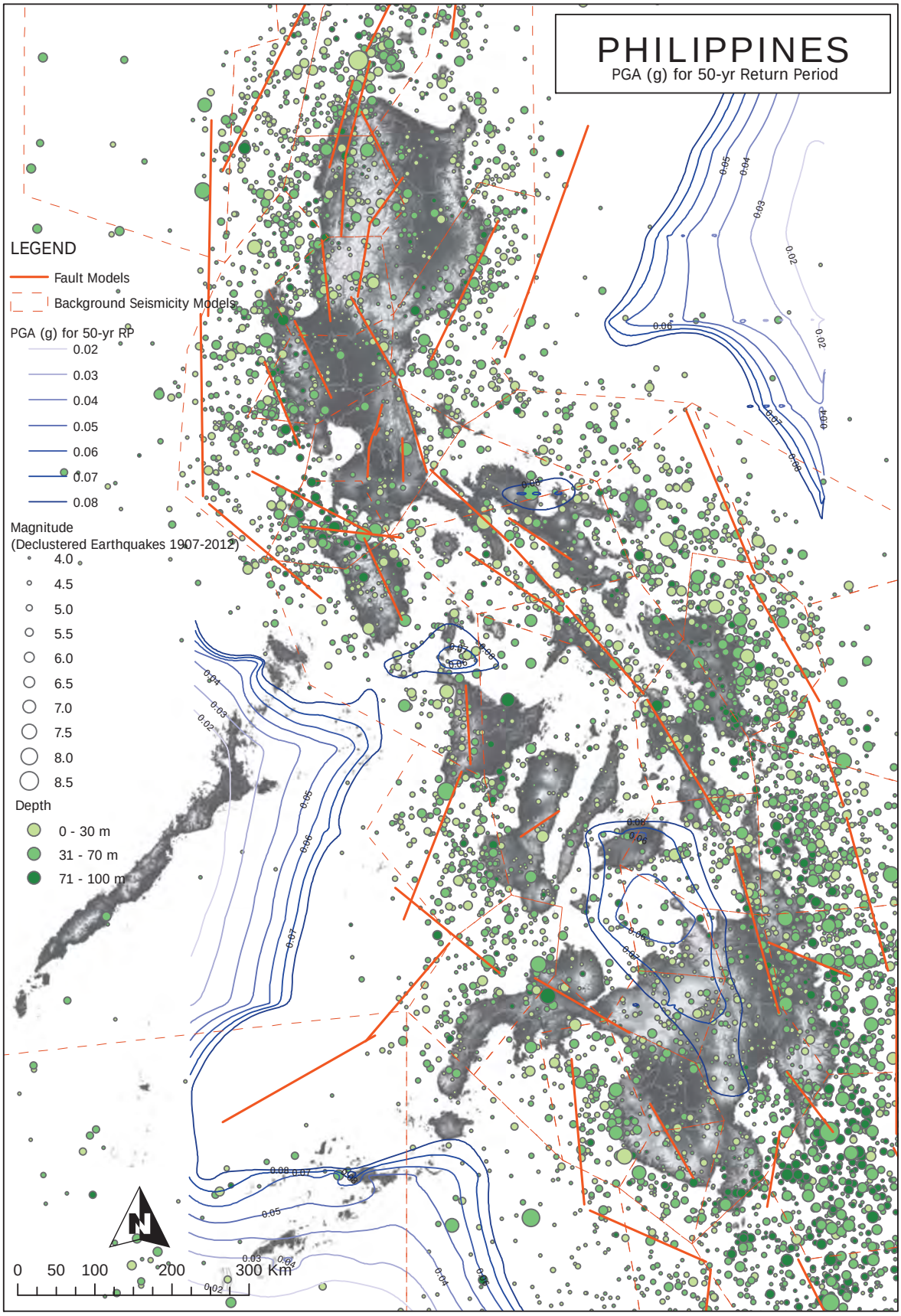

Figure 2A-13 Contoured result of PGA for 50-year return period superimposed on seismic source models and declustered earthquake plots used in analysis

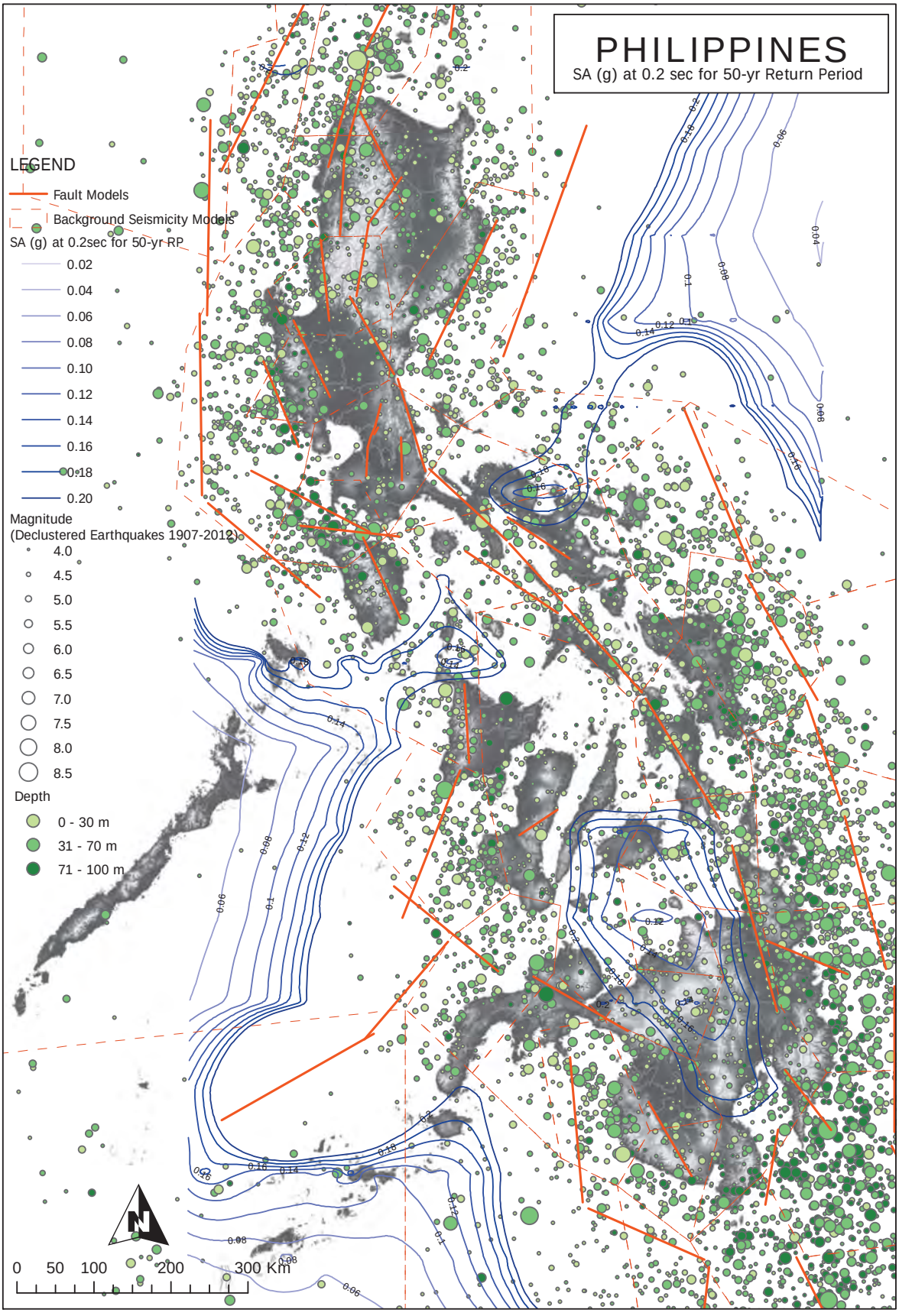

Figure 2A-14 Contoured result of S_a at 0.2 sec. for 50-year return period superimposed on seismic source models and declustered earthquake plots used in analysis

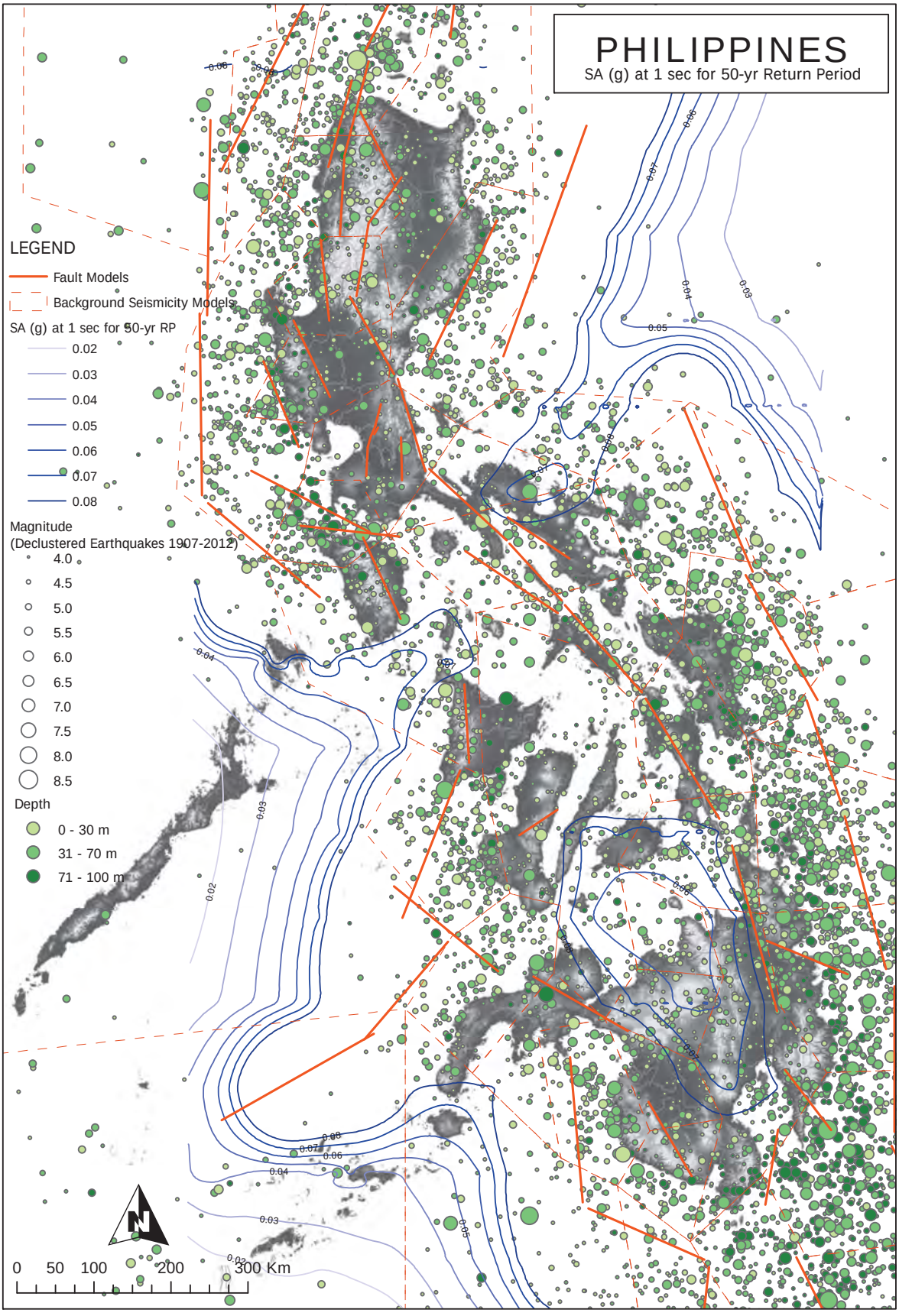

Figure 2A-15 Contoured result of S_a at 1. sec. for 50-year return period superimposed on seismic source models and declustered earthquake plots used in analysis

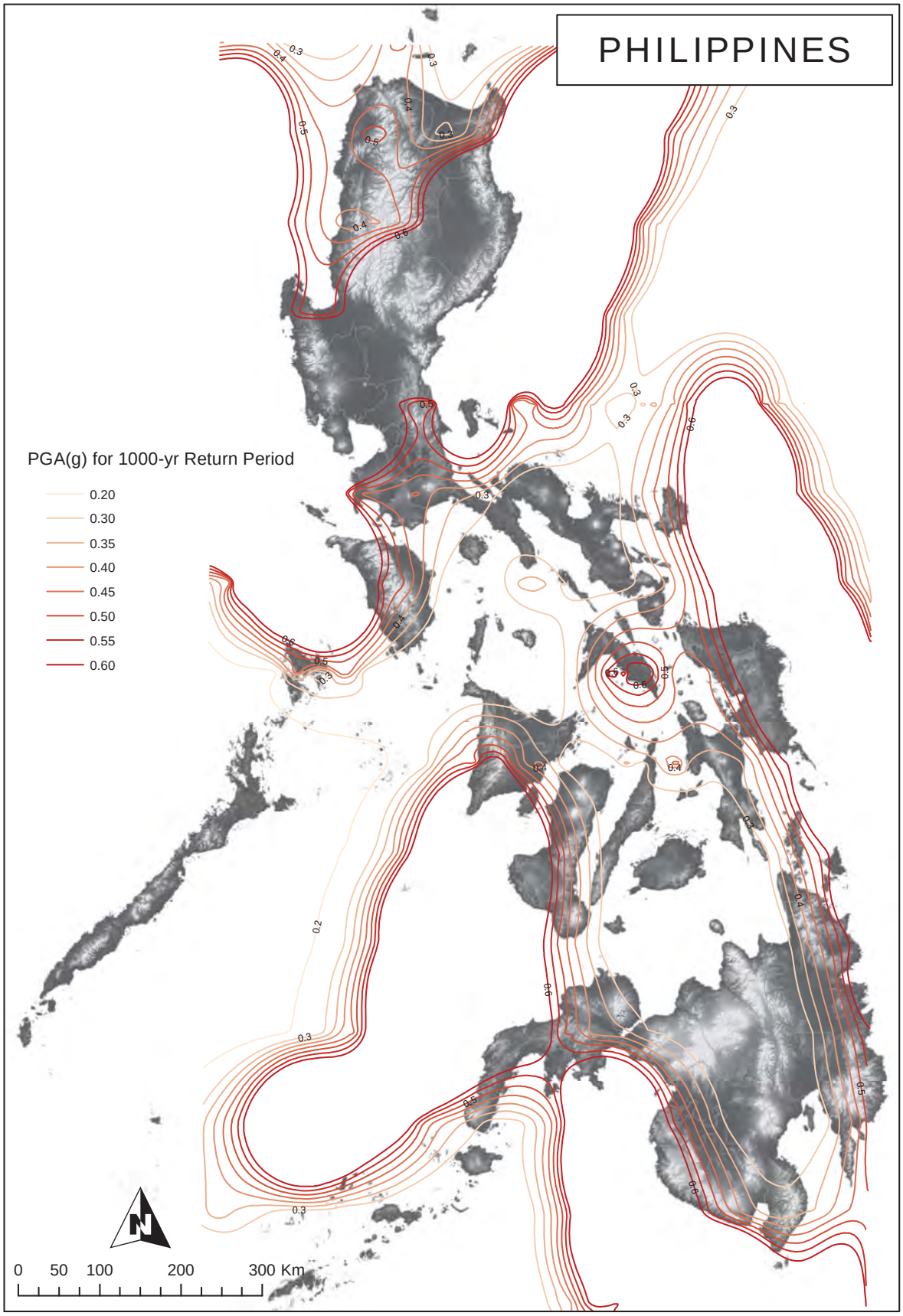

Figure 2A-16 Contour map of peak ground acceleration for 1,000-year return period

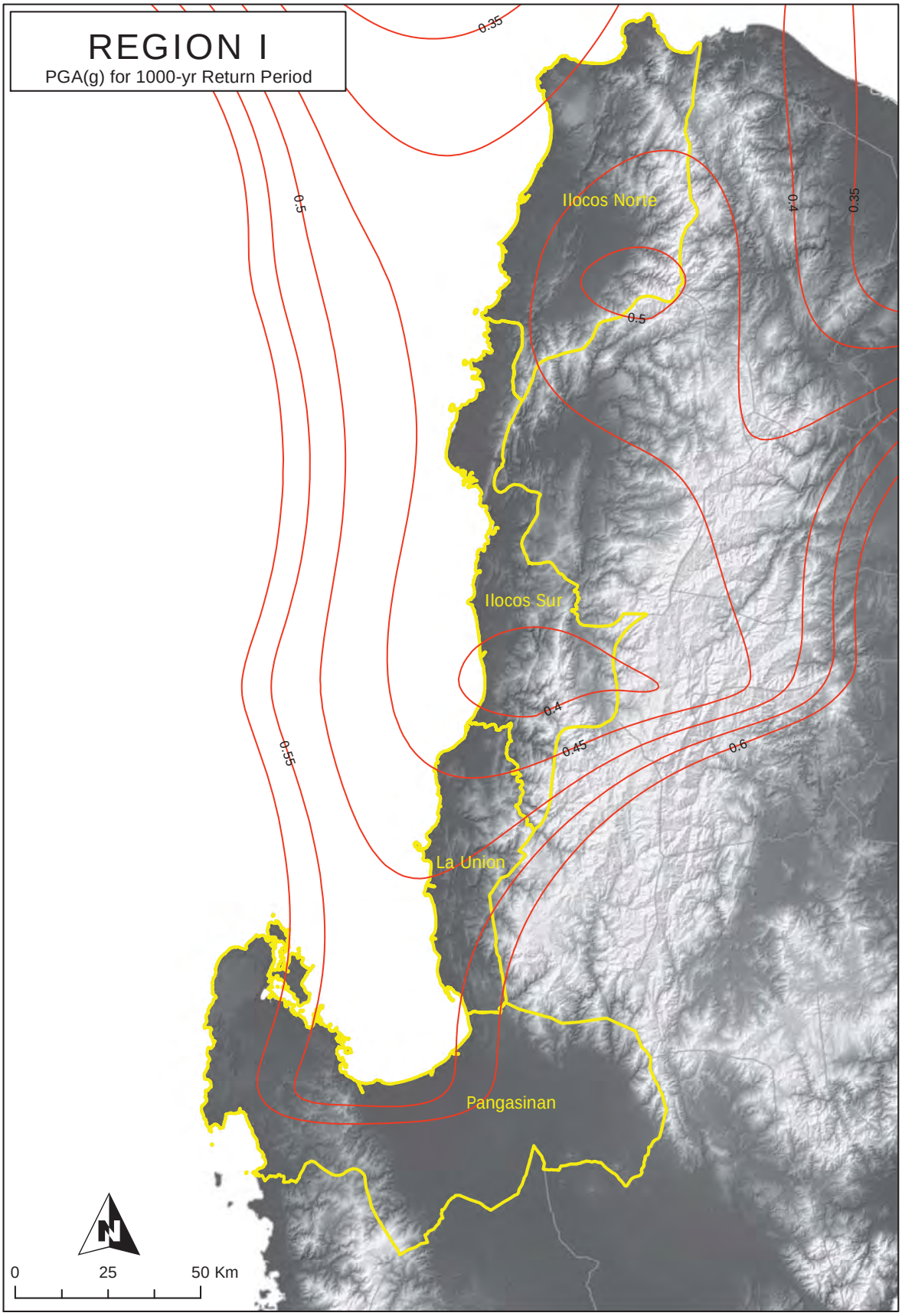

Figure 2A-17 Region I map of peak ground acceleration for 1,000-year return period

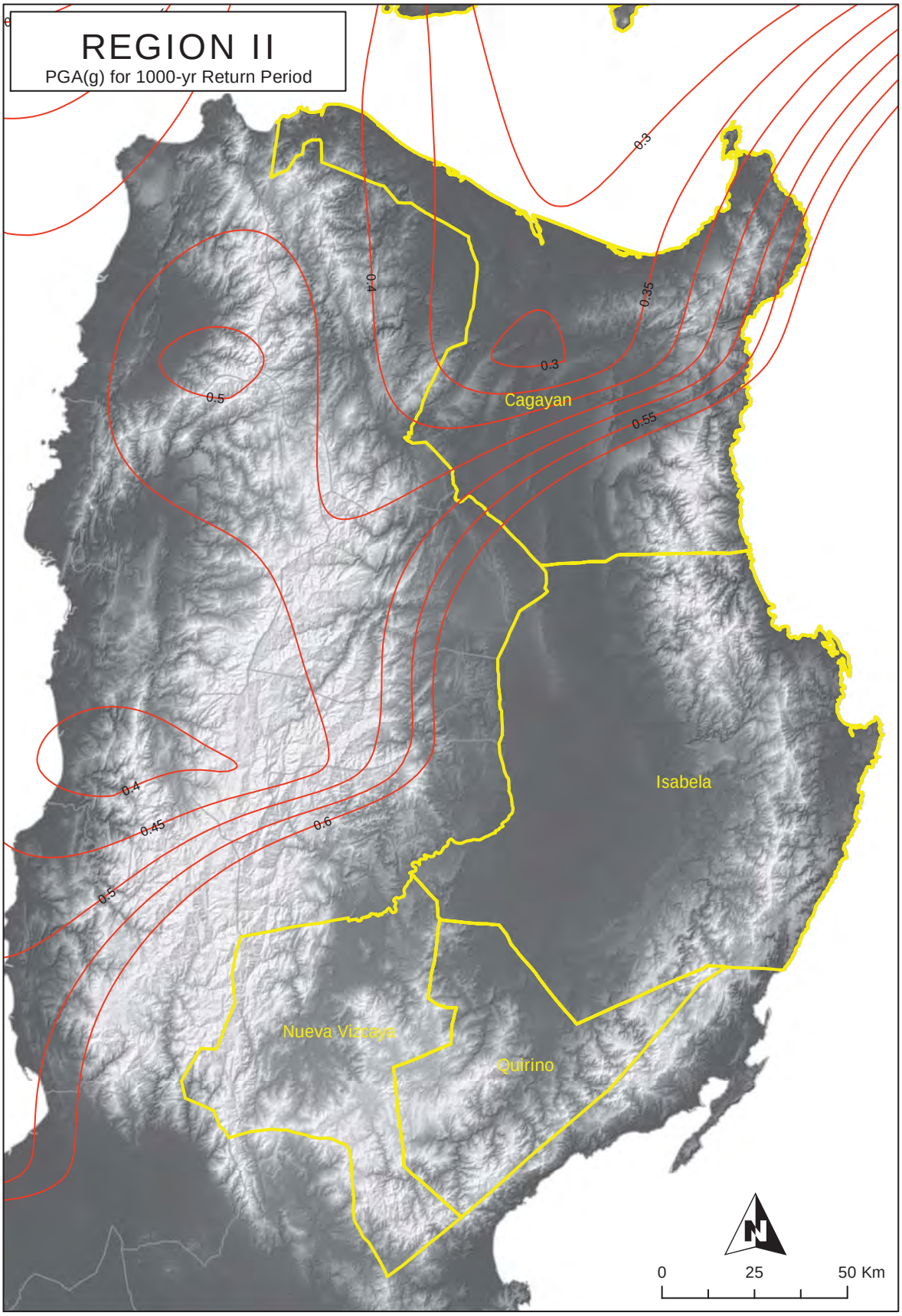

Figure 2A-18 Region II map of peak ground acceleration for 1,000-year return period

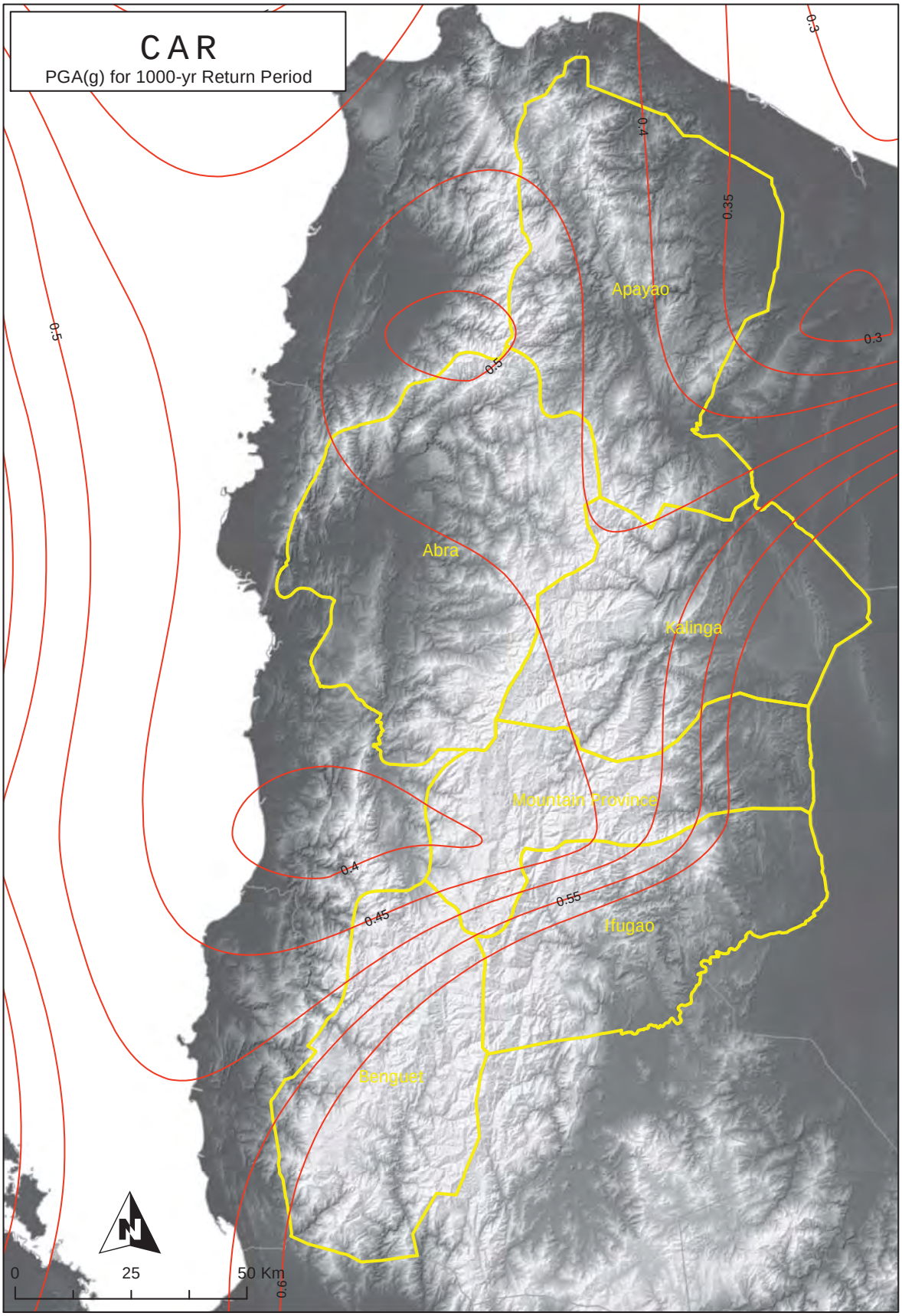

Figure 2A-19 CAR map of peak ground acceleration for 1,000-year return period

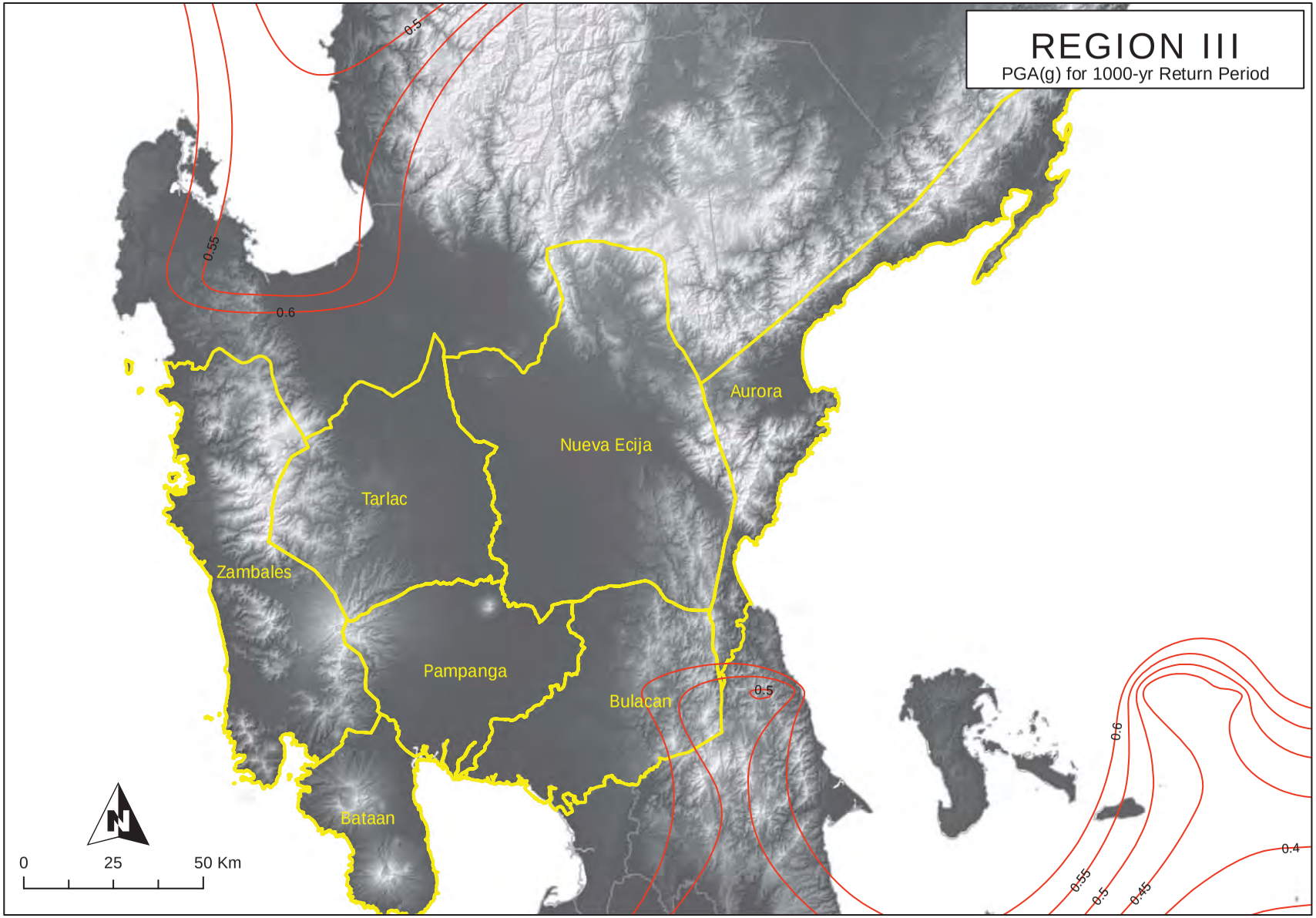

Figure 2A-20 Region III map of peak ground acceleration for 1,000-year return period

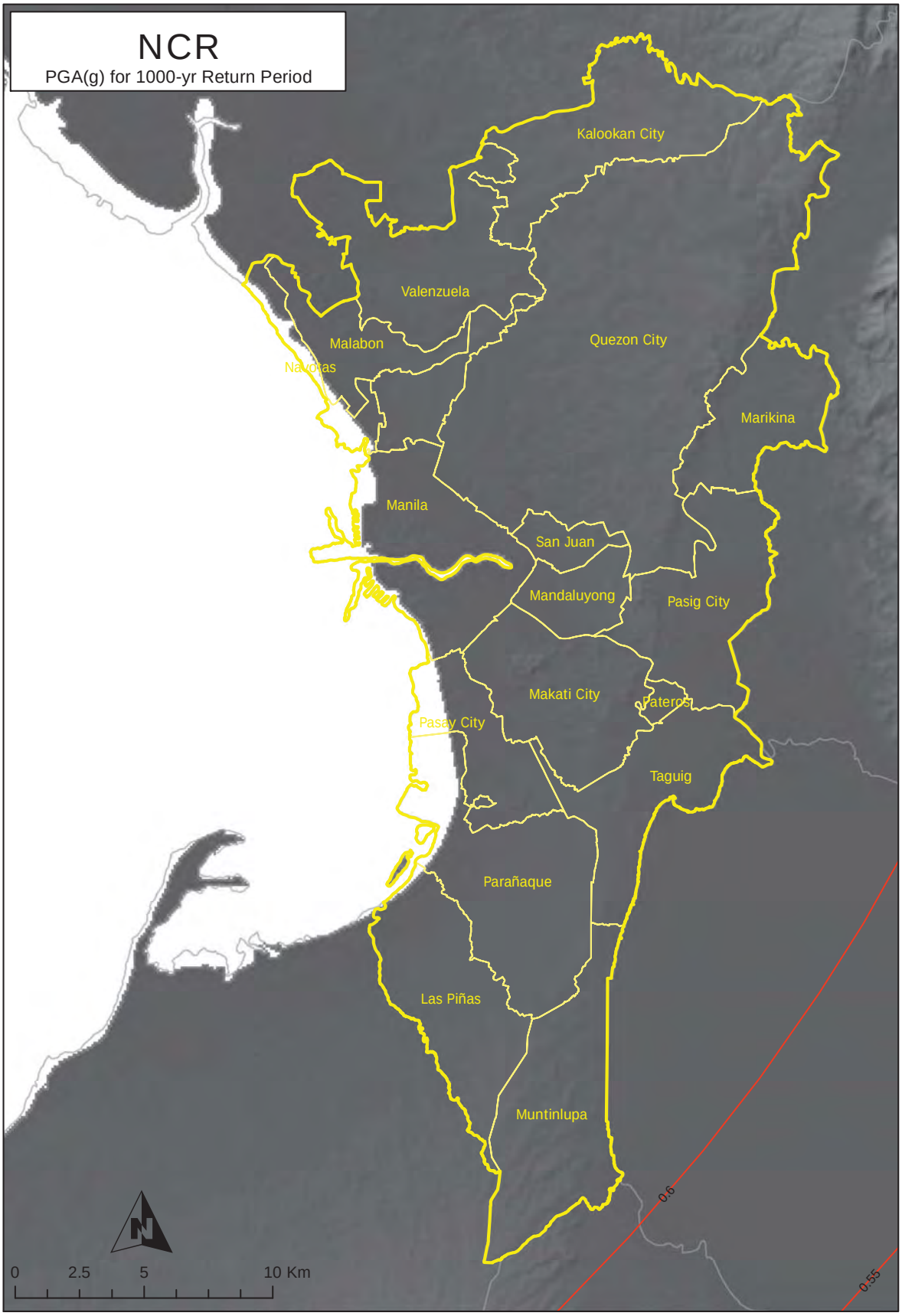

Figure 2A-21 NCR map of peak ground acceleration for 1,000-year return period

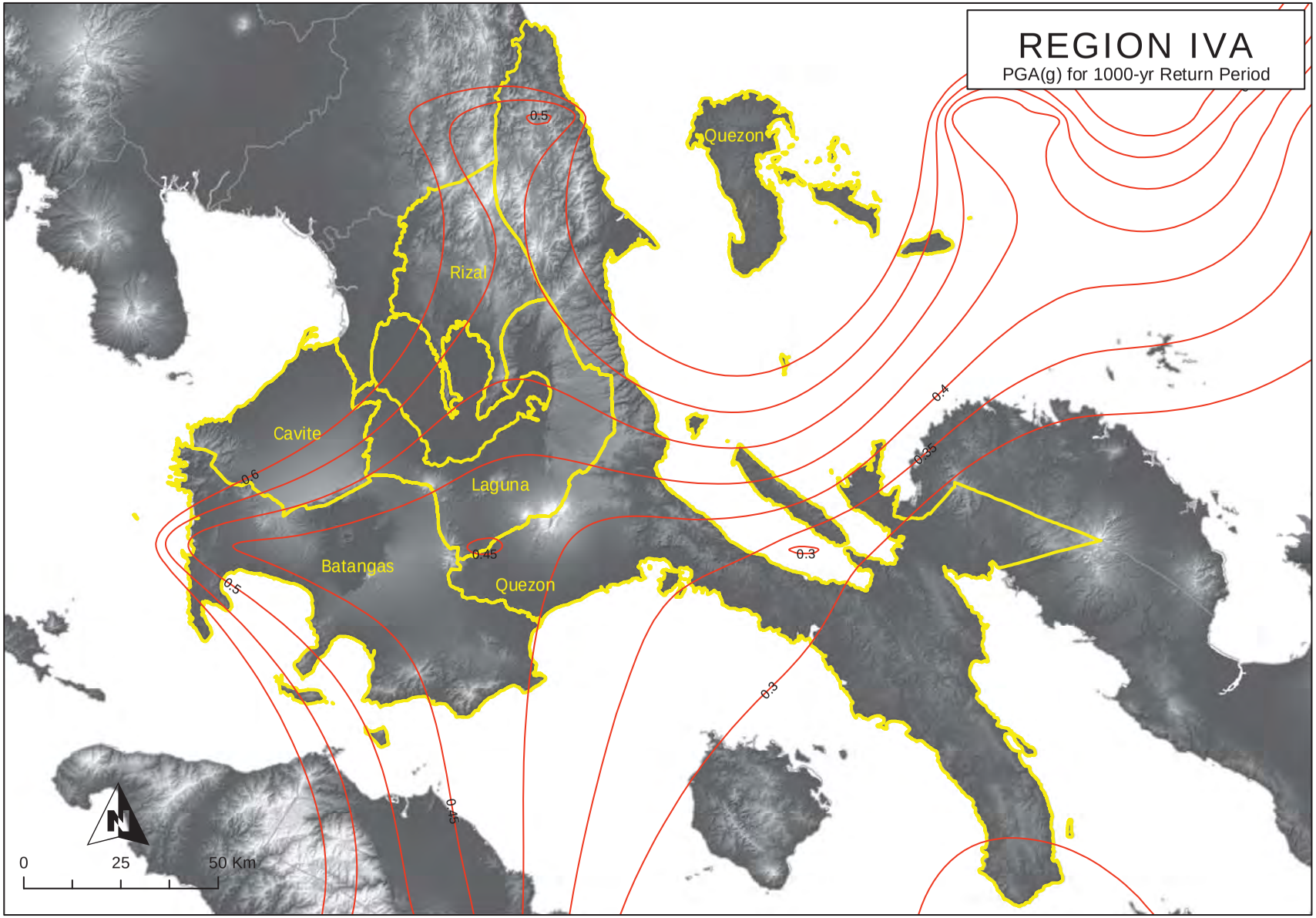

Figure 2A-22 Region IV-A map of peak ground acceleration for 1,000-year return period

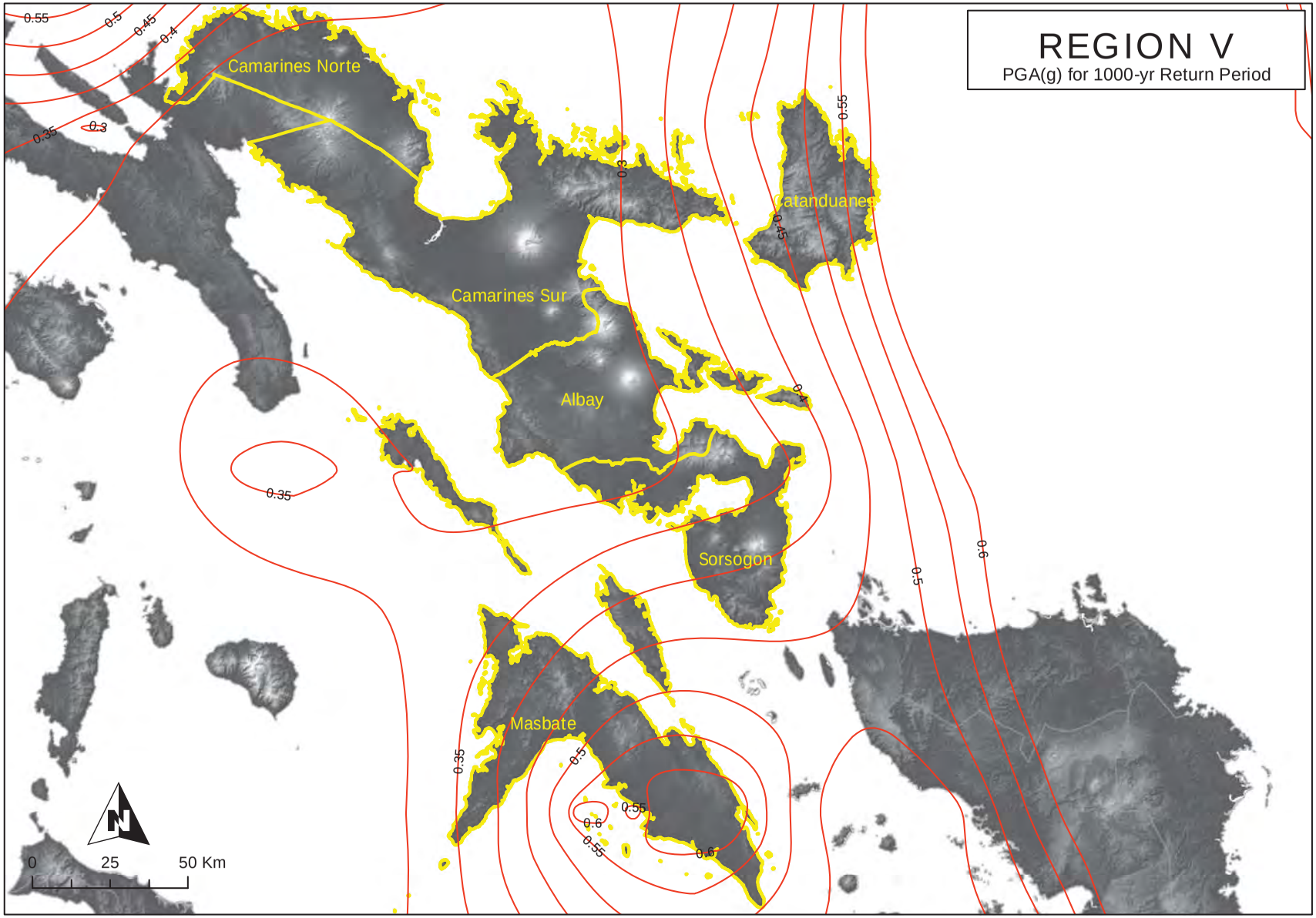

Figure 2A-23 Region V map of peak ground acceleration for 1,000-year return period

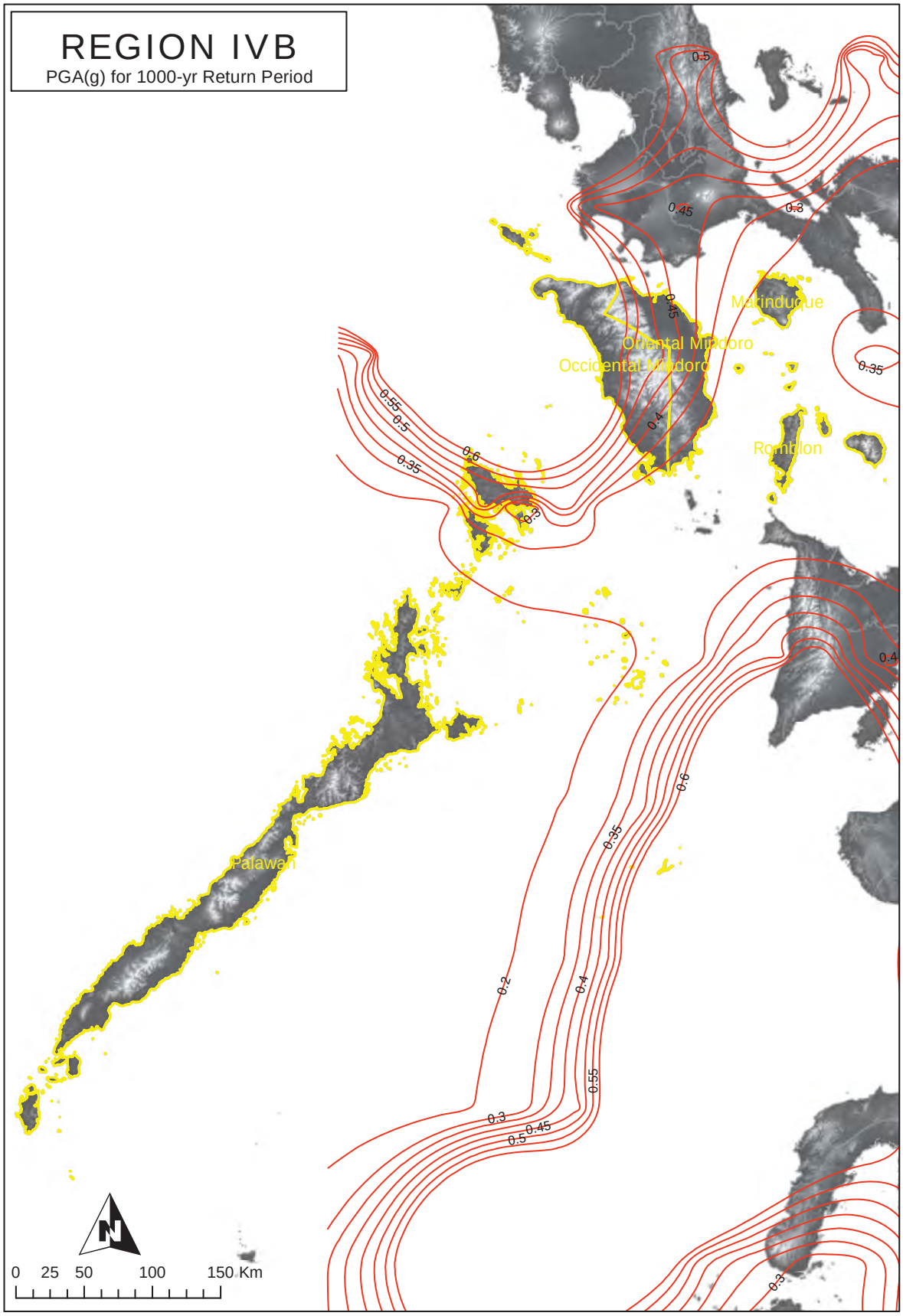

Figure 2A-24 Region IV-B map of peak ground acceleration for 1,000-year return period

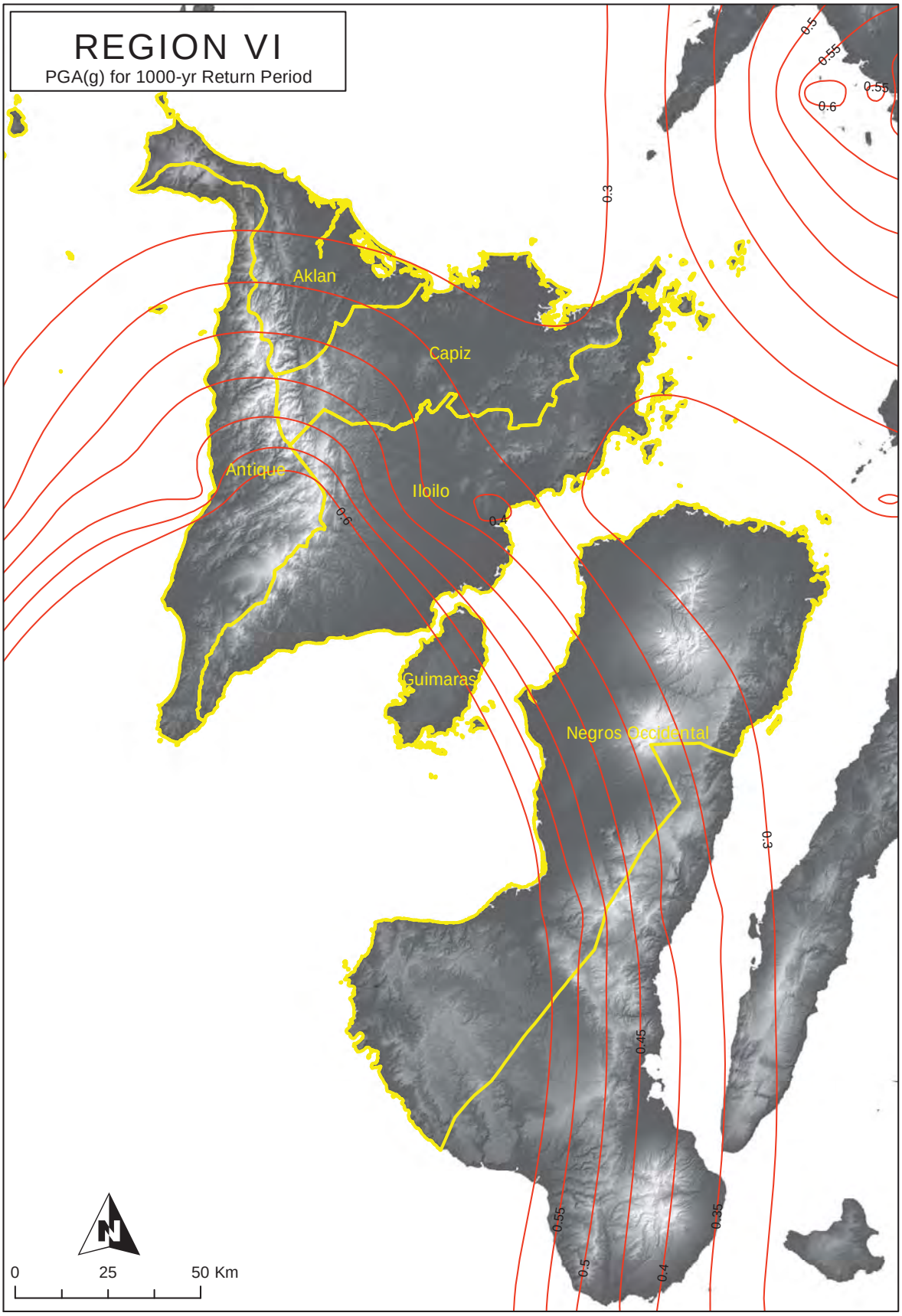

Figure 2A-25 Region VI map of peak ground acceleration for 1,000-year return period

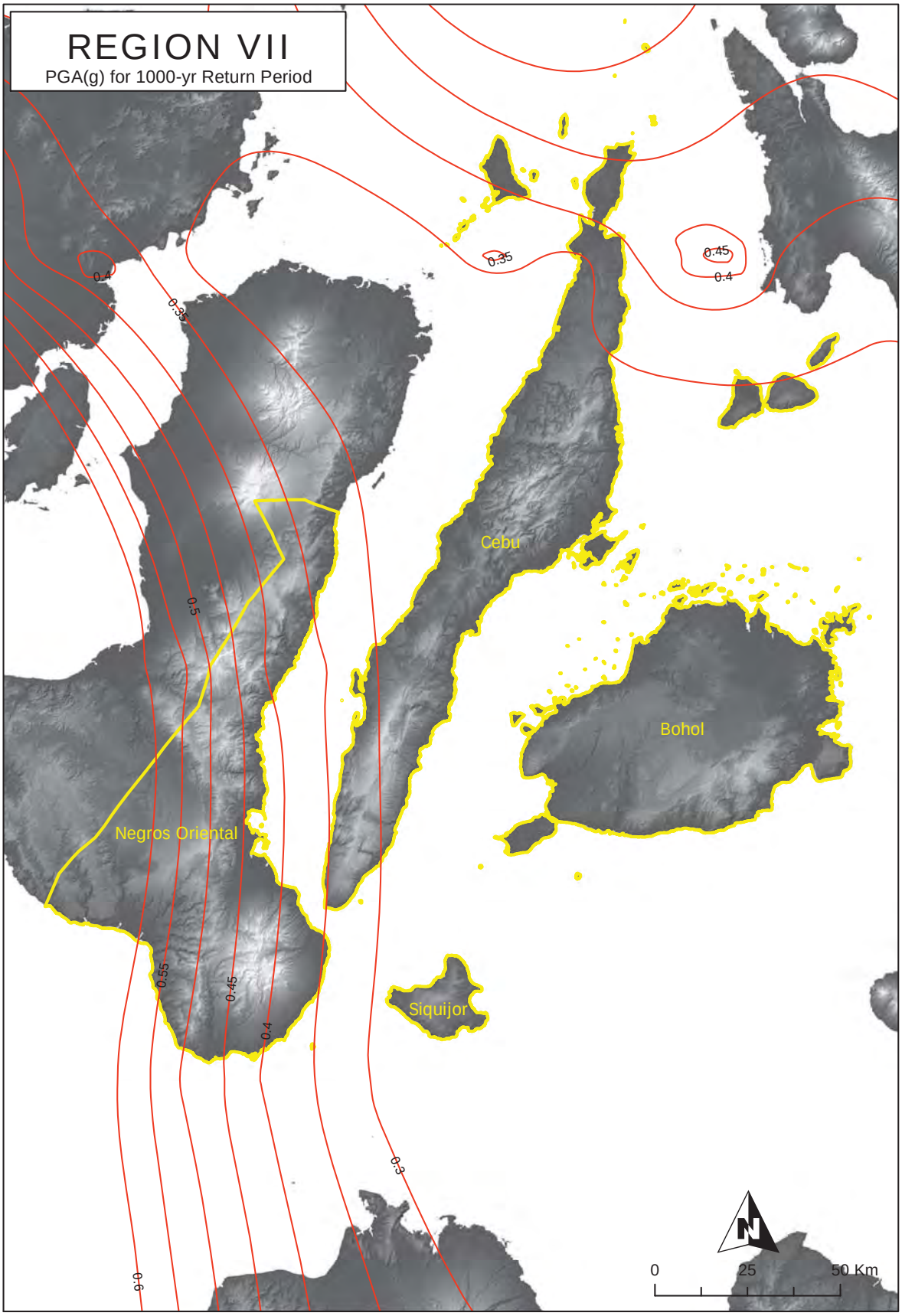

Figure 2A-26 Region VII map of peak ground acceleration for 1,000-year return period

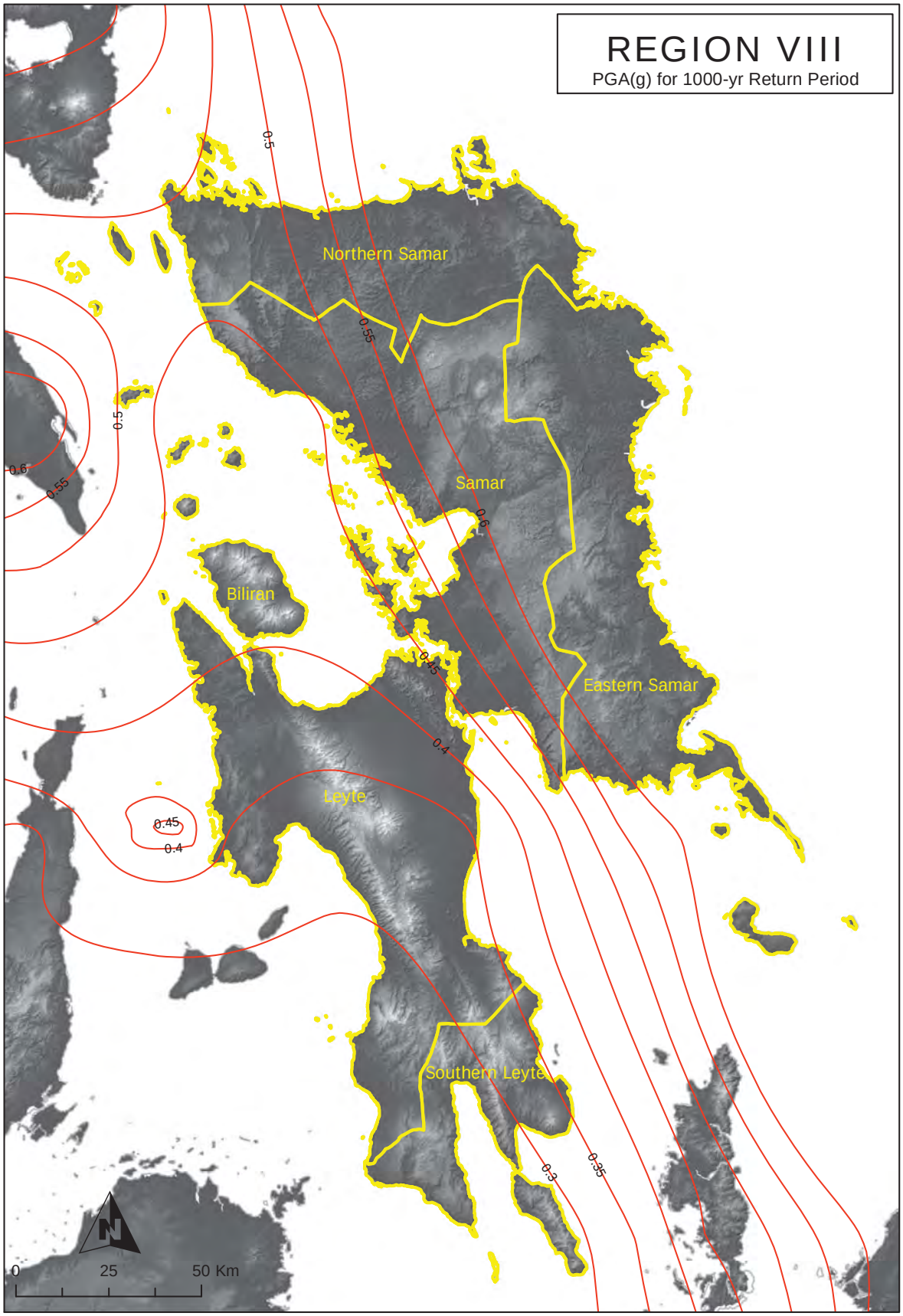

Figure 2A-27 Region VIII map of peak ground acceleration for 1,000-year return period

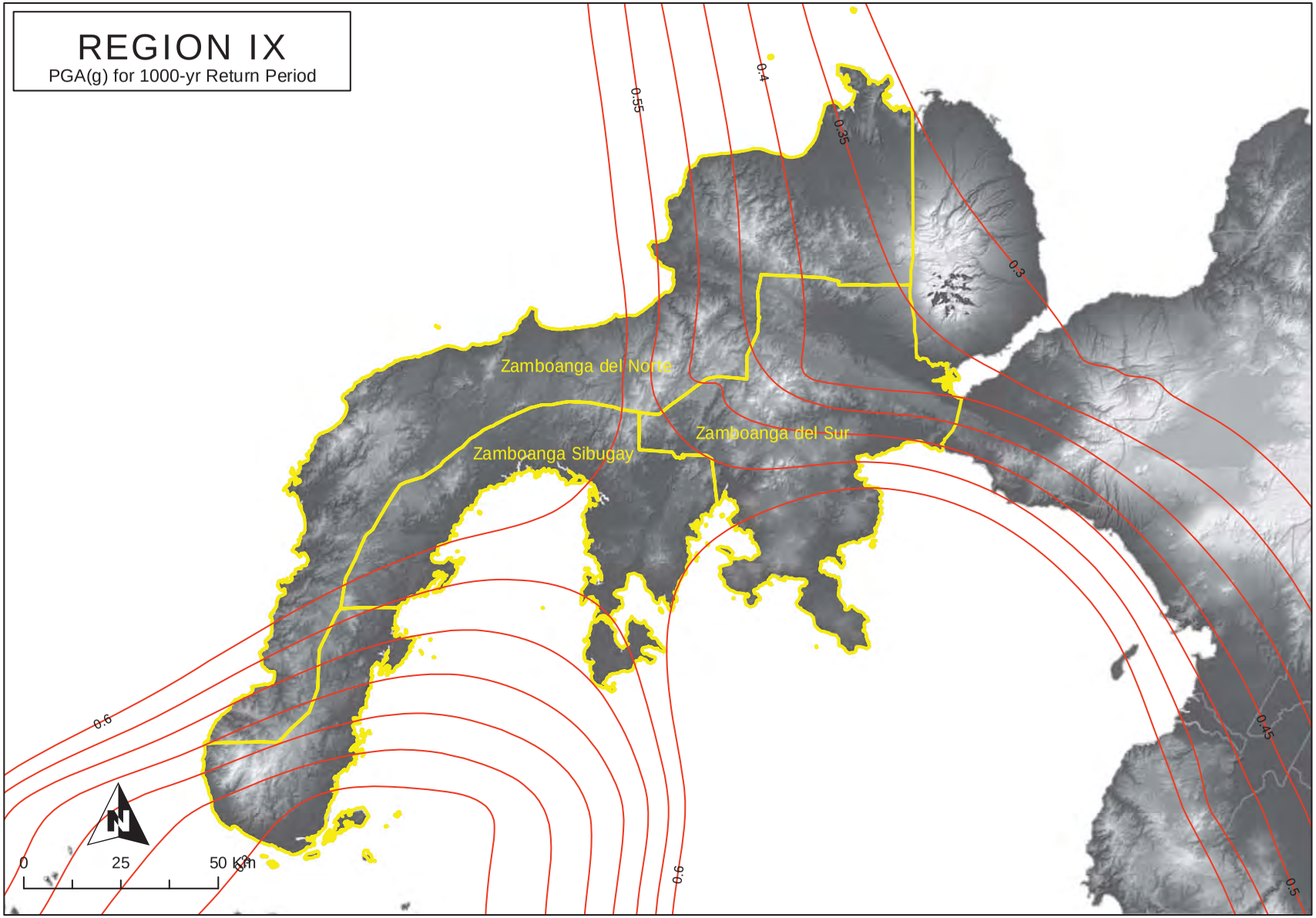

Figure 2A-28 Region IX map of peak ground acceleration for 1,000-year return period

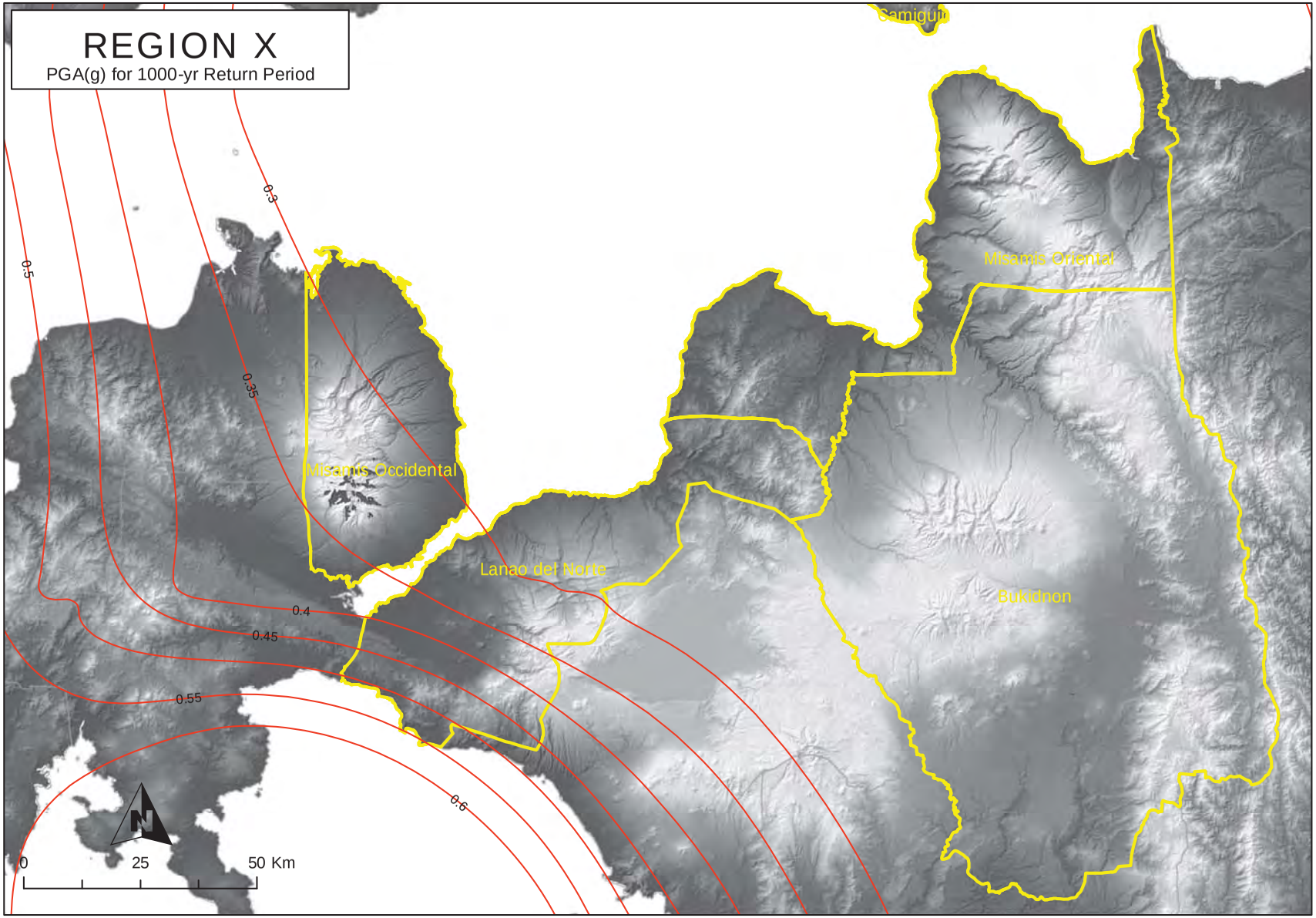

Figure 2A-29 Region X map of peak ground acceleration for 1,000-year return period

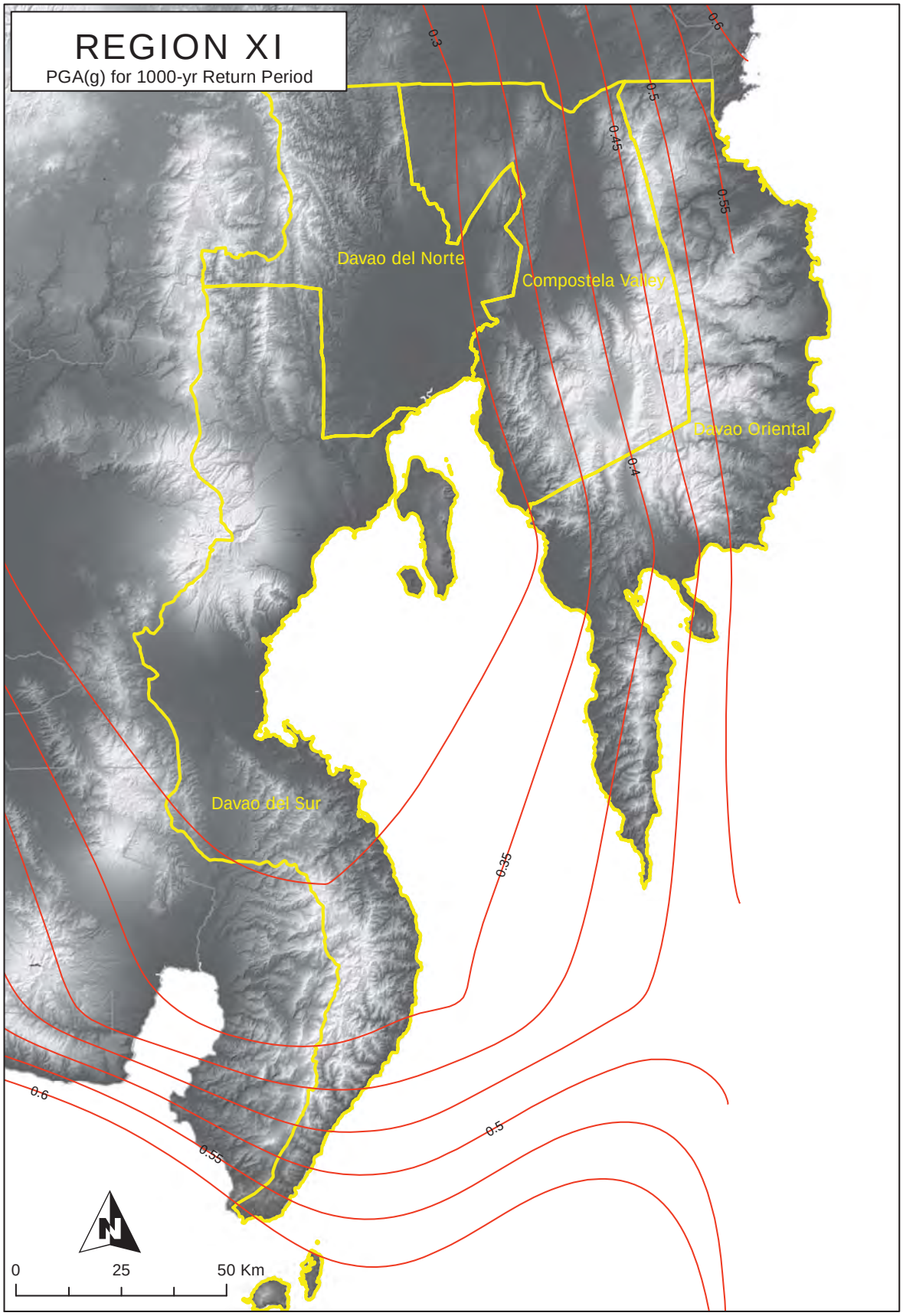

Figure 2A-30 Region XI map of peak ground acceleration for 1,000-year return period

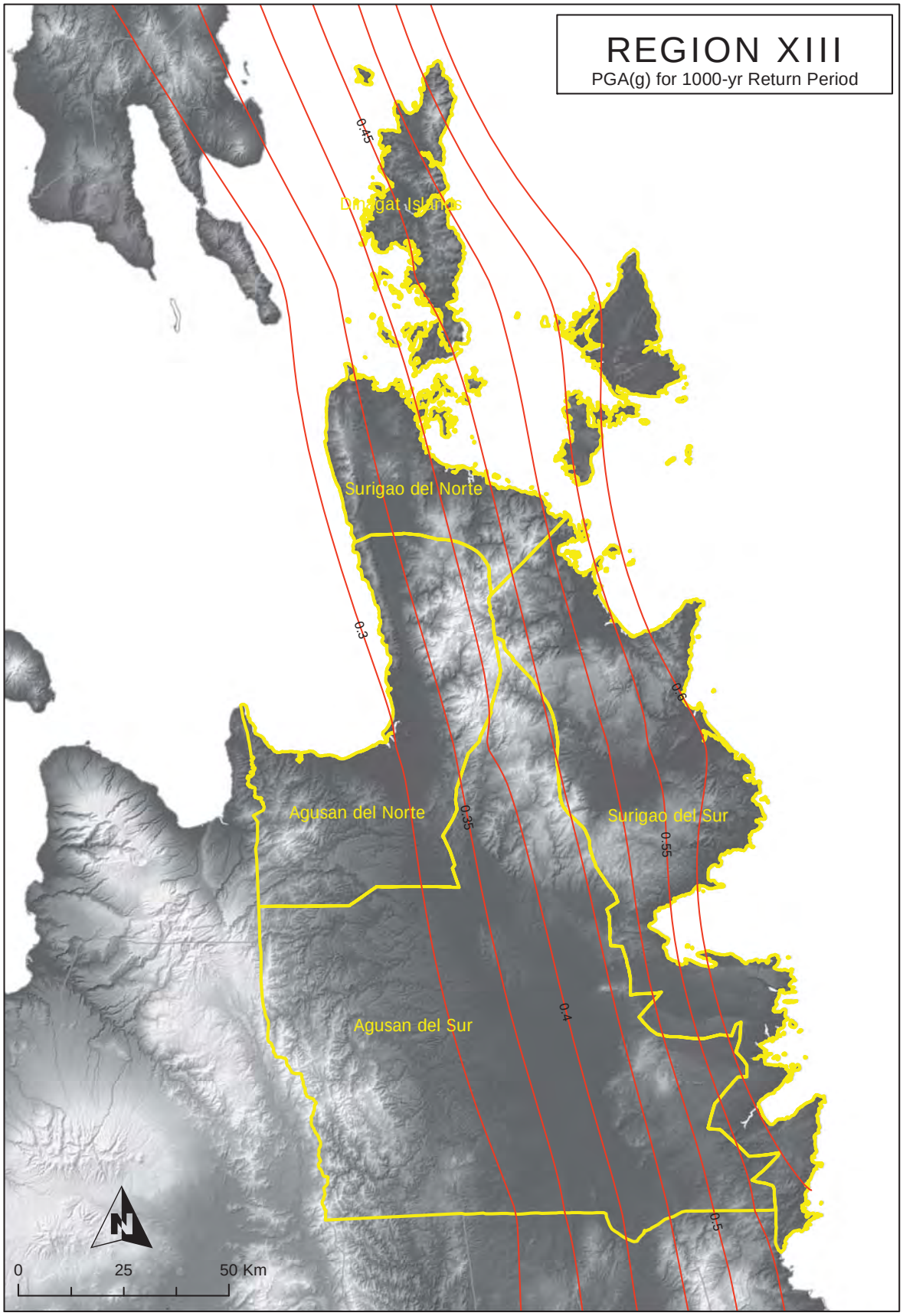

Figure 2A-31 Region XIII map of peak ground acceleration for 1,000-year return period

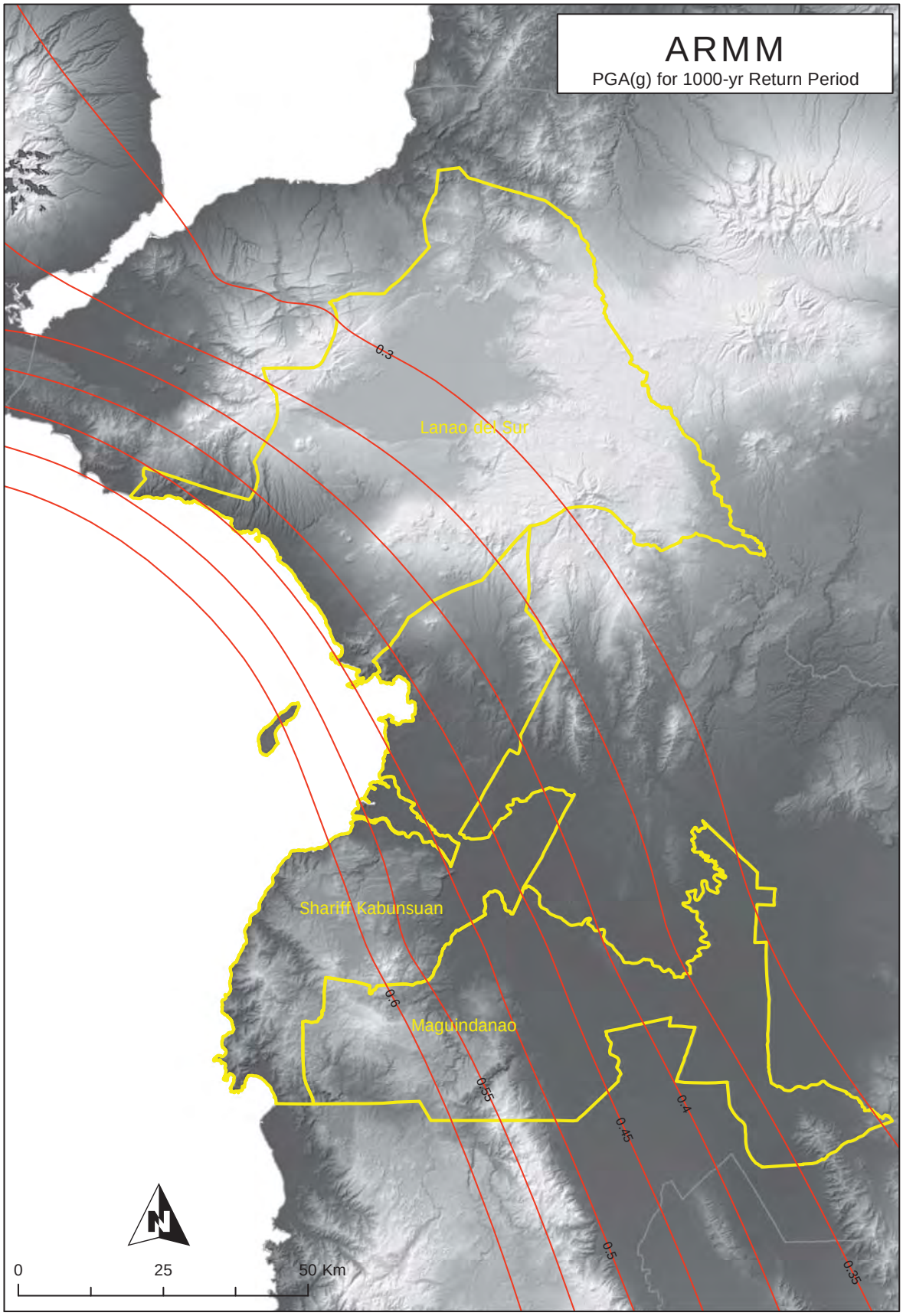

Figure 2A-32 ARMM map of peak ground acceleration for 1,000-year return period

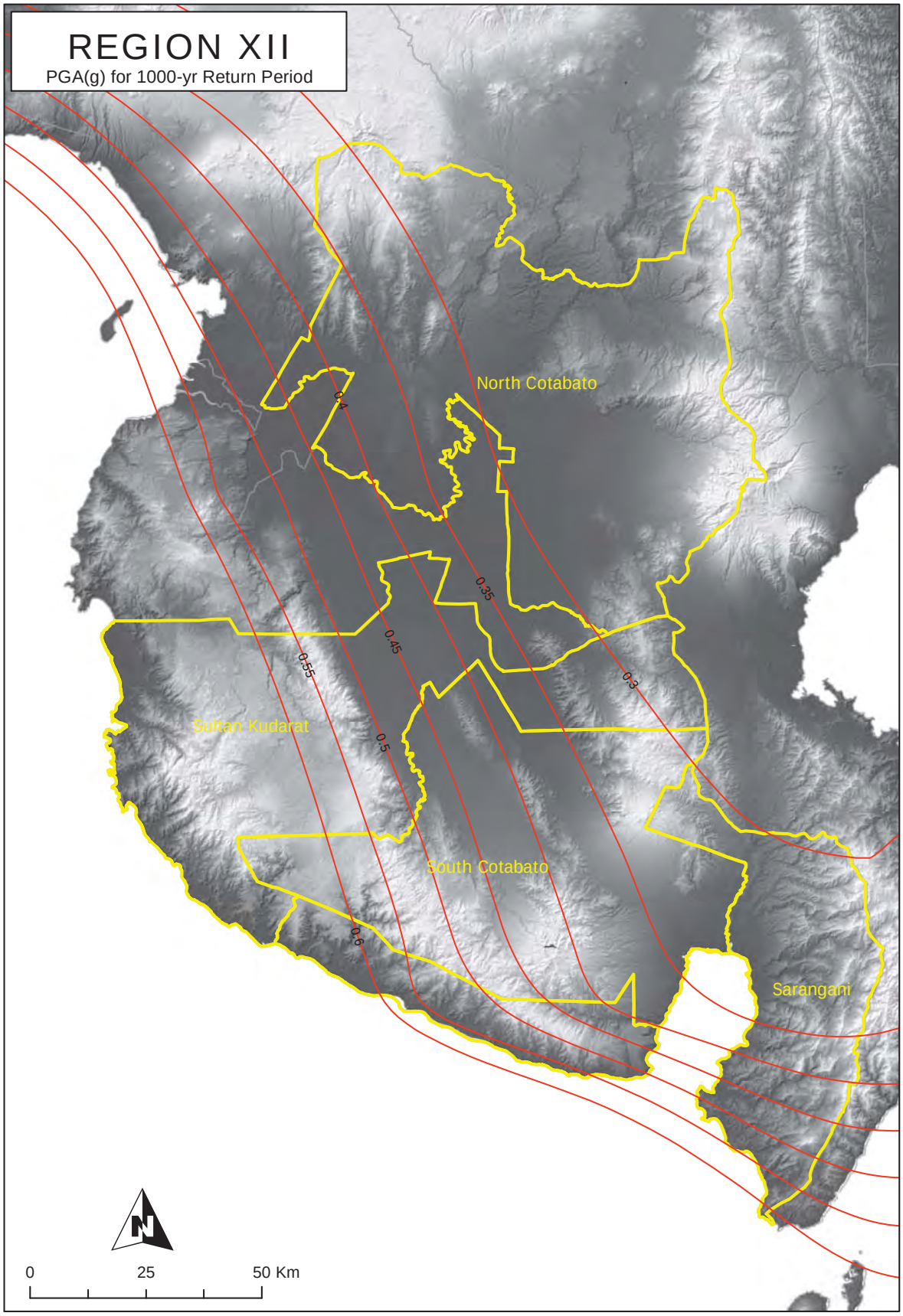

Figure 2A-33 Region XII map of peak ground acceleration for 1,000-year return period

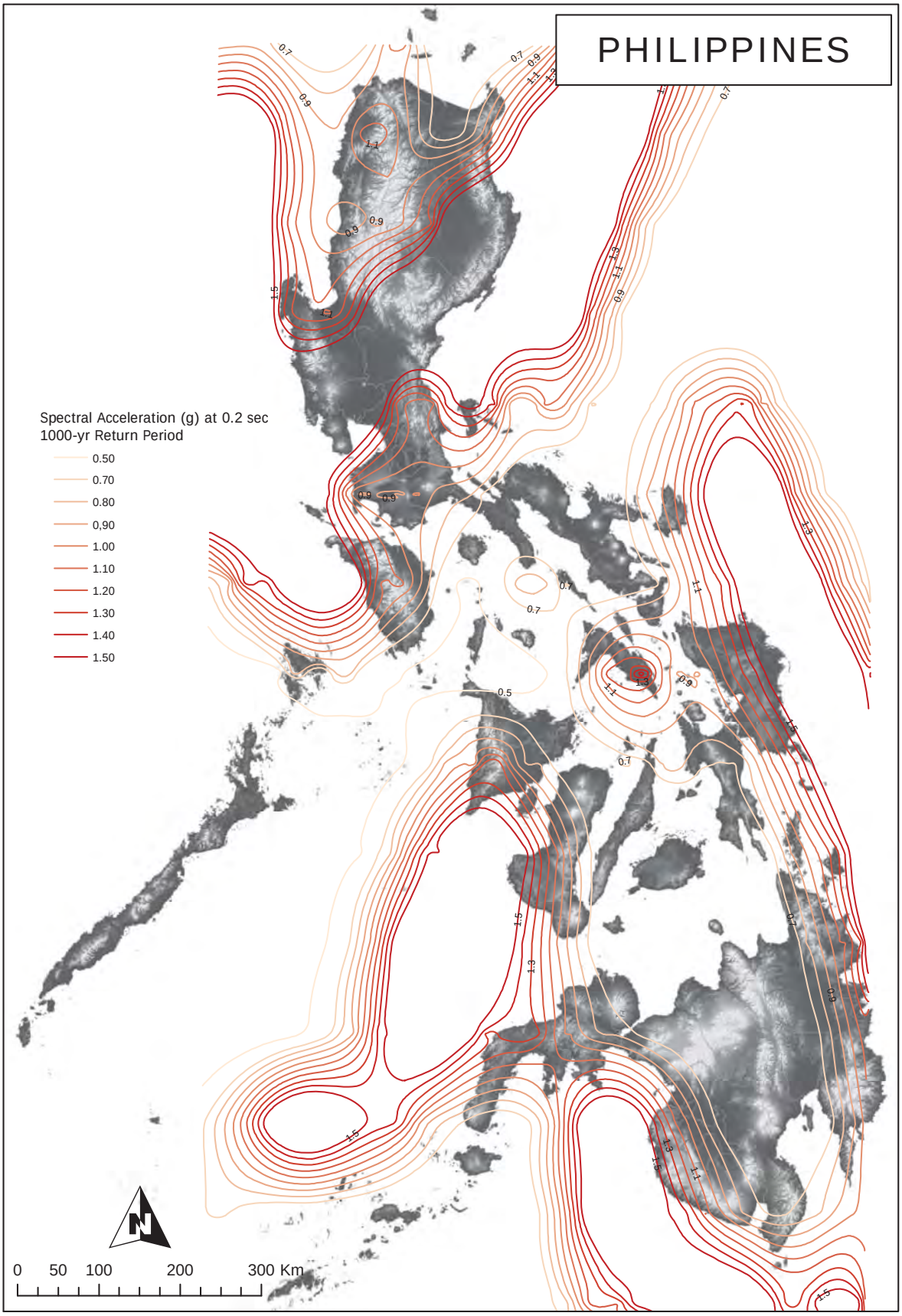

Figure 2A-34 Contour map of spectral acceleration at 0.2 sec. for 1,000-year return period

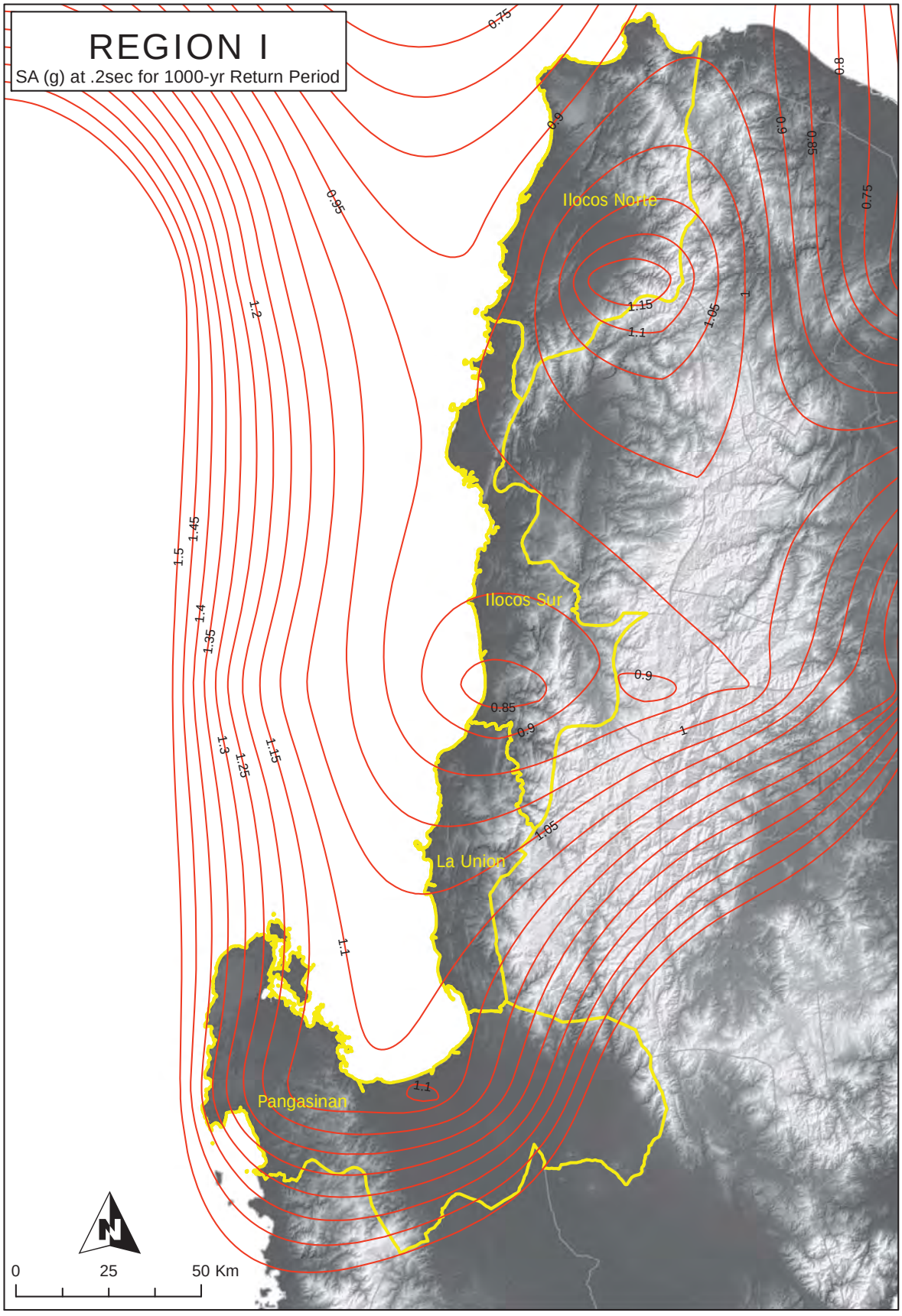

Figure 2A-35 Region I map of spectral acceleration at 0.2 sec. for 1,000-year return period

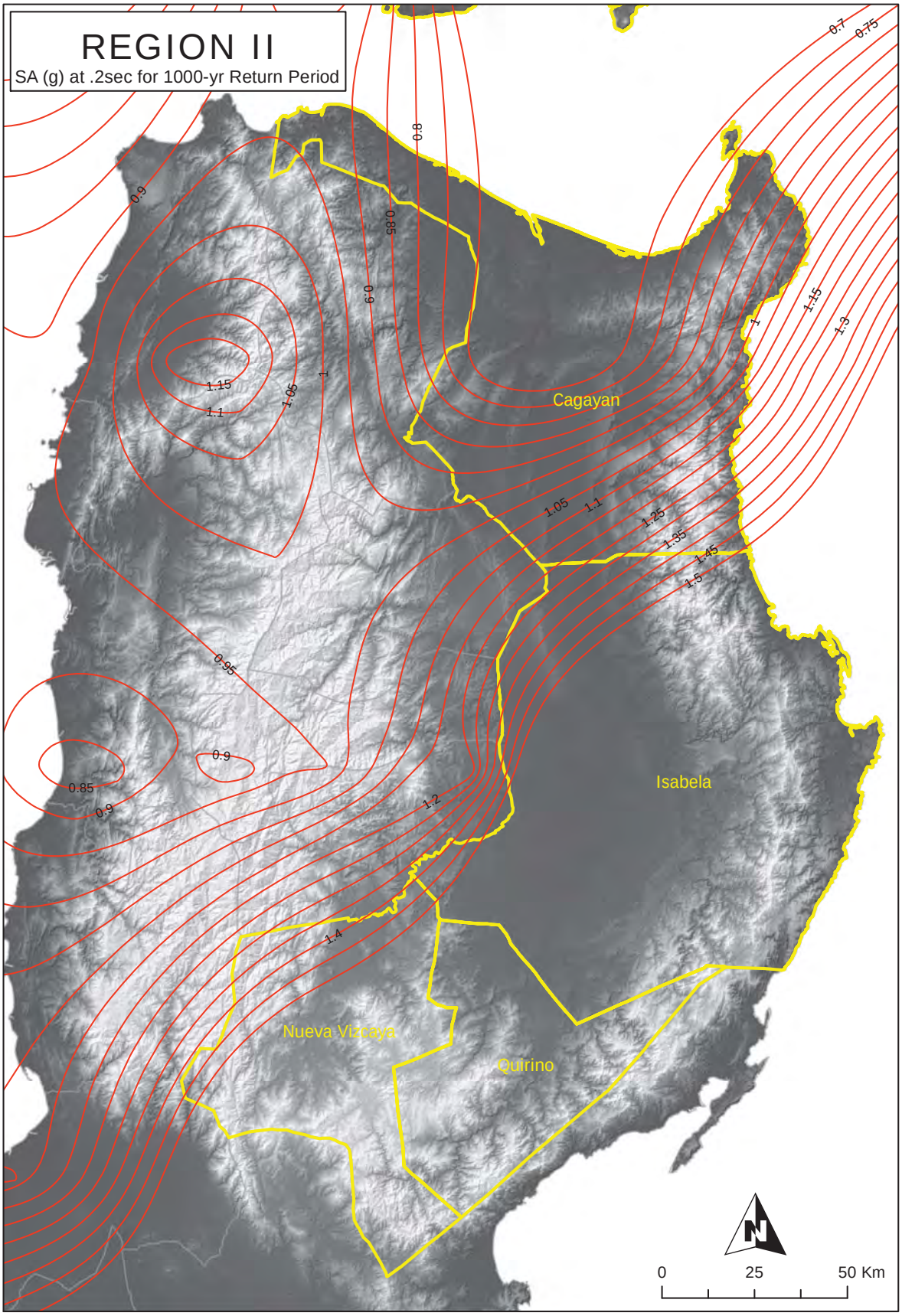

Figure 2A-36 Region II map of spectral acceleration at 0.2 sec. for 1,000-year return period

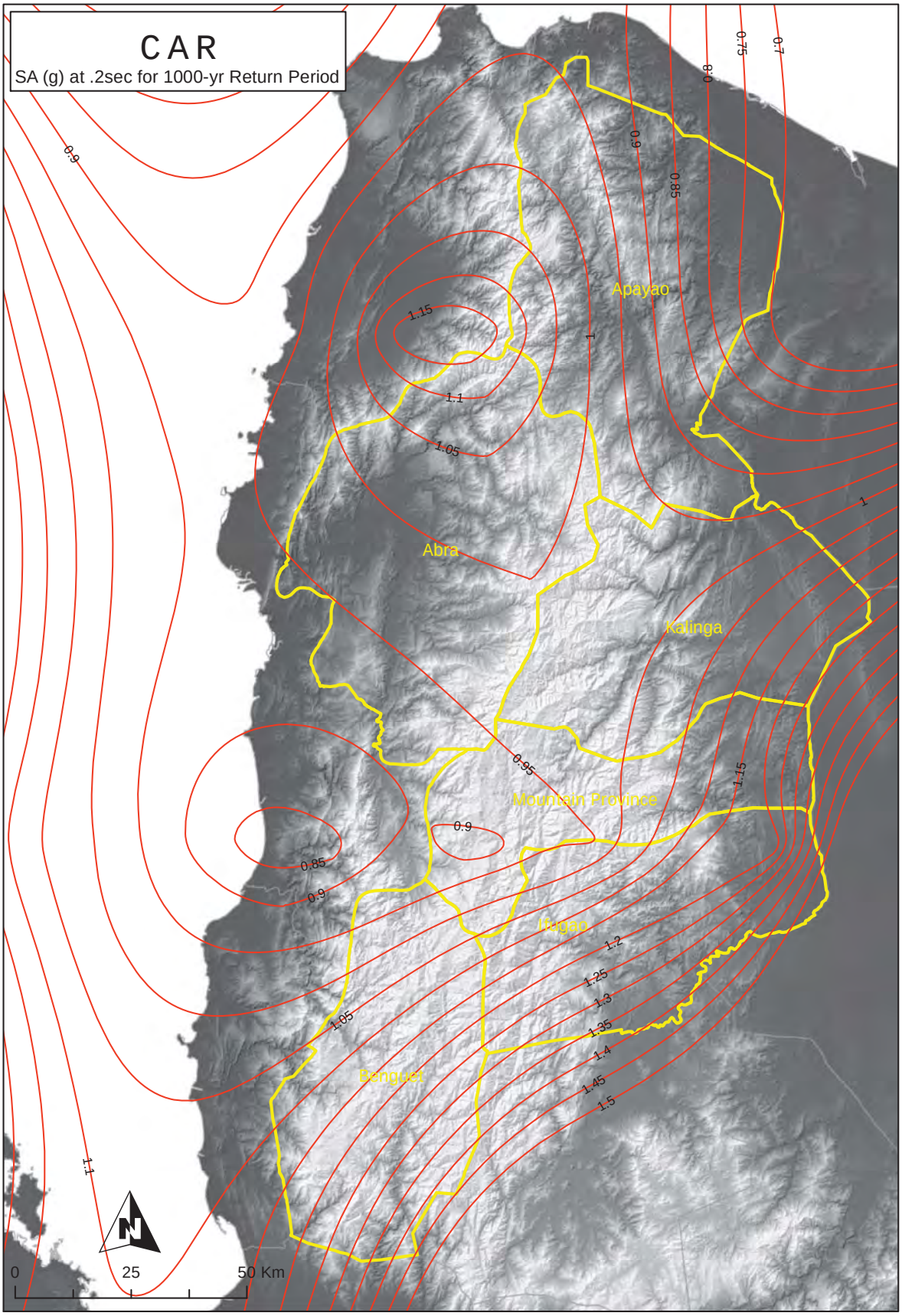

Figure 2A-37 CAR map of spectral acceleration at 0.2 sec. for 1,000-year return period

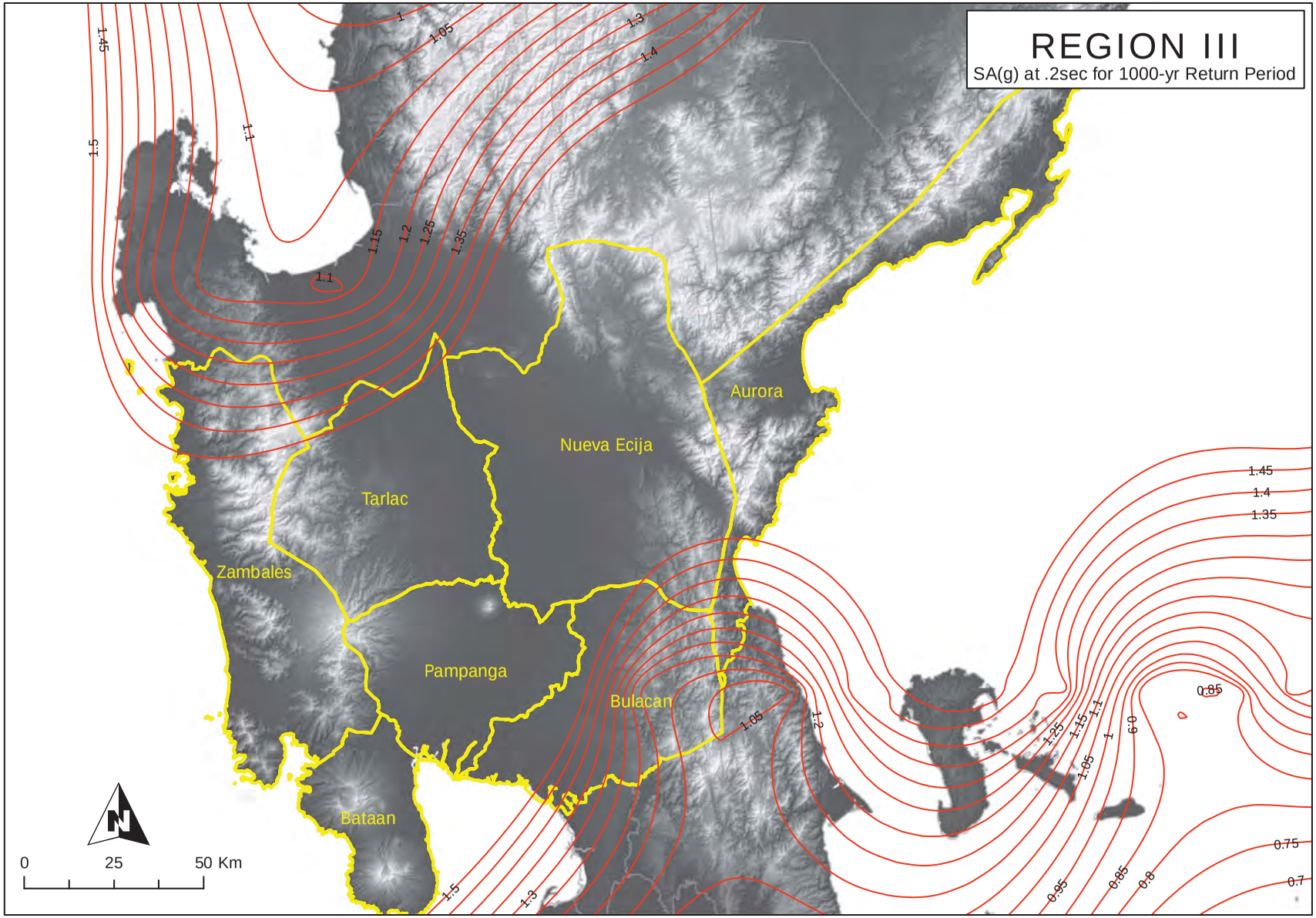

Figure 2A-38 Region III map of spectral acceleration at 0.2 sec. for 1,000-year return period

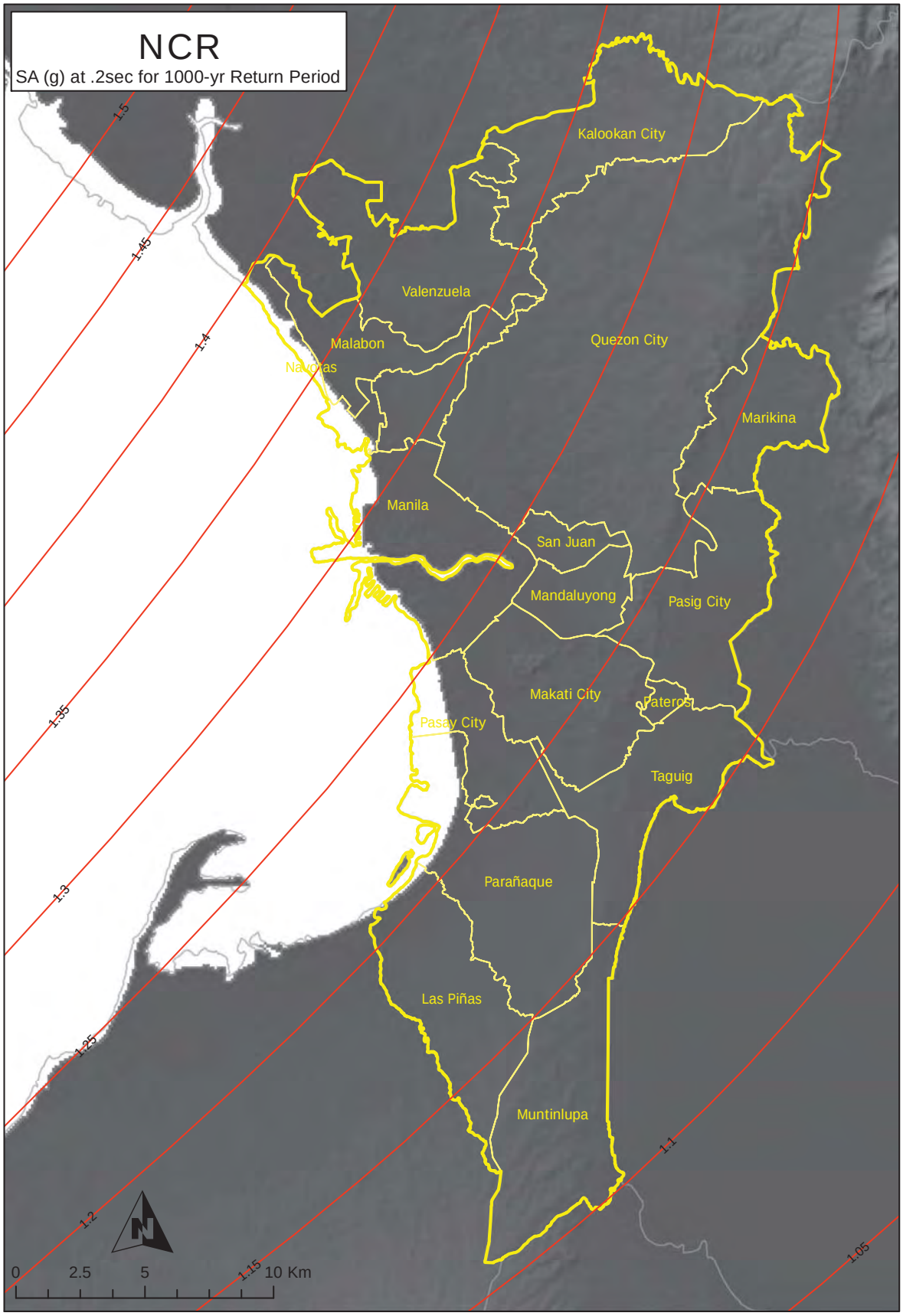

Figure 2A-39 NCR map of spectral acceleration at 0.2 sec. for 1,000-year return period

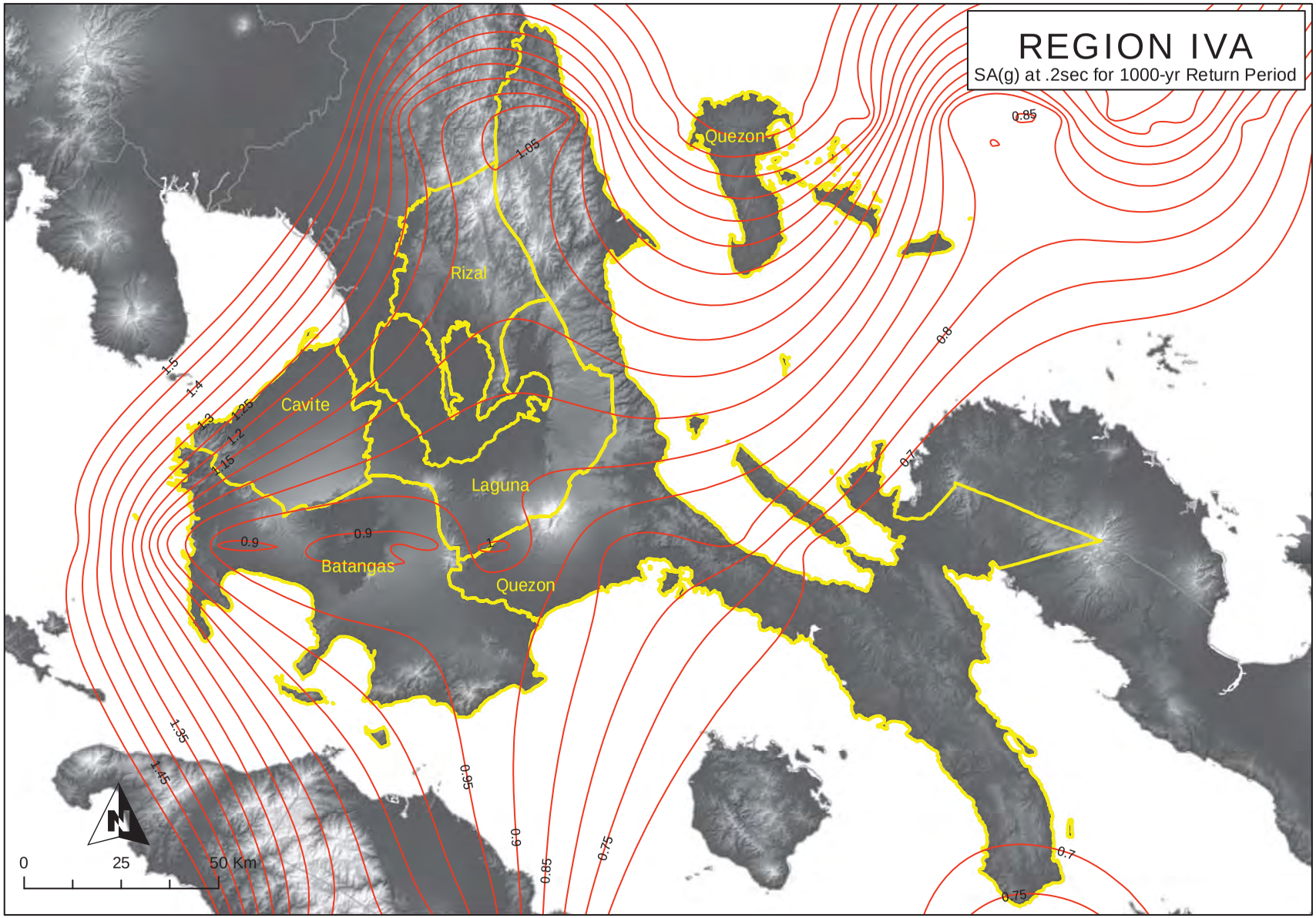

Figure 2A-40 Region IV-A map of spectral acceleration at 0.2 sec. for 1,000-year return period

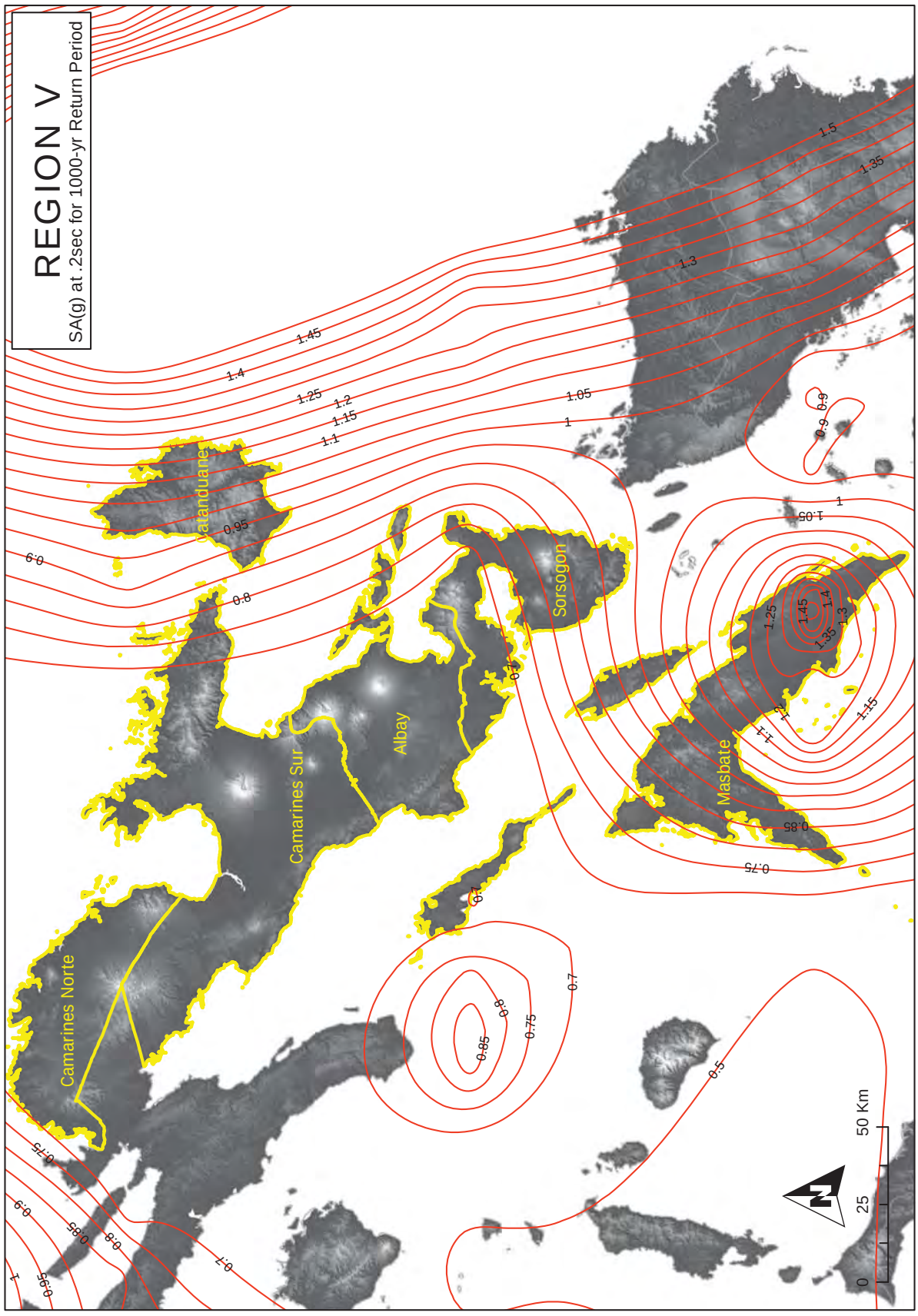

Figure 2A-41 Region V map of spectral acceleration at 0.2 sec. for 1,000-year return period

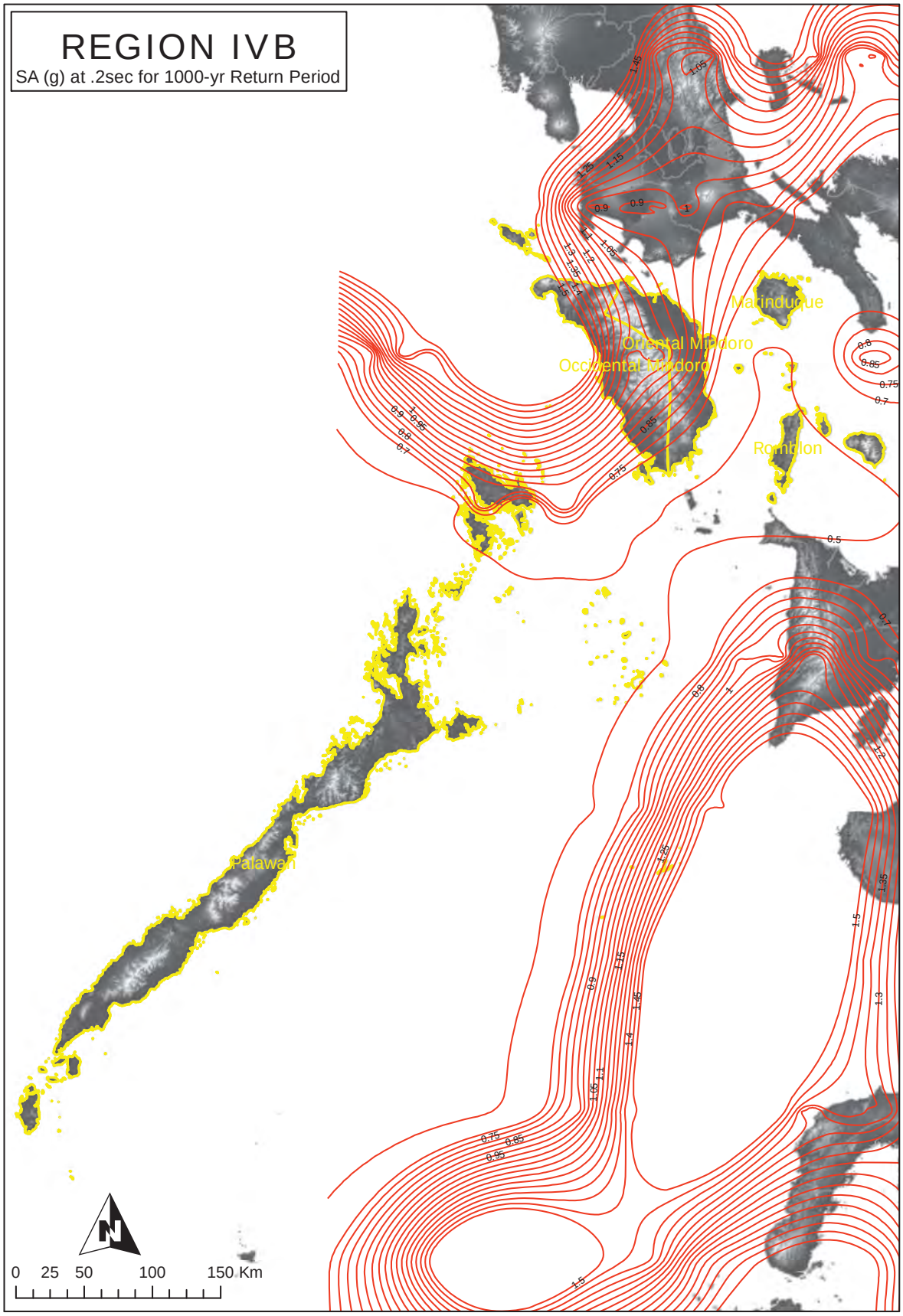

Figure 2A-42 Region IV-B map of spectral acceleration at 0.2 sec. for 1,000-year return period

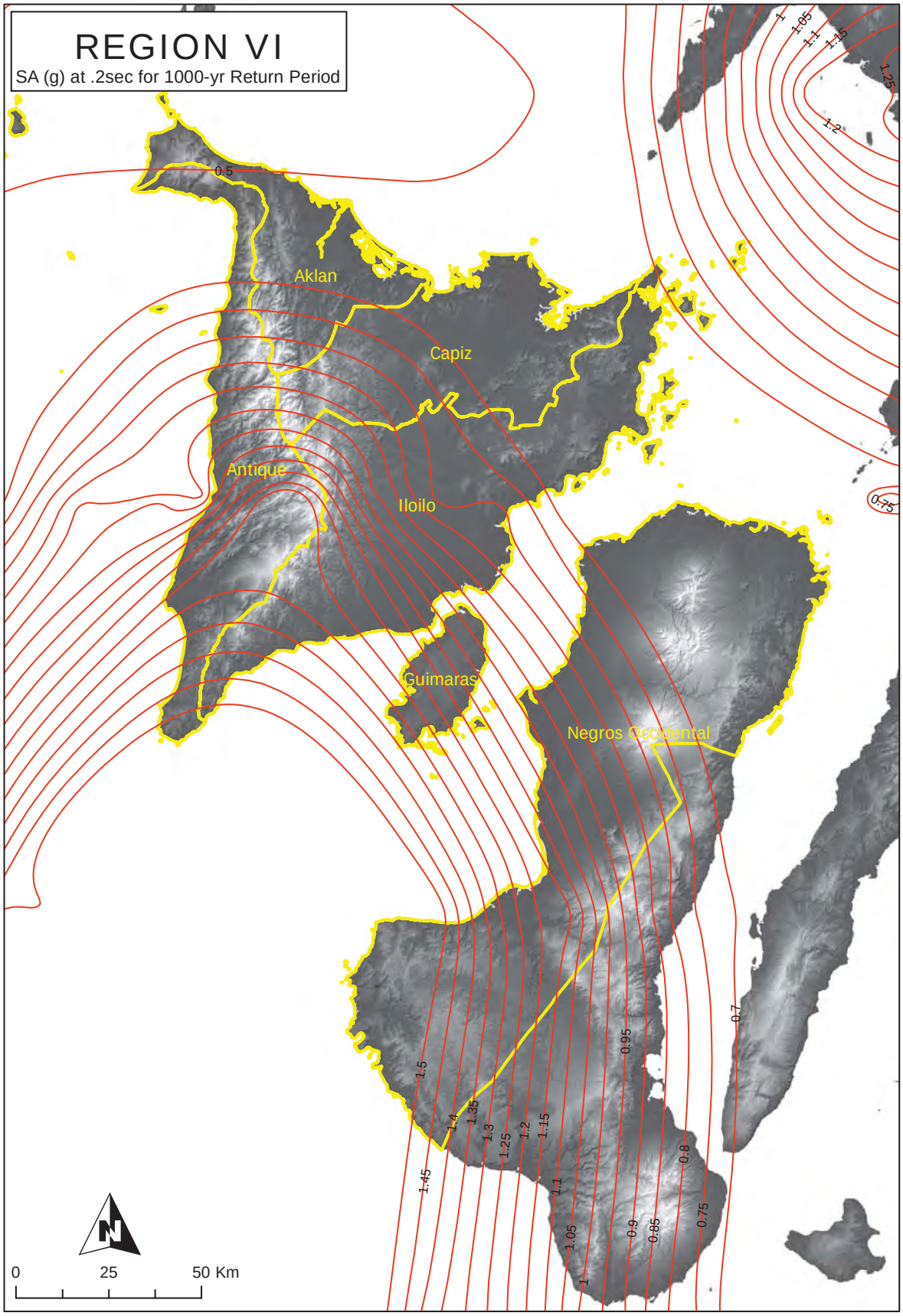

Figure 2A-43 Region VI map of spectral acceleration at 0.2 sec. for 1,000-year return period

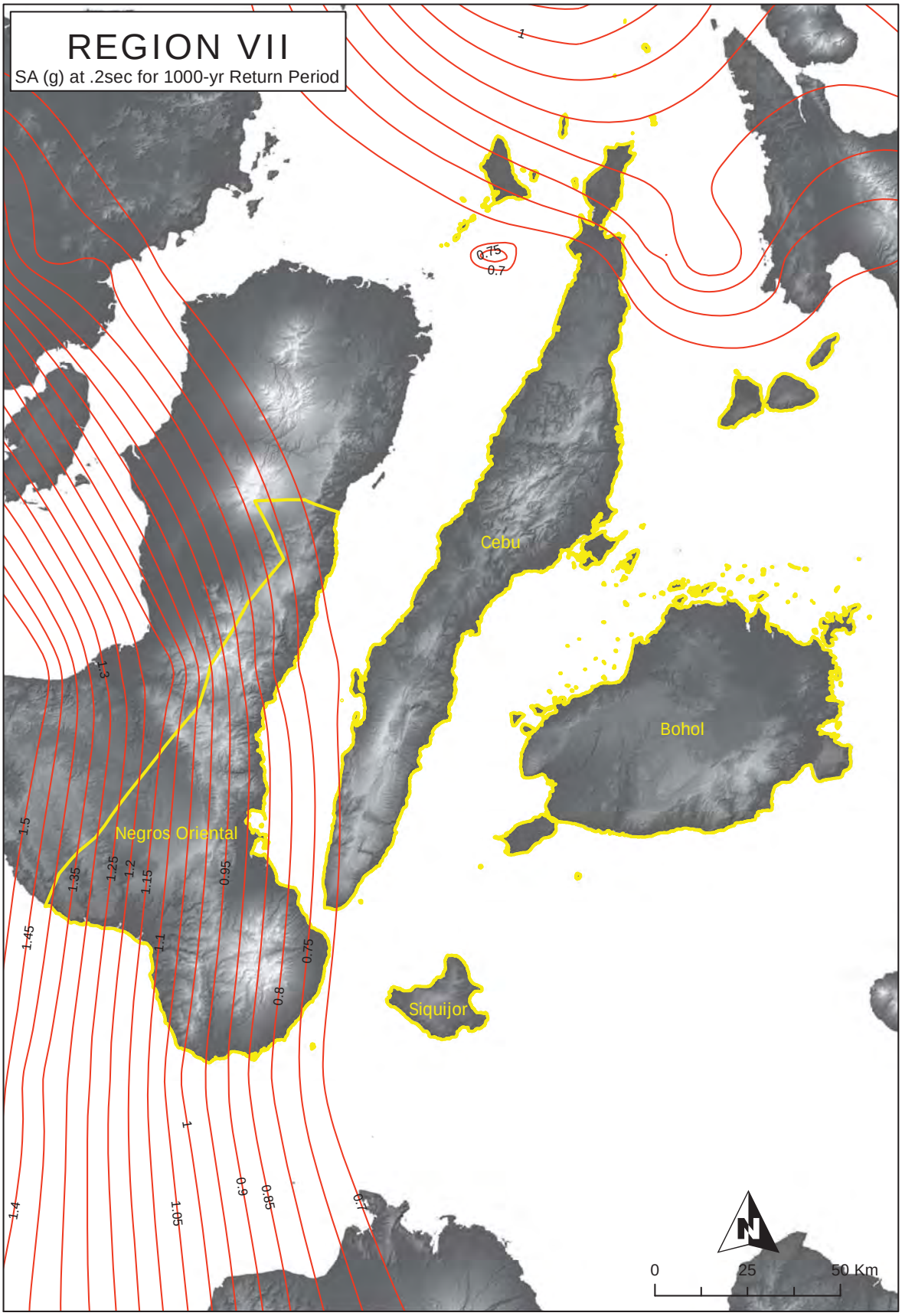

Figure 2A-44 Region VII map of spectral acceleration at 0.2 sec. for 1,000-year return period

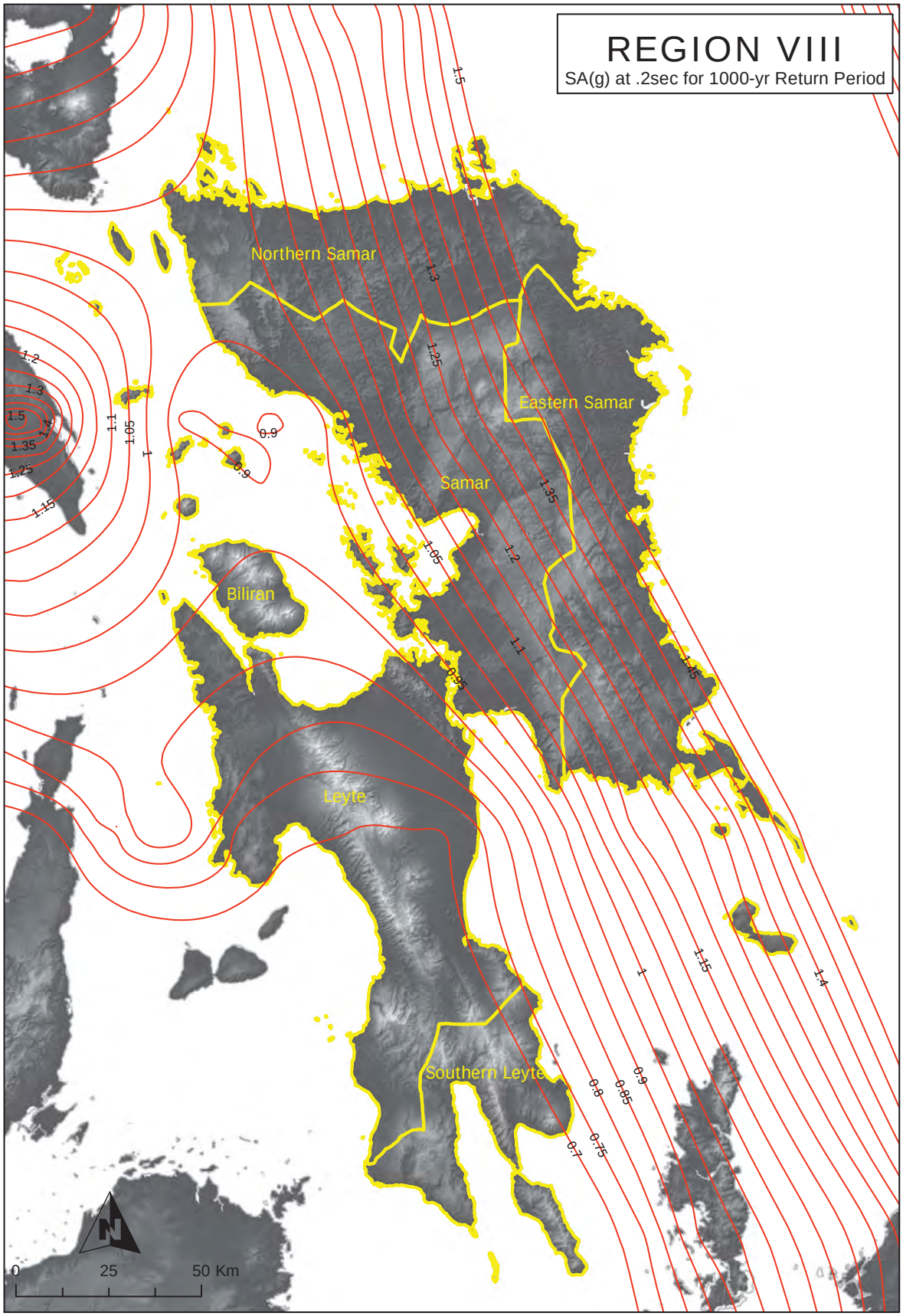

Figure 2A-45 Region VIII map of spectral acceleration at 0.2 sec. for 1,000-year return period

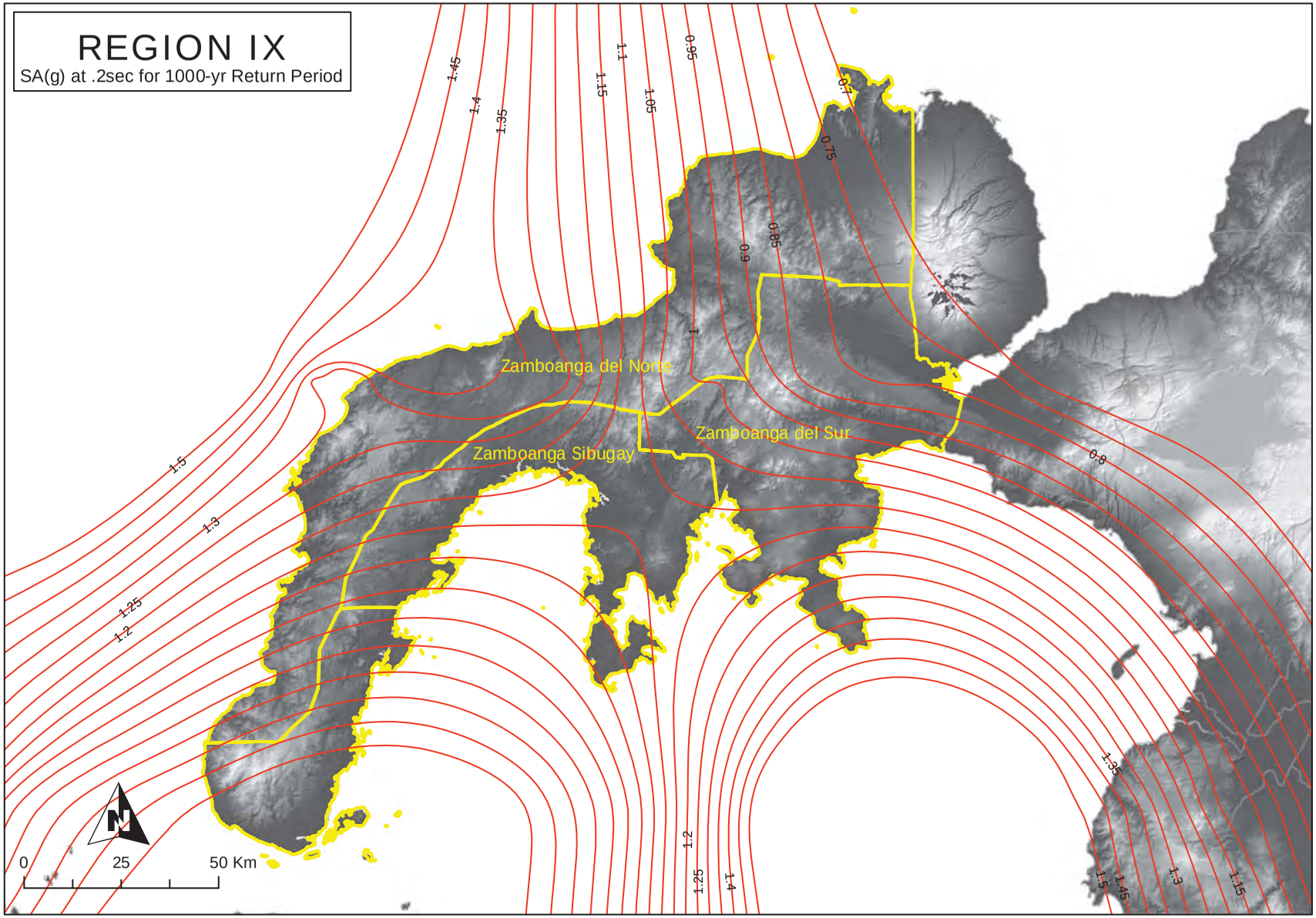

Figure 2A-46 Region IX map of spectral acceleration at 0.2 sec. for 1,000-year return period

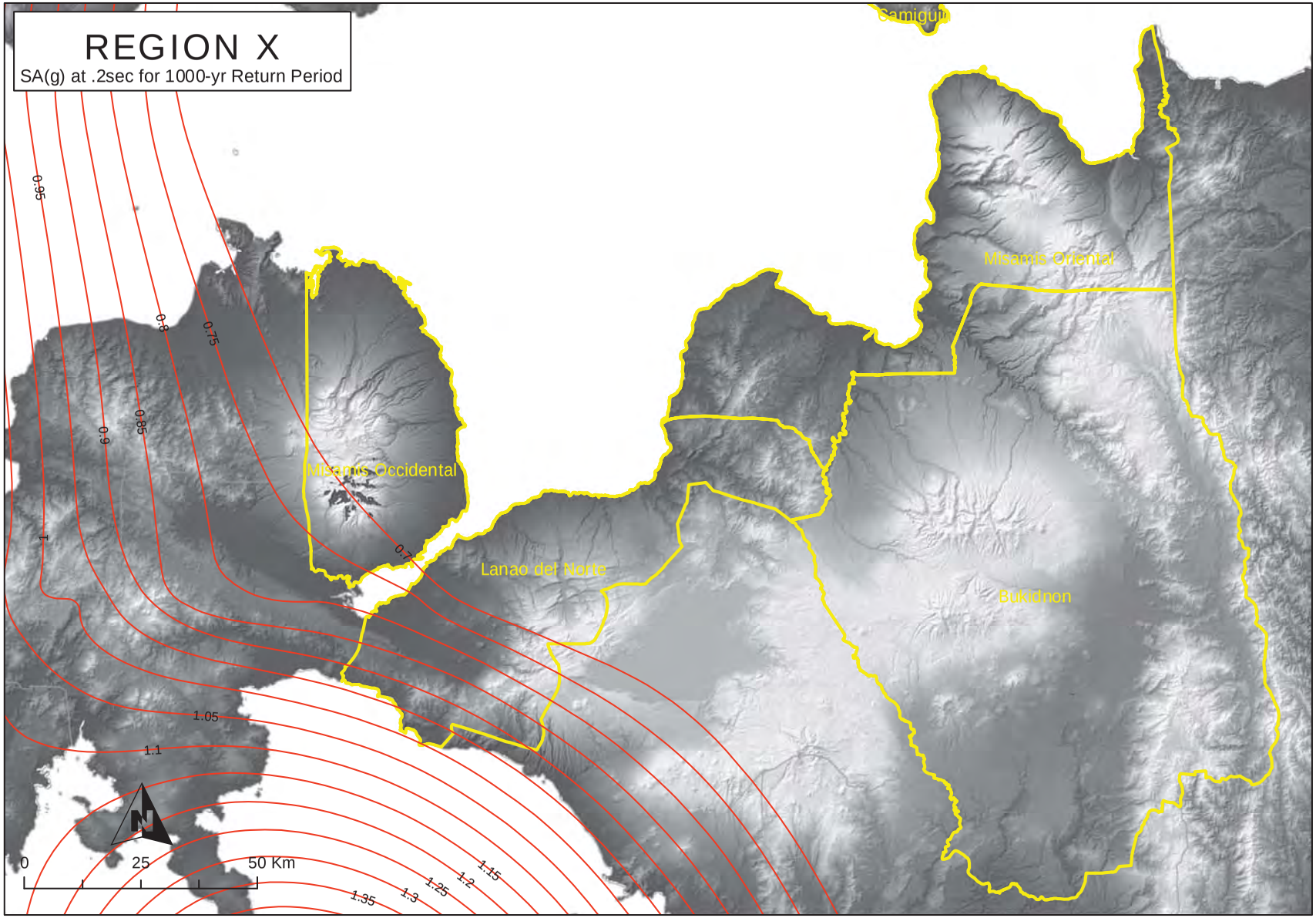

Figure 2A-47 Region X map of spectral acceleration at 0.2 sec. for 1,000-year return period

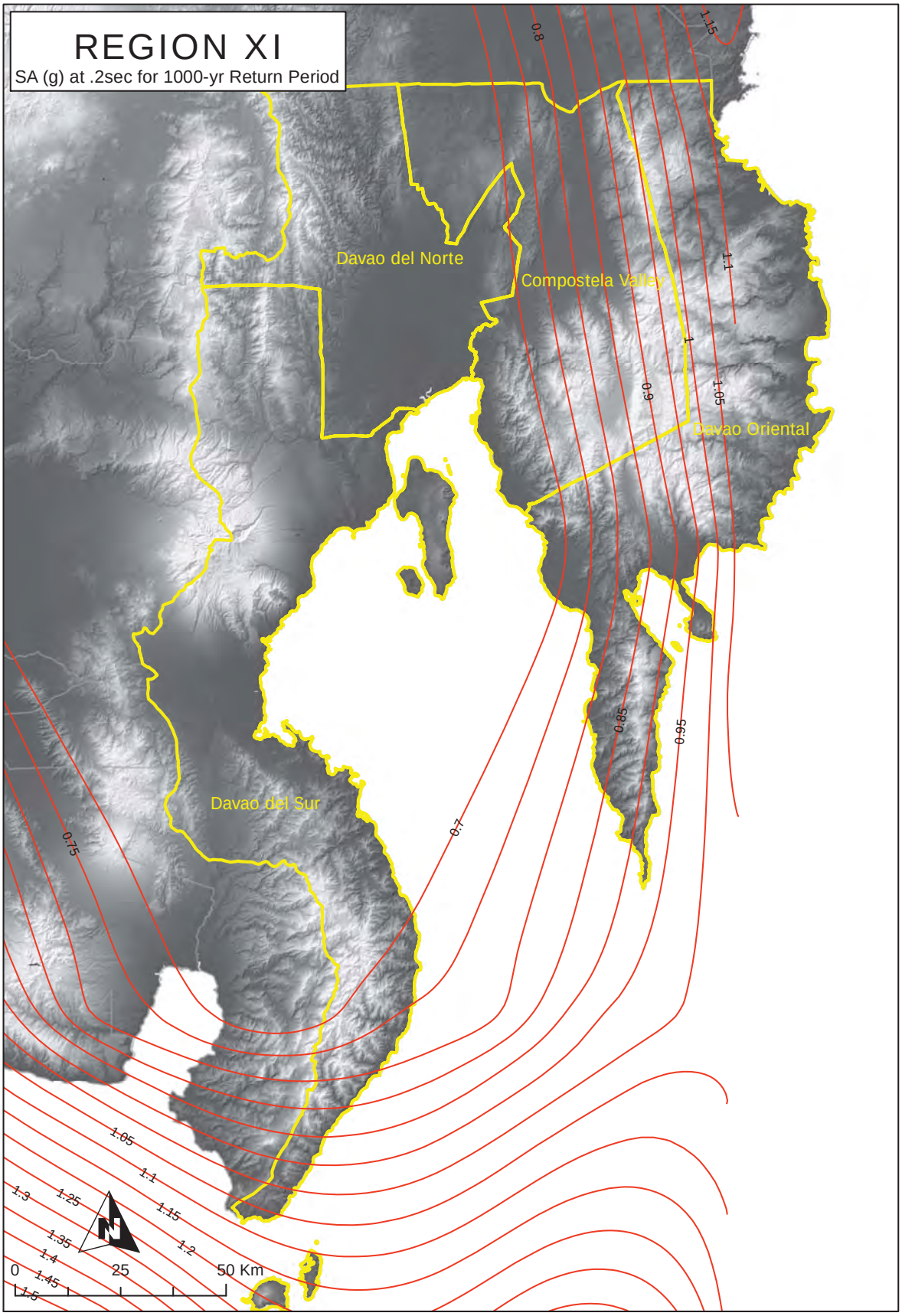

Figure 2A-48 Region XI map of spectral acceleration at 0.2 sec. for 1,000-year return period

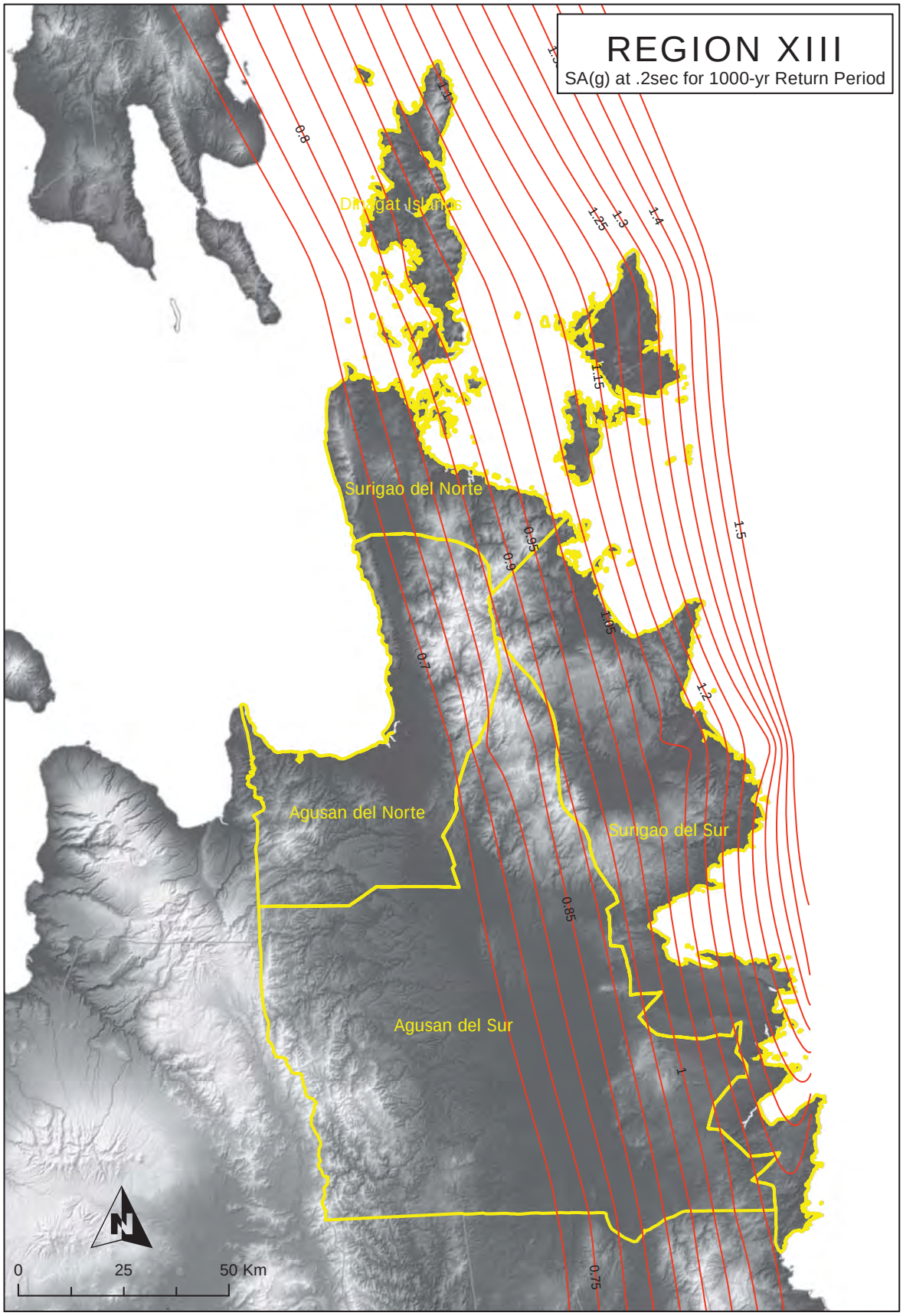

Figure 2A-49 Region XIII map of spectral acceleration at 0.2 sec. for 1,000-year return period

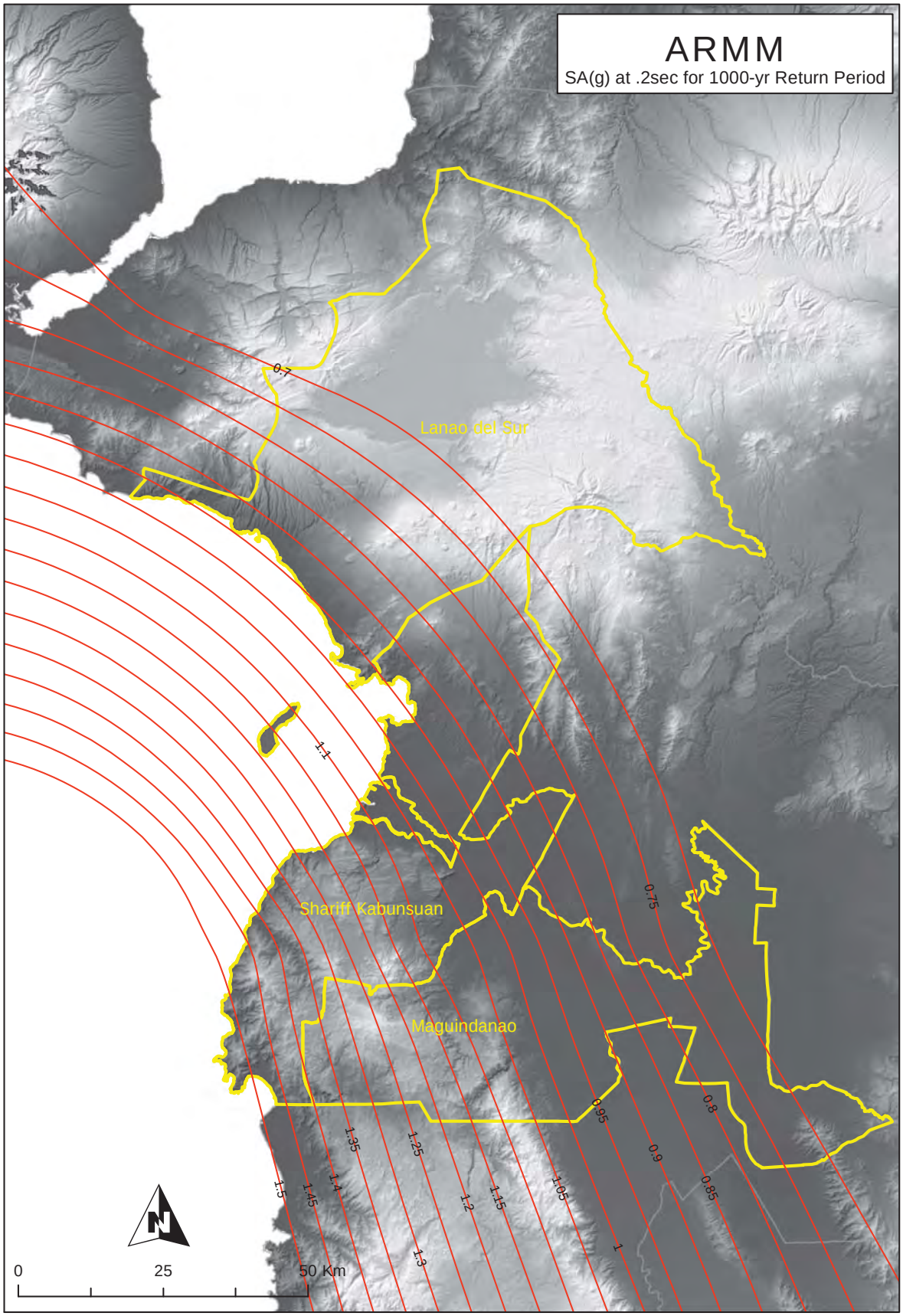

Figure 2A-50 ARMM map of spectral acceleration at 0.2 sec. for 1,000-year return period

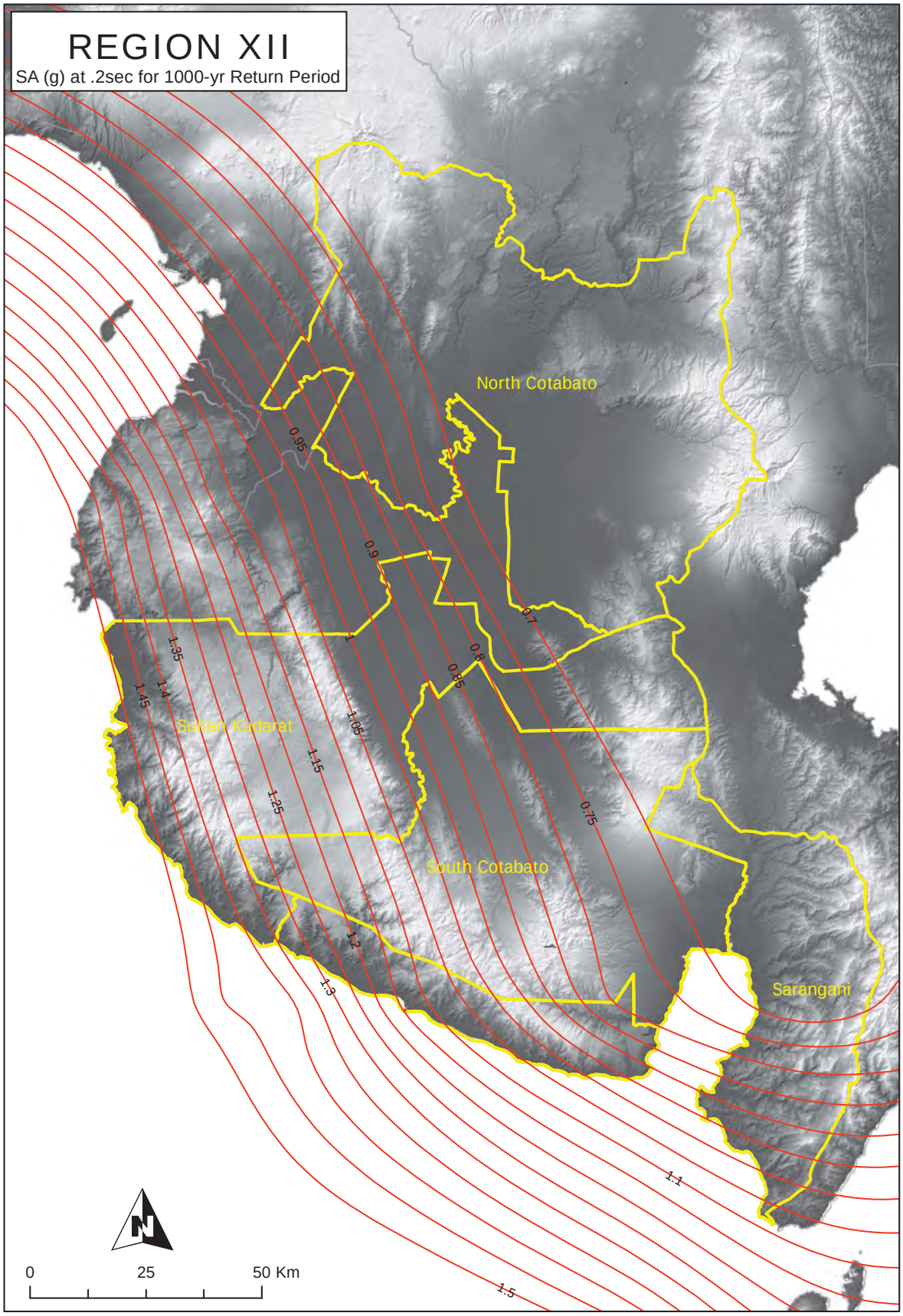

Figure 2A-51 Region XII map of spectral acceleration at 0.2 sec. for 1,000-year return period

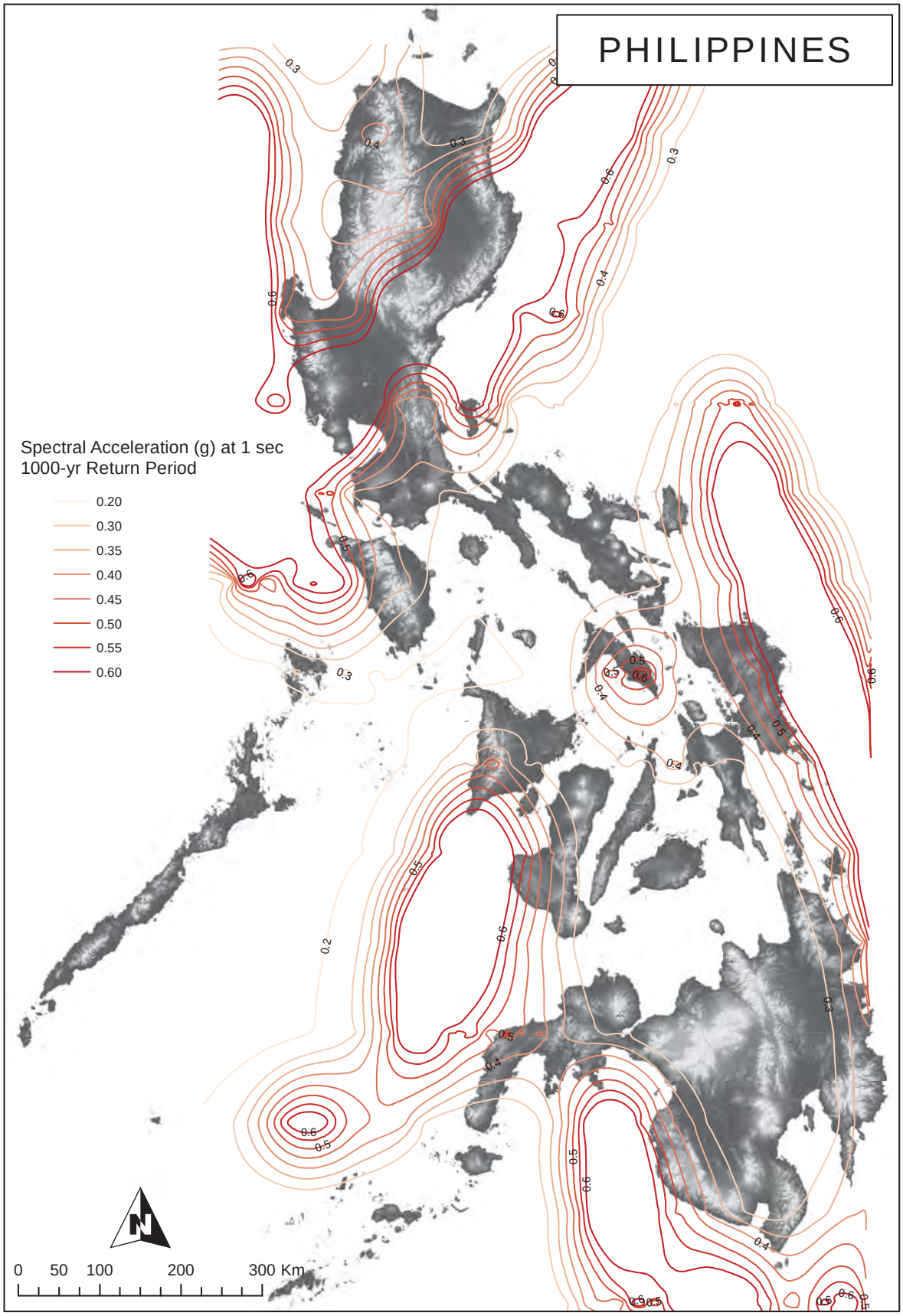

Figure 2A-52 Contour map of spectral acceleration at 1. sec. for 1,000-year return period

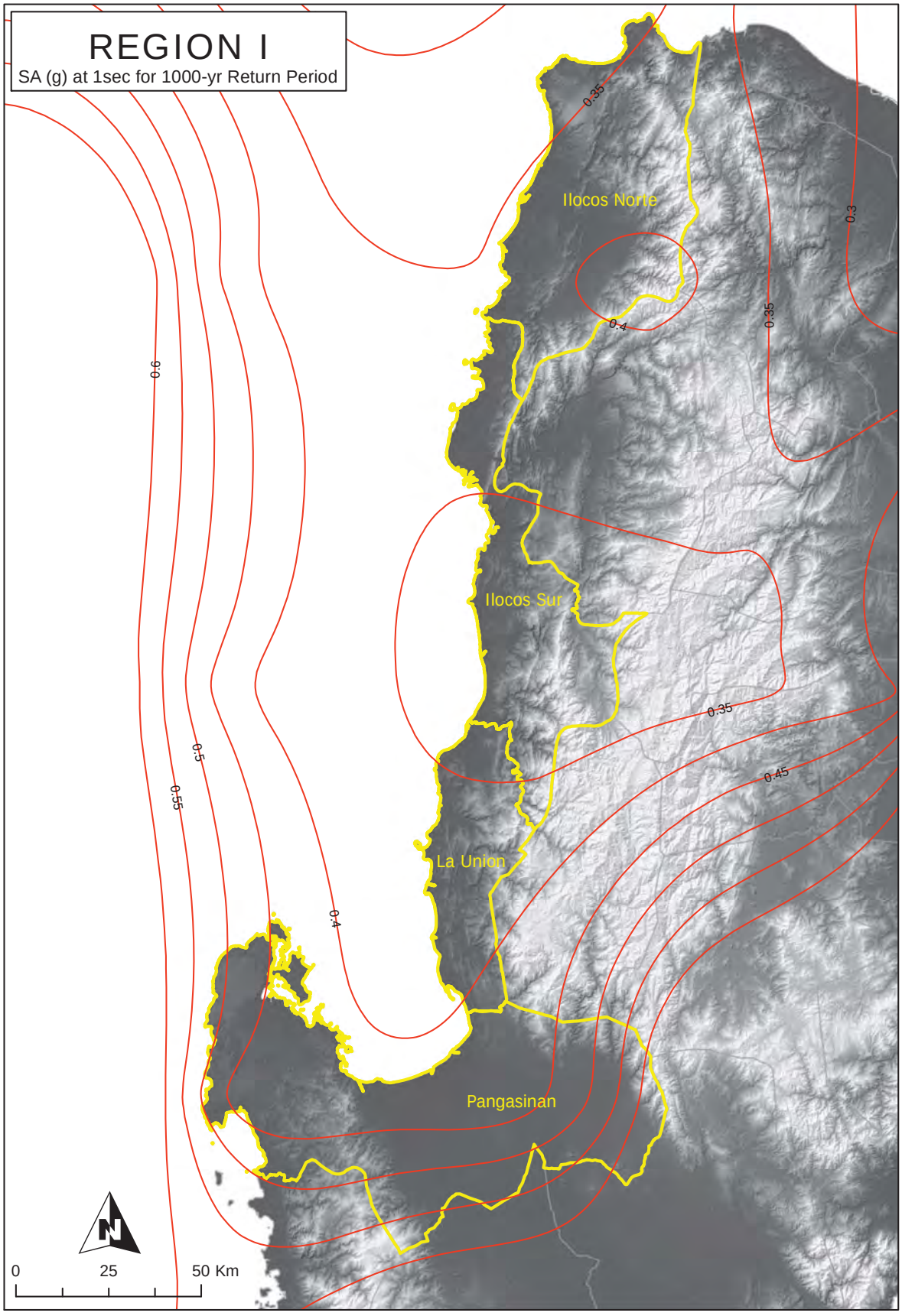

Figure 2A-53 Region I map of spectral acceleration at 1. sec. for 1,000-year return period

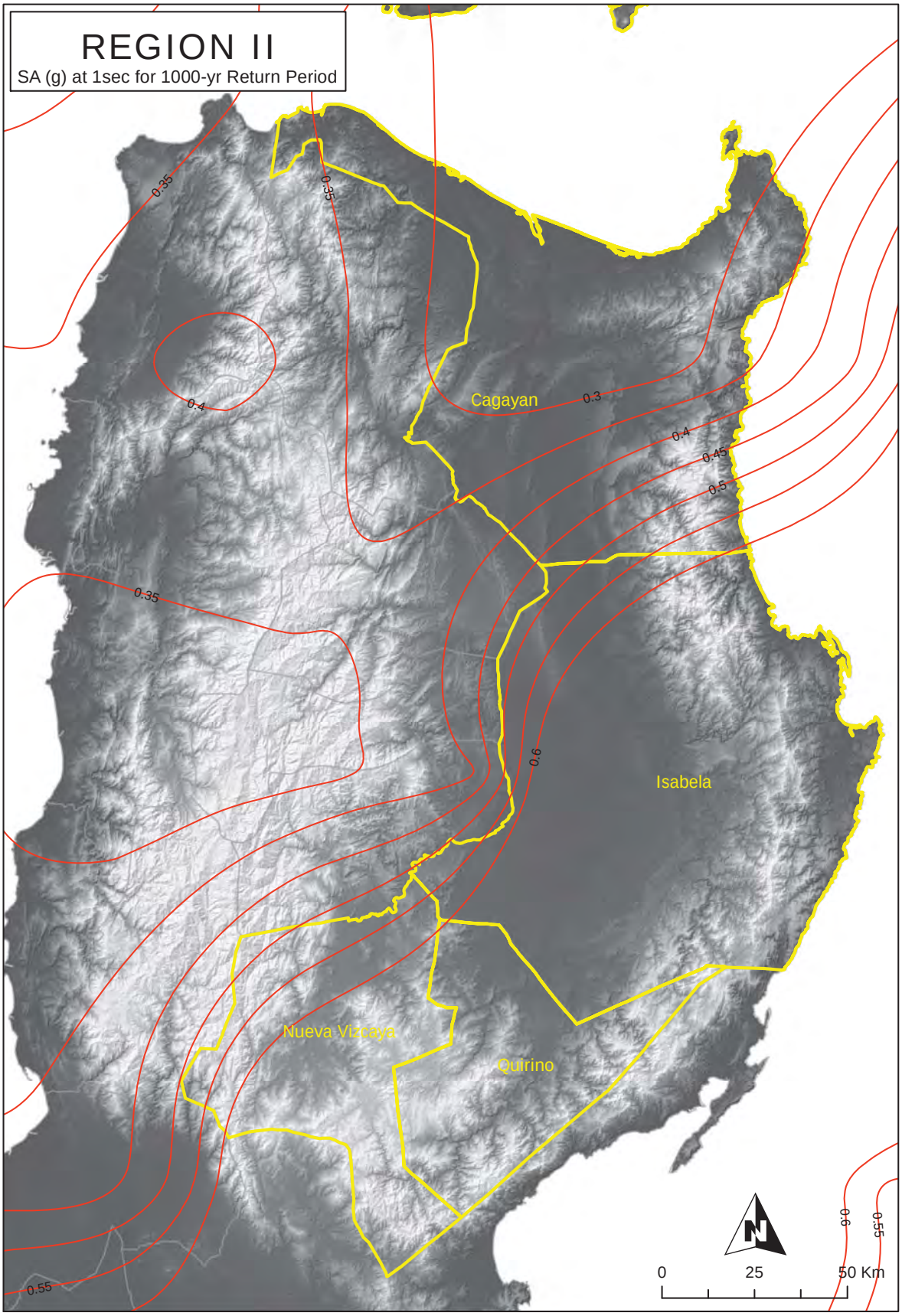

Figure 2A-54 Region II map of spectral acceleration at 1. sec. for 1,000-year return period

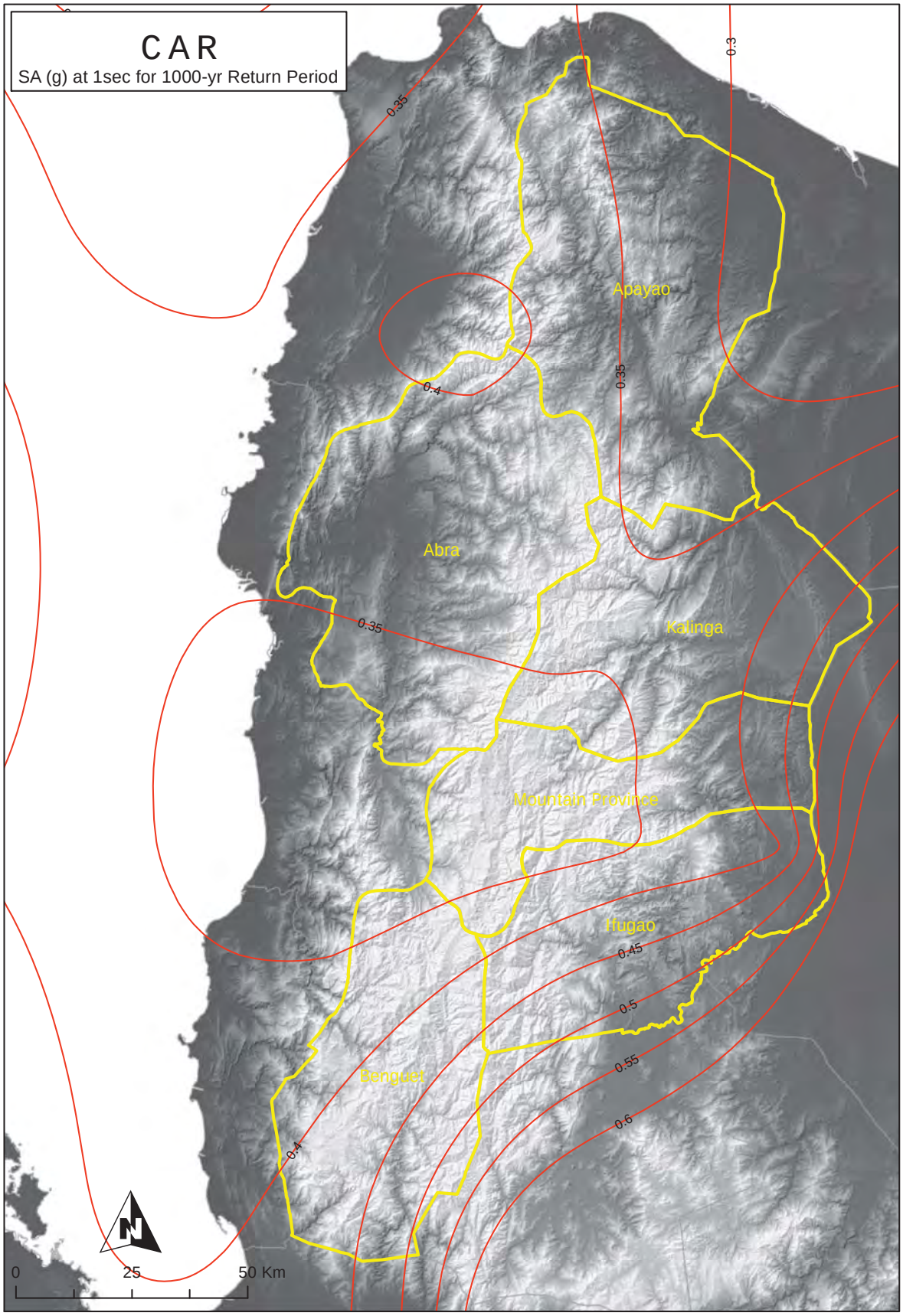

Figure 2A-55 CAR map of spectral acceleration at 1. sec. for 1,000-year return period

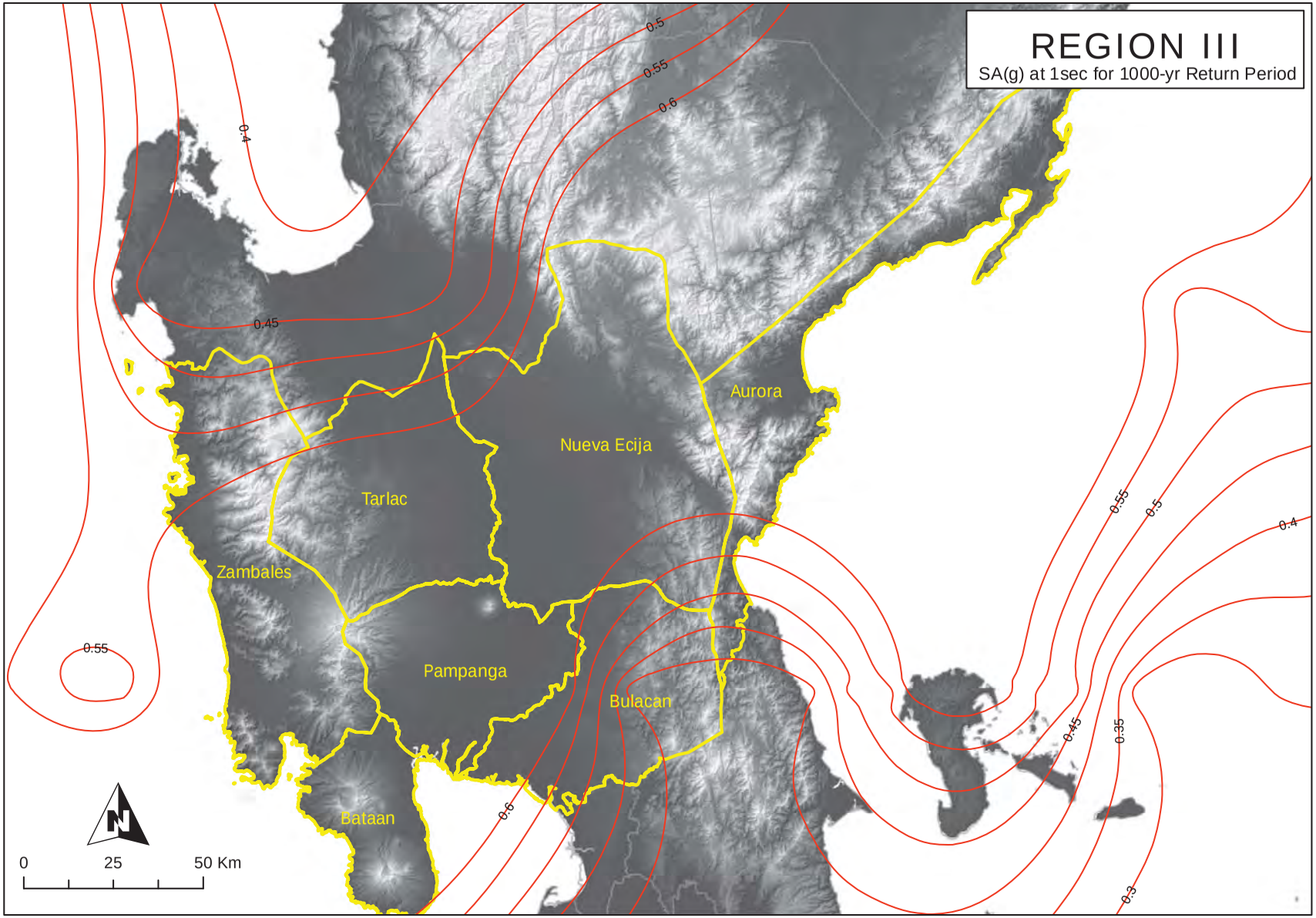

Figure 2A-56 Region III map of spectral acceleration at 1. sec. for 1,000-year return period

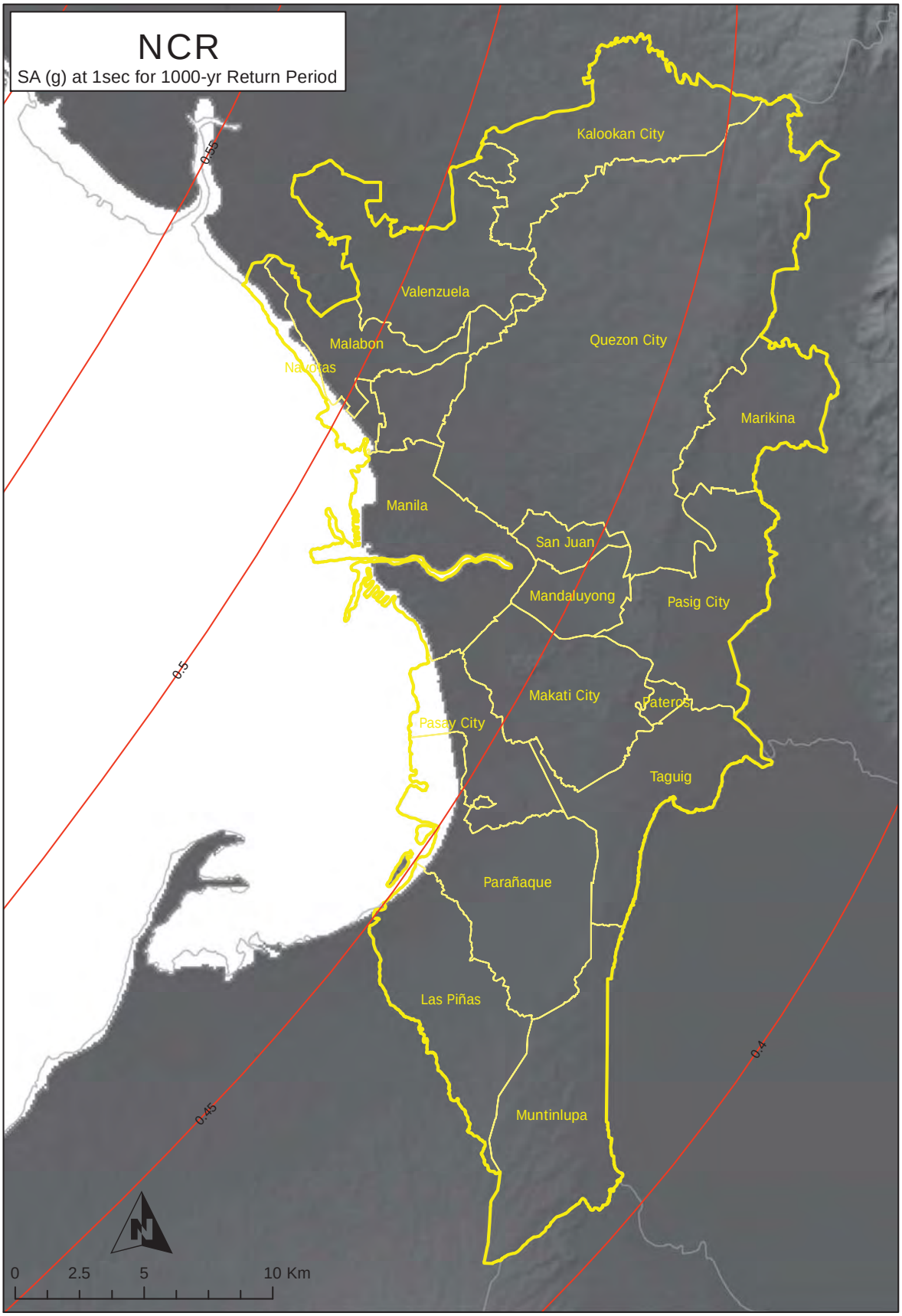

Figure 2A-57 NCR map of spectral acceleration at 1. sec. for 1,000-year return period

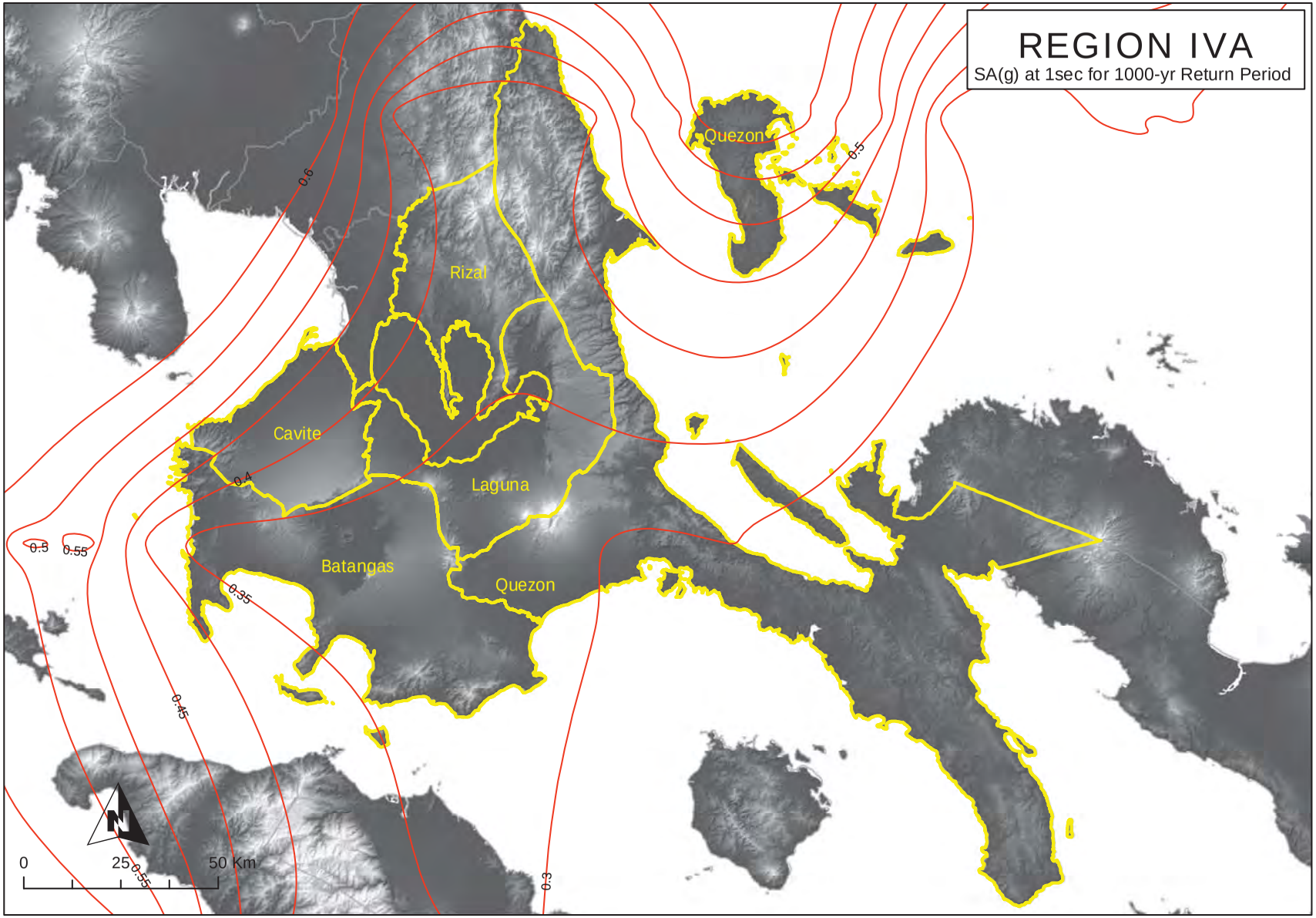

Figure 2A-58 Region IV-A map of spectral acceleration at 1. sec. for 1,000-year return period

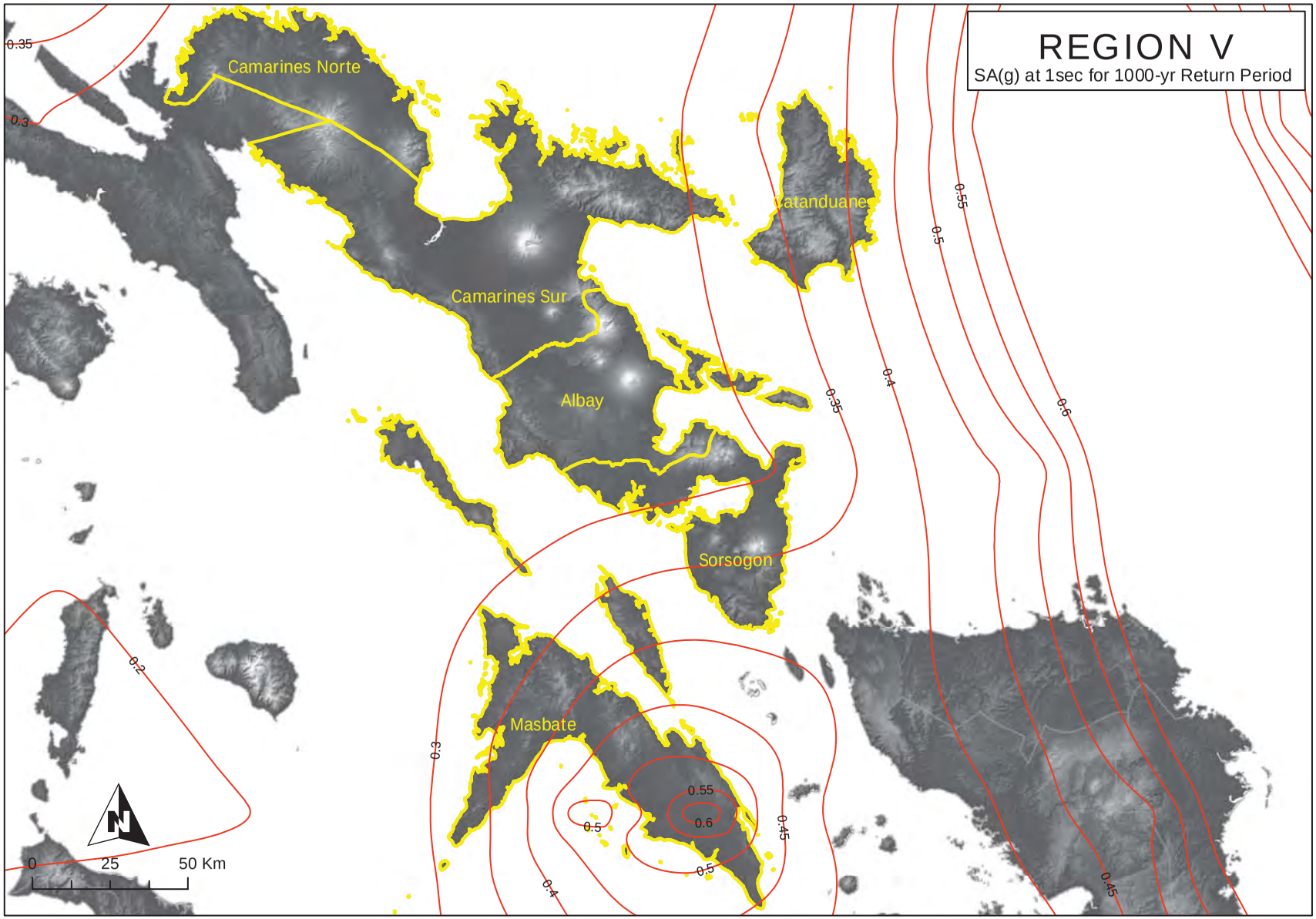

Figure 2A-59 Region V map of spectral acceleration at 1. sec. for 1,000-year return period

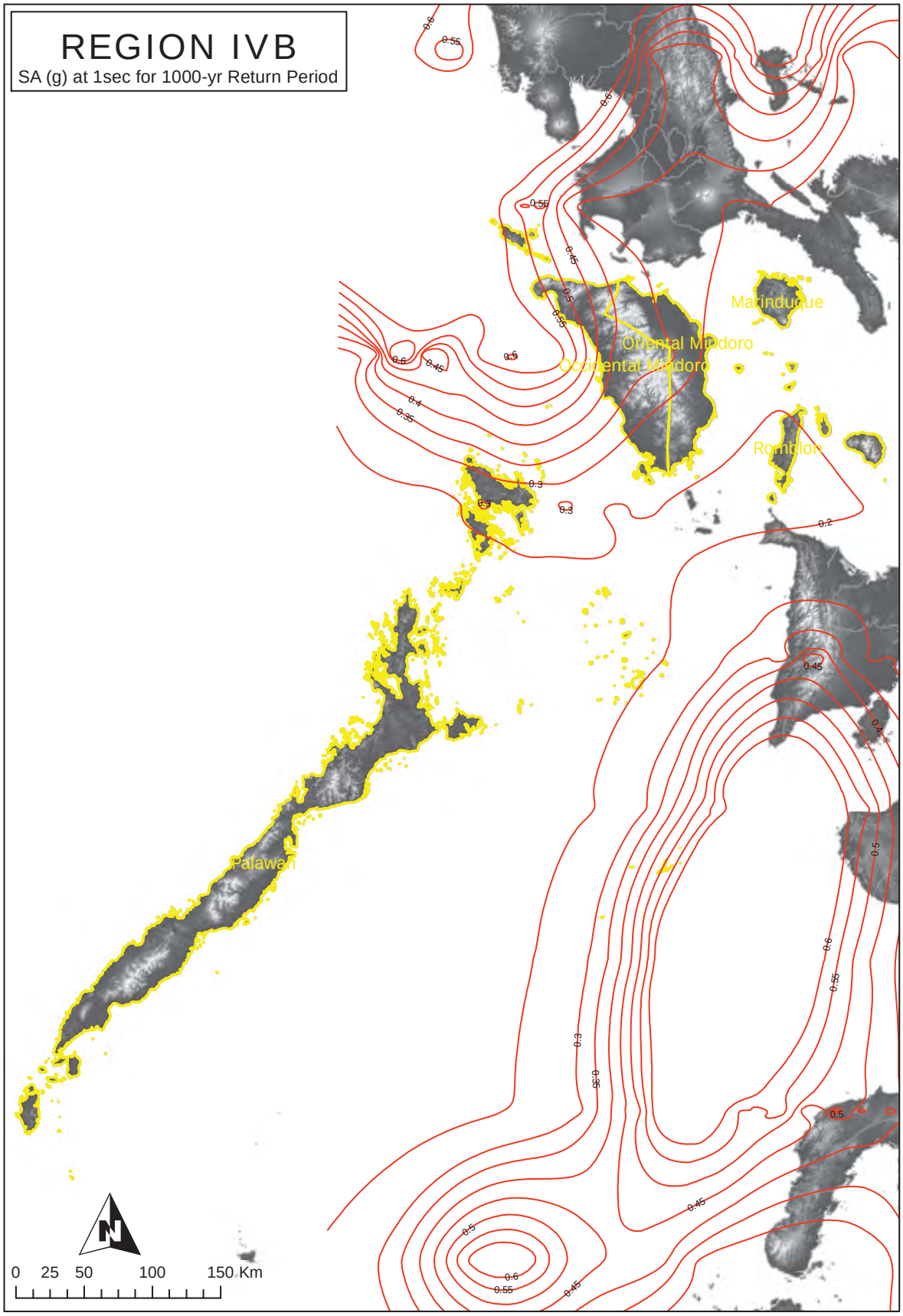

Figure 2A-60 Region IV-B map of spectral acceleration at 1. sec. for 1,000-year return period

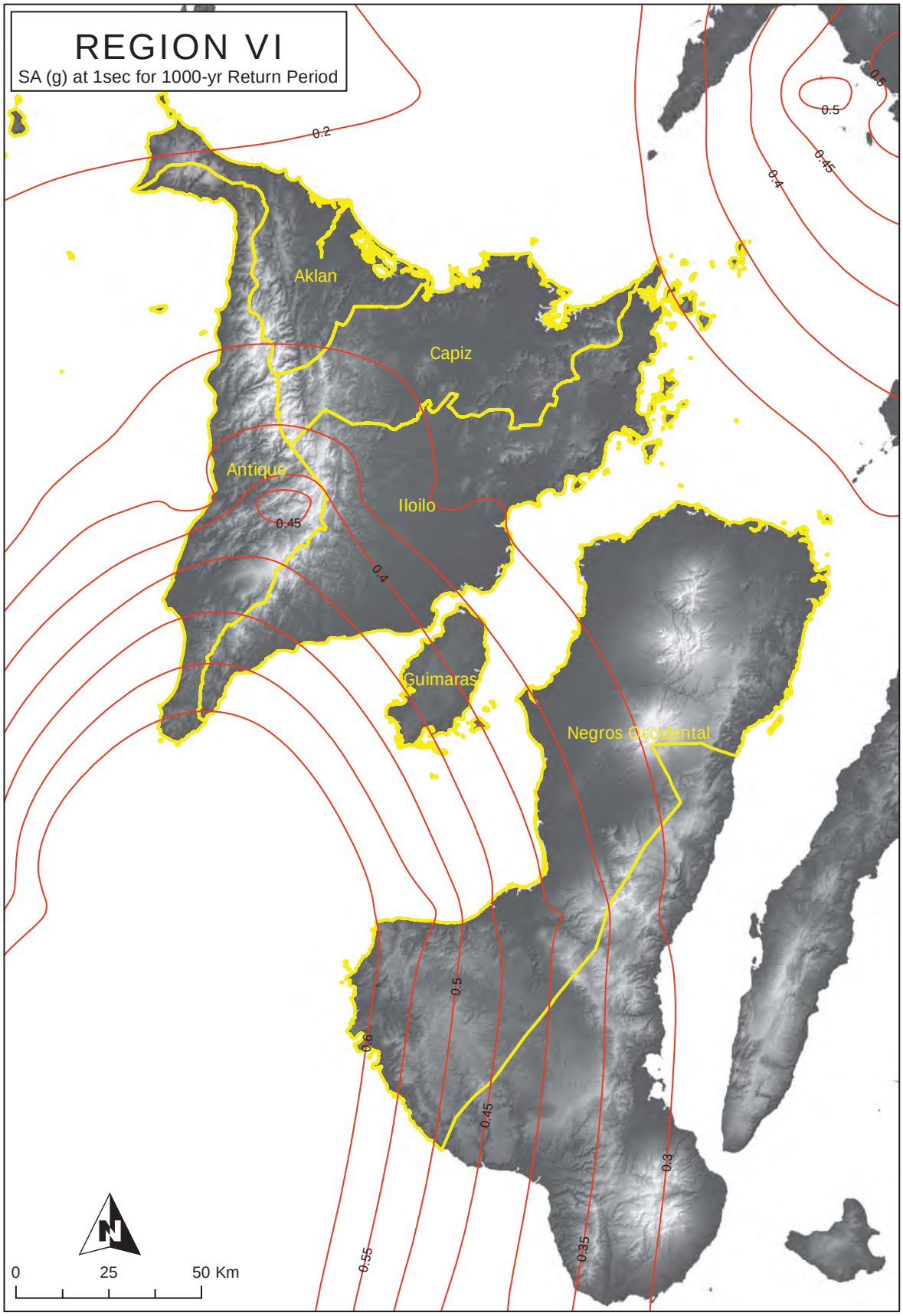

Figure 2A-61 Region VI map of spectral acceleration at 1. sec. for 1,000-year return period

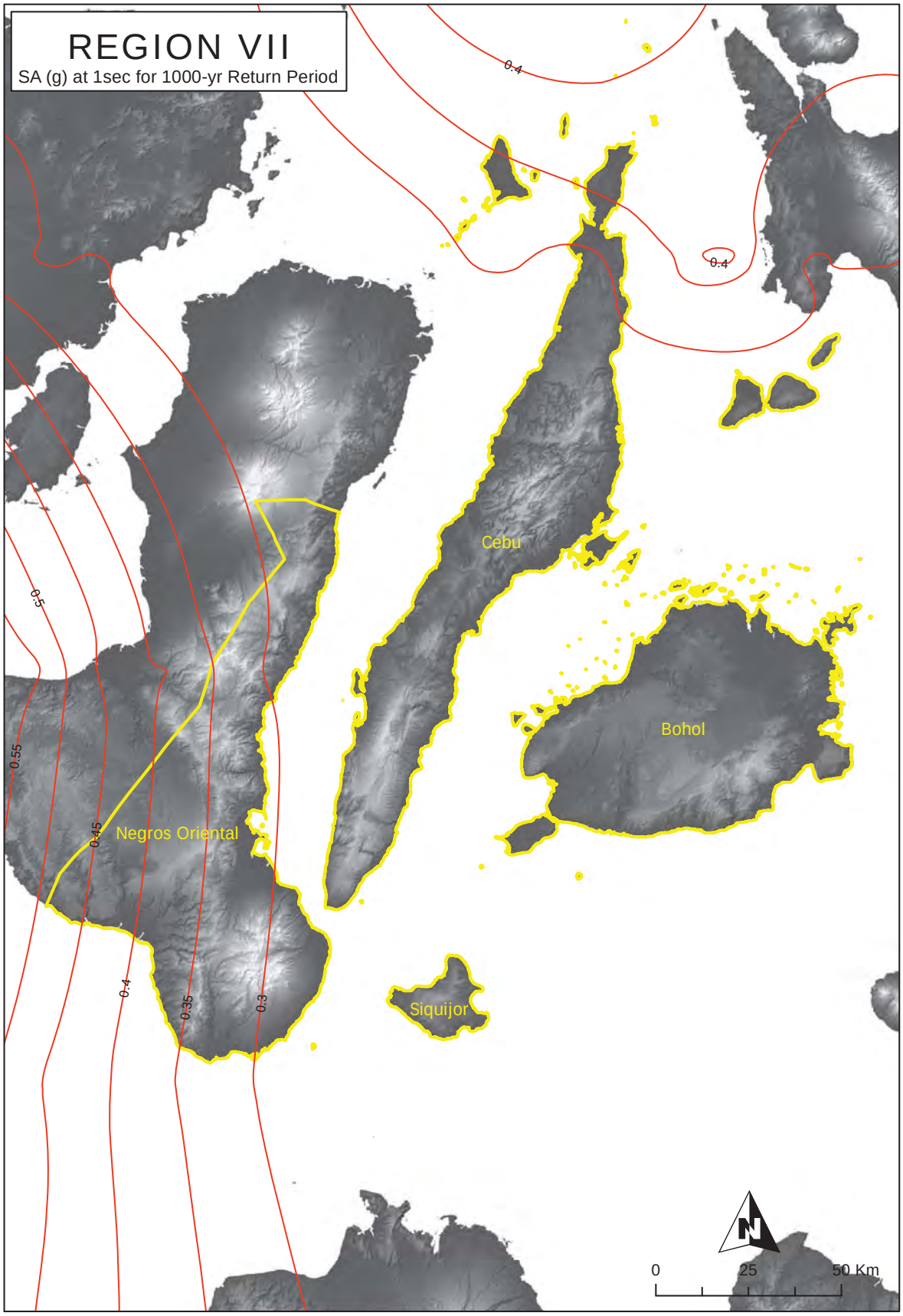

Figure 2A-62 Region VII map of spectral acceleration at 1. sec. for 1,000-year return period

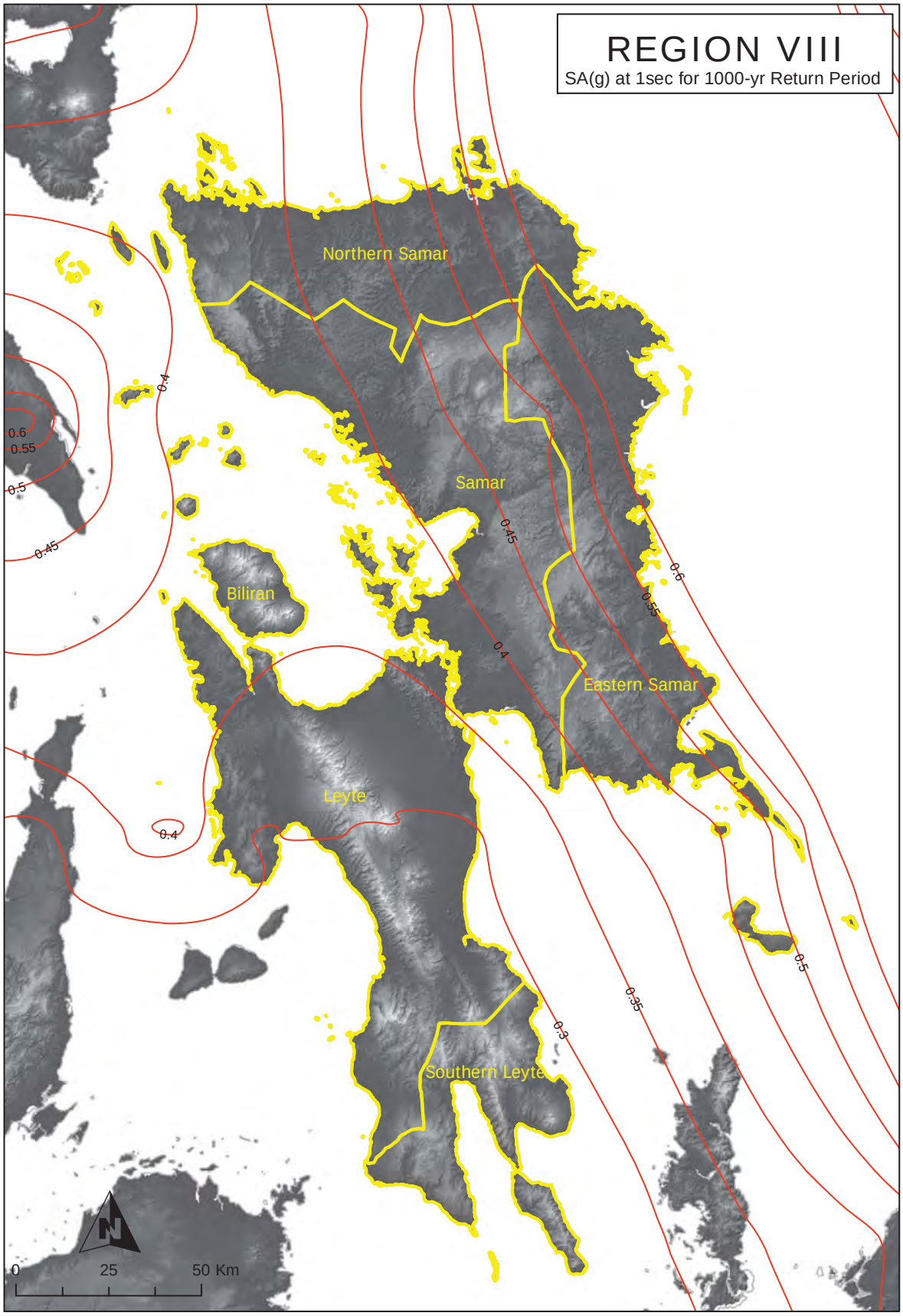

Figure 2A-63 Region VIII map of spectral acceleration at 1. sec. for 1,000-year return period

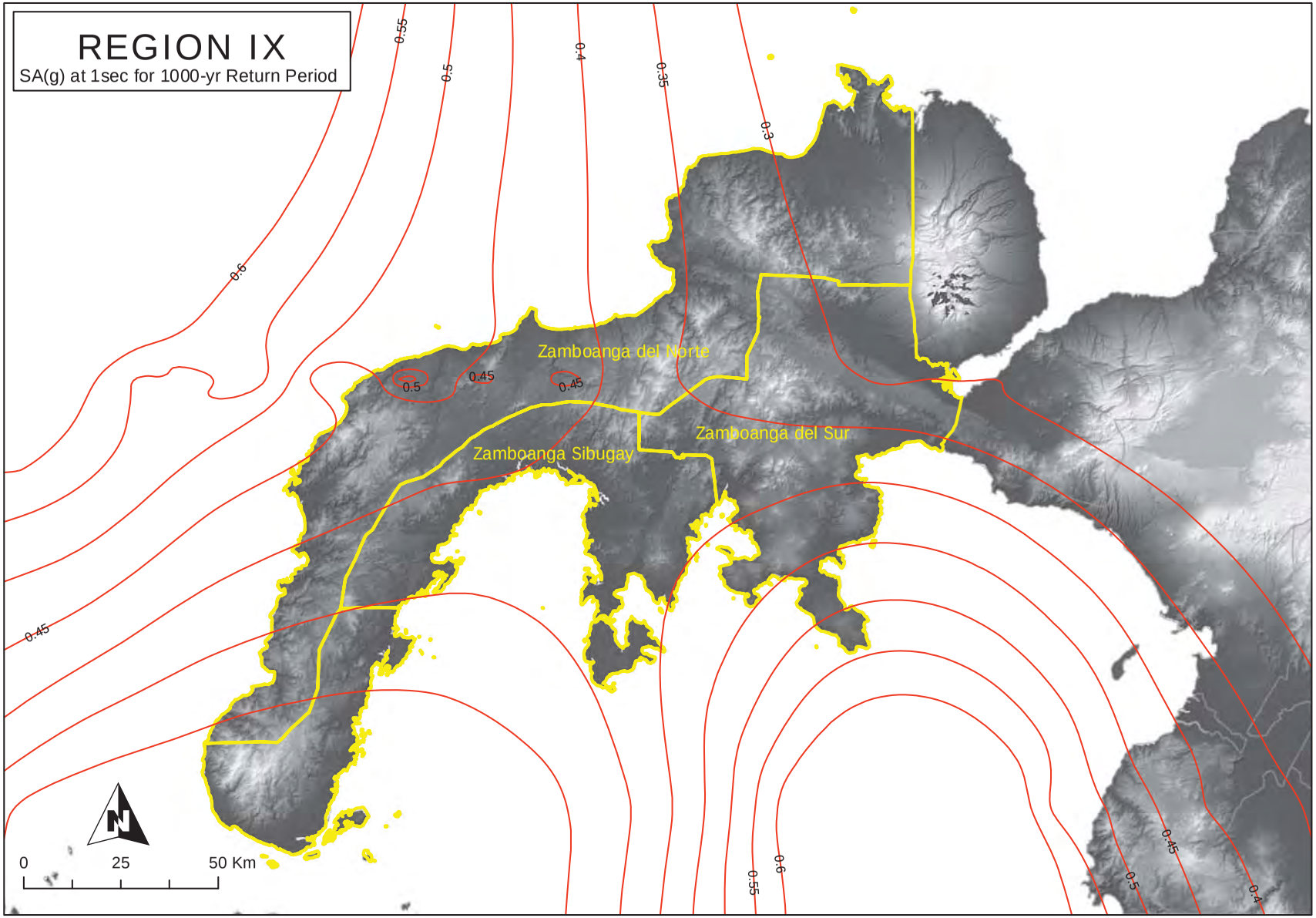

Figure 2A-64 Region IX map of spectral acceleration at 1. sec. for 1,000-year return period

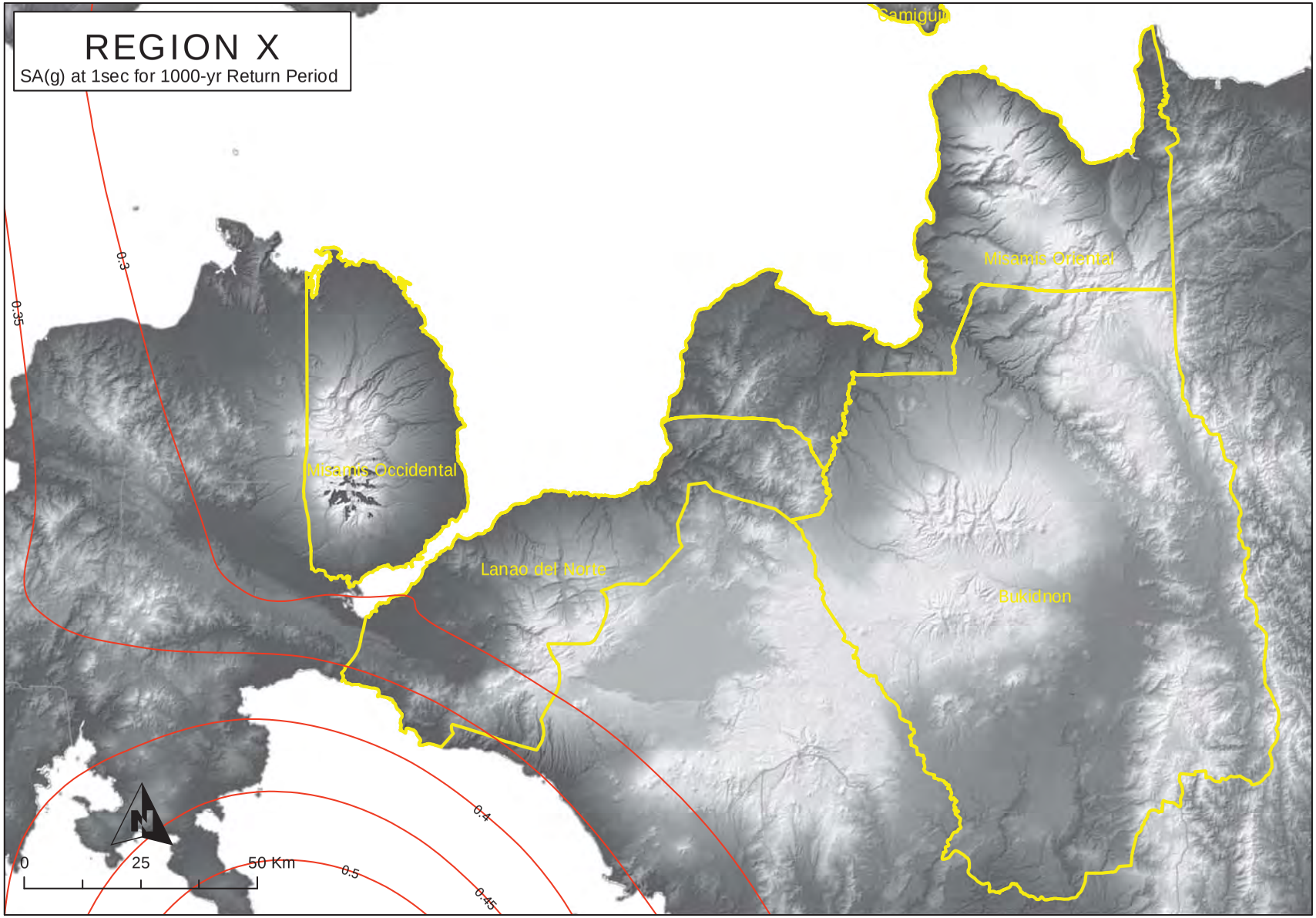

Figure 2A-65 Region X map of spectral acceleration at 1. sec. for 1,000-year return period

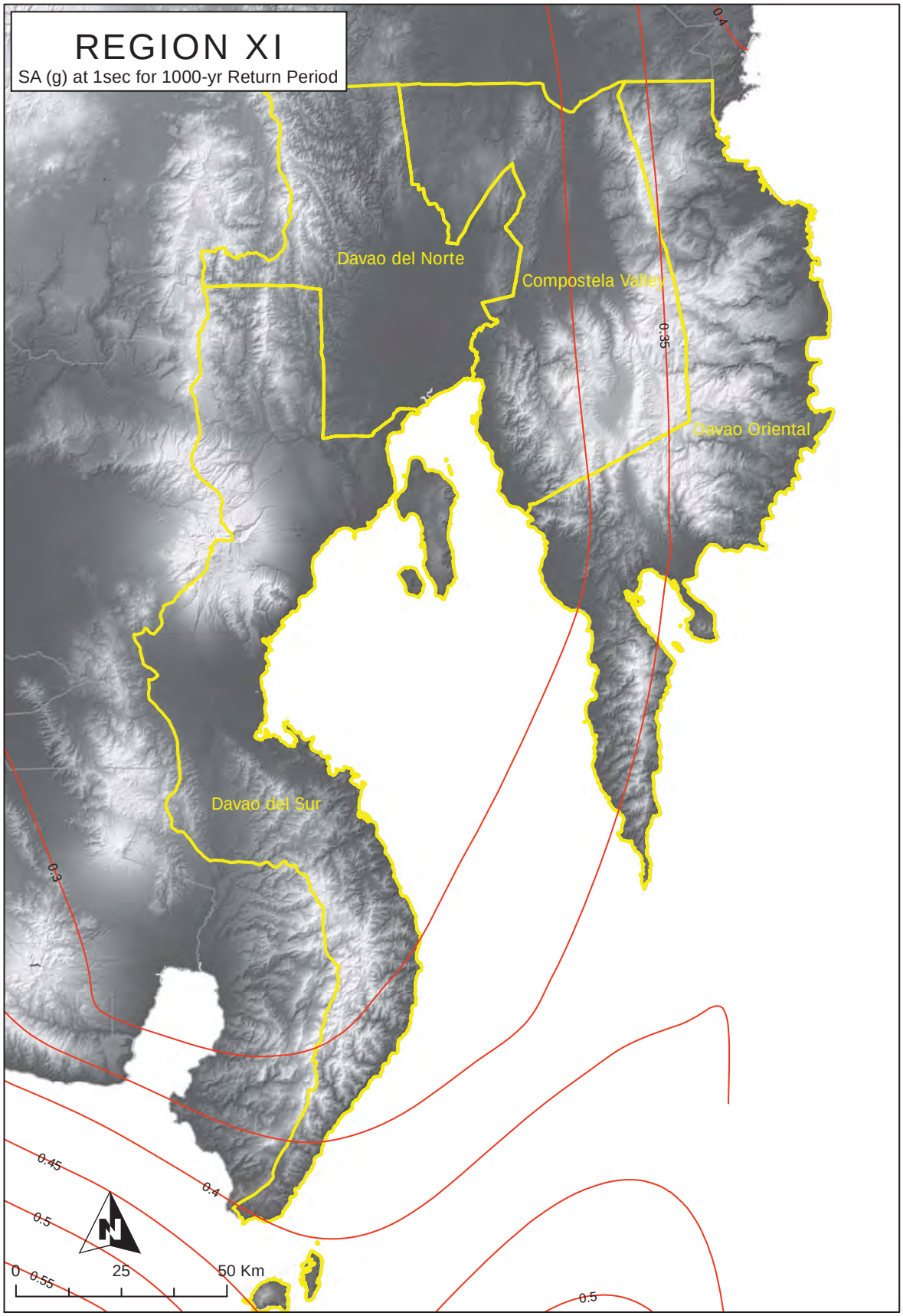

Figure 2A-66 Region XI map of spectral acceleration at 1. sec. for 1,000-year return period

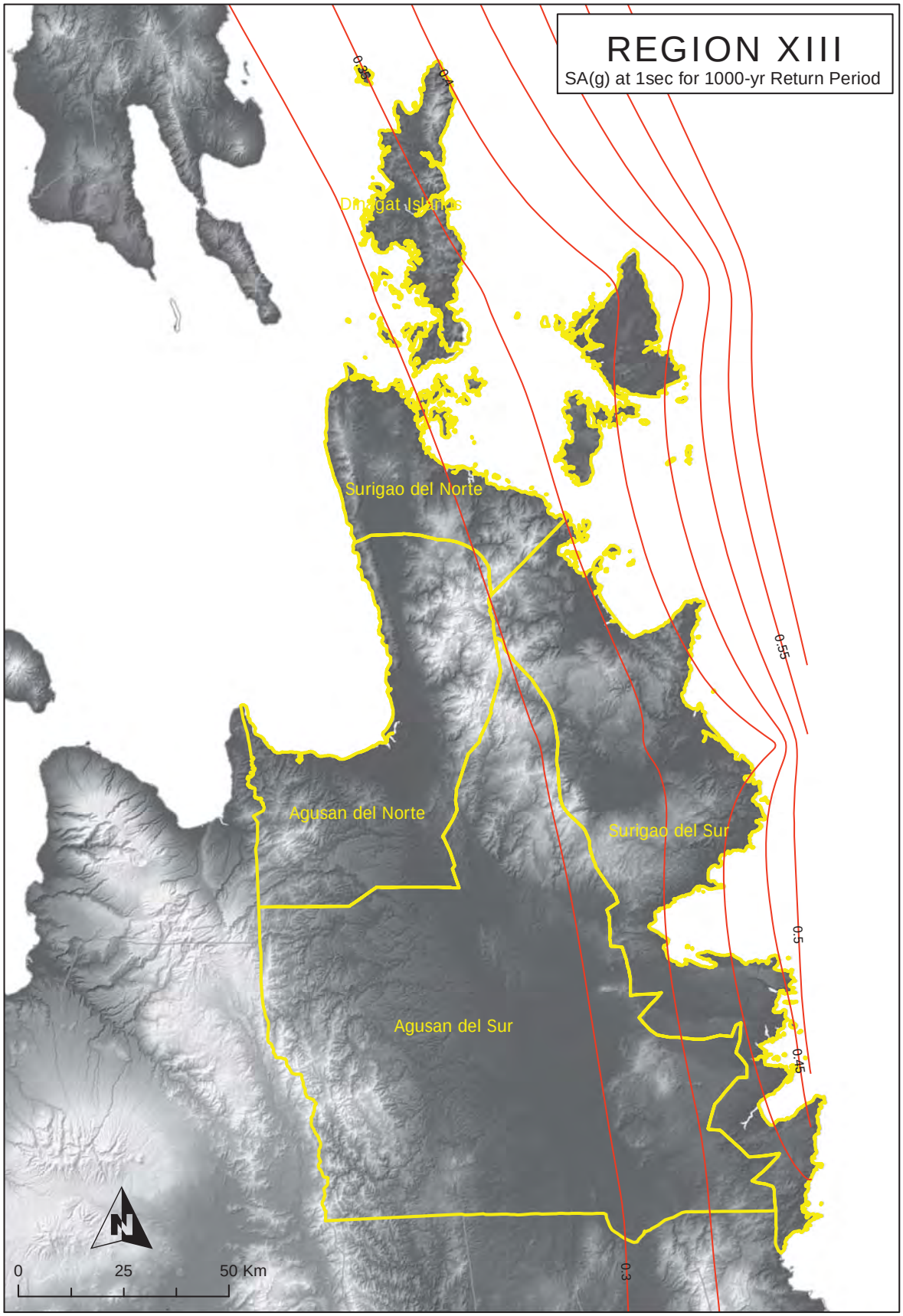

Figure 2A-67 Region XIII map of spectral acceleration at 1. sec. for 1,000-year return period

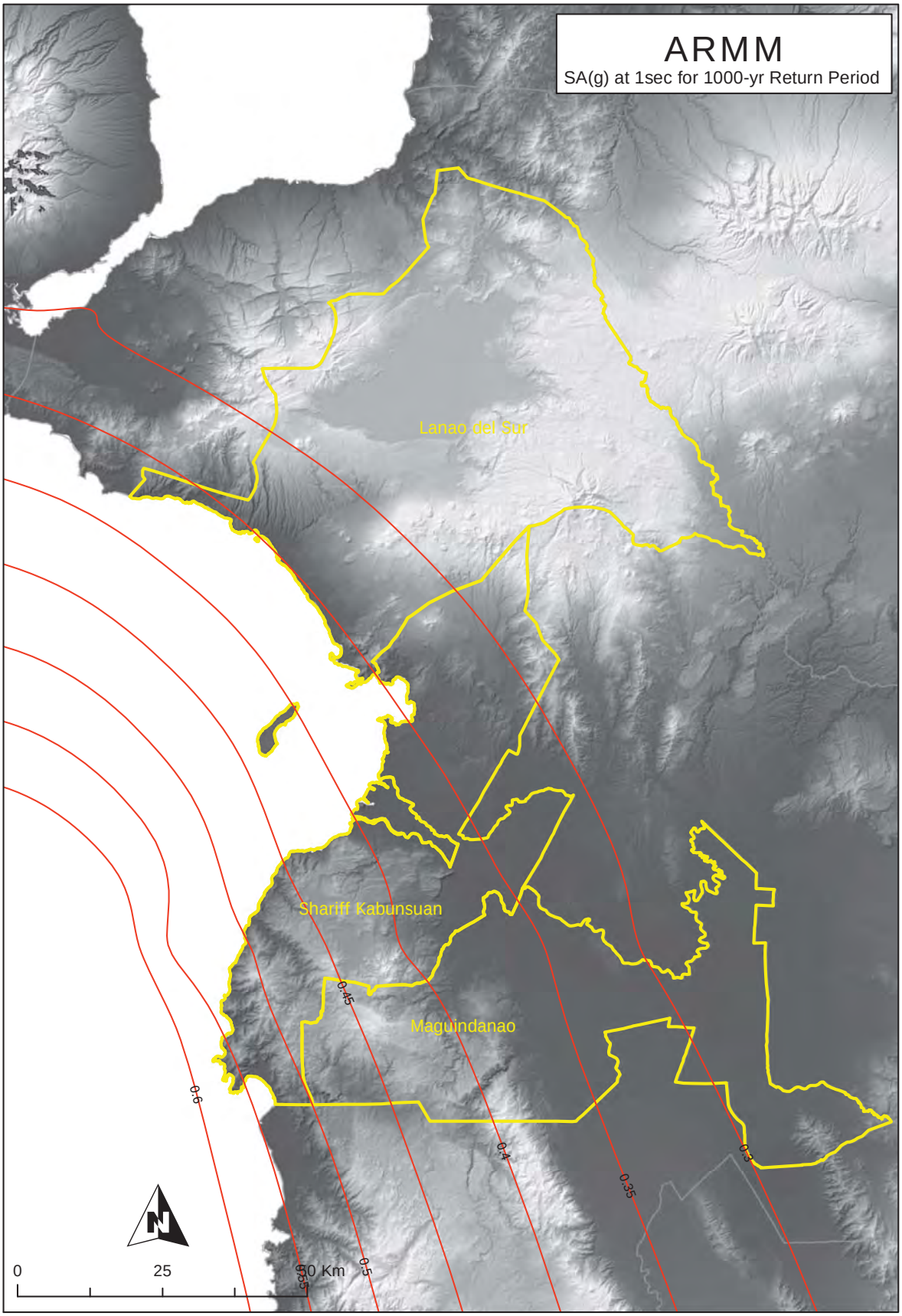

Figure 2A-68 ARMM map of spectral acceleration at 1. sec. for 1,000-year return period

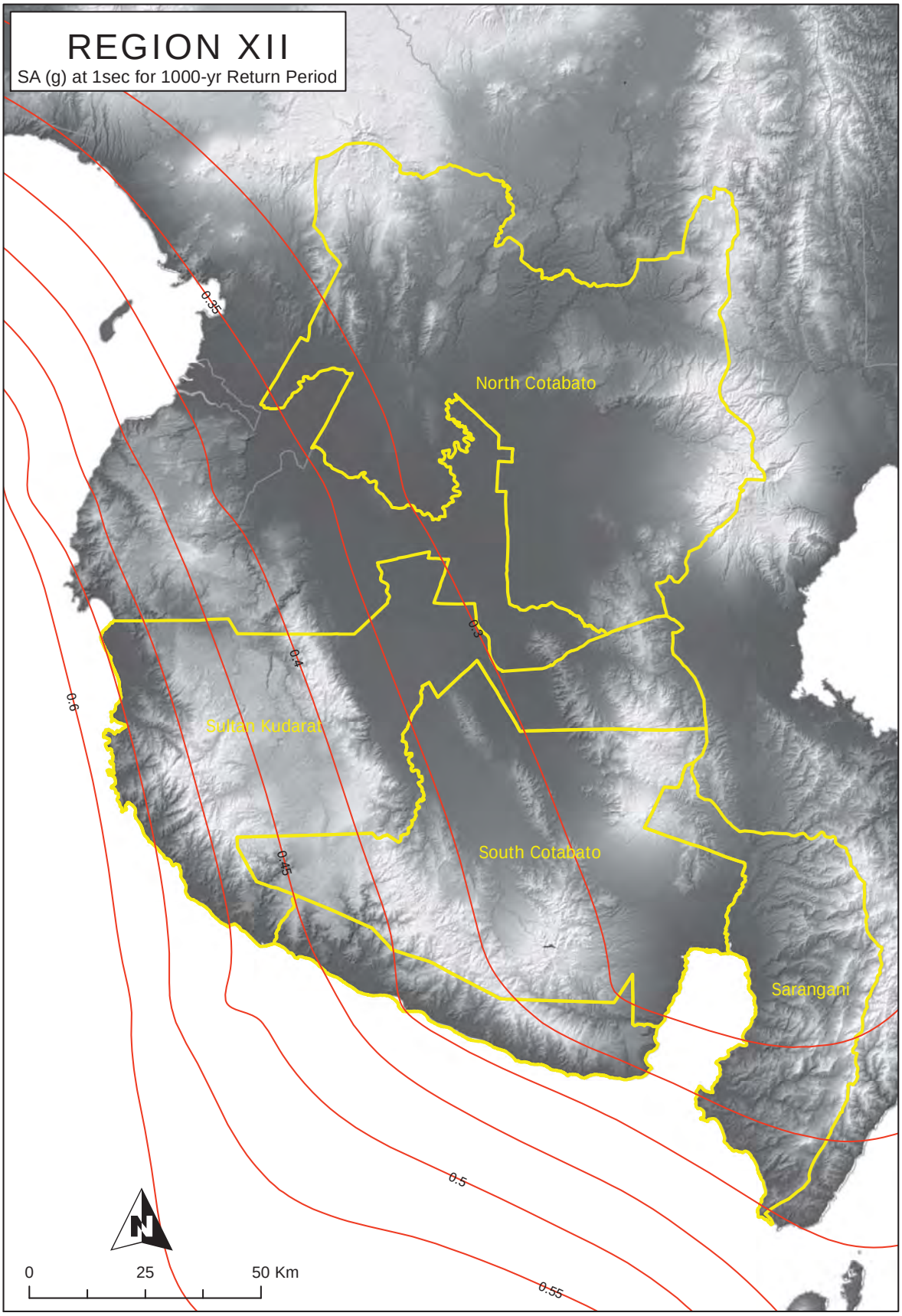

Figure 2A-69 Region XII map of spectral acceleration at 1. sec. for 1,000-year return period

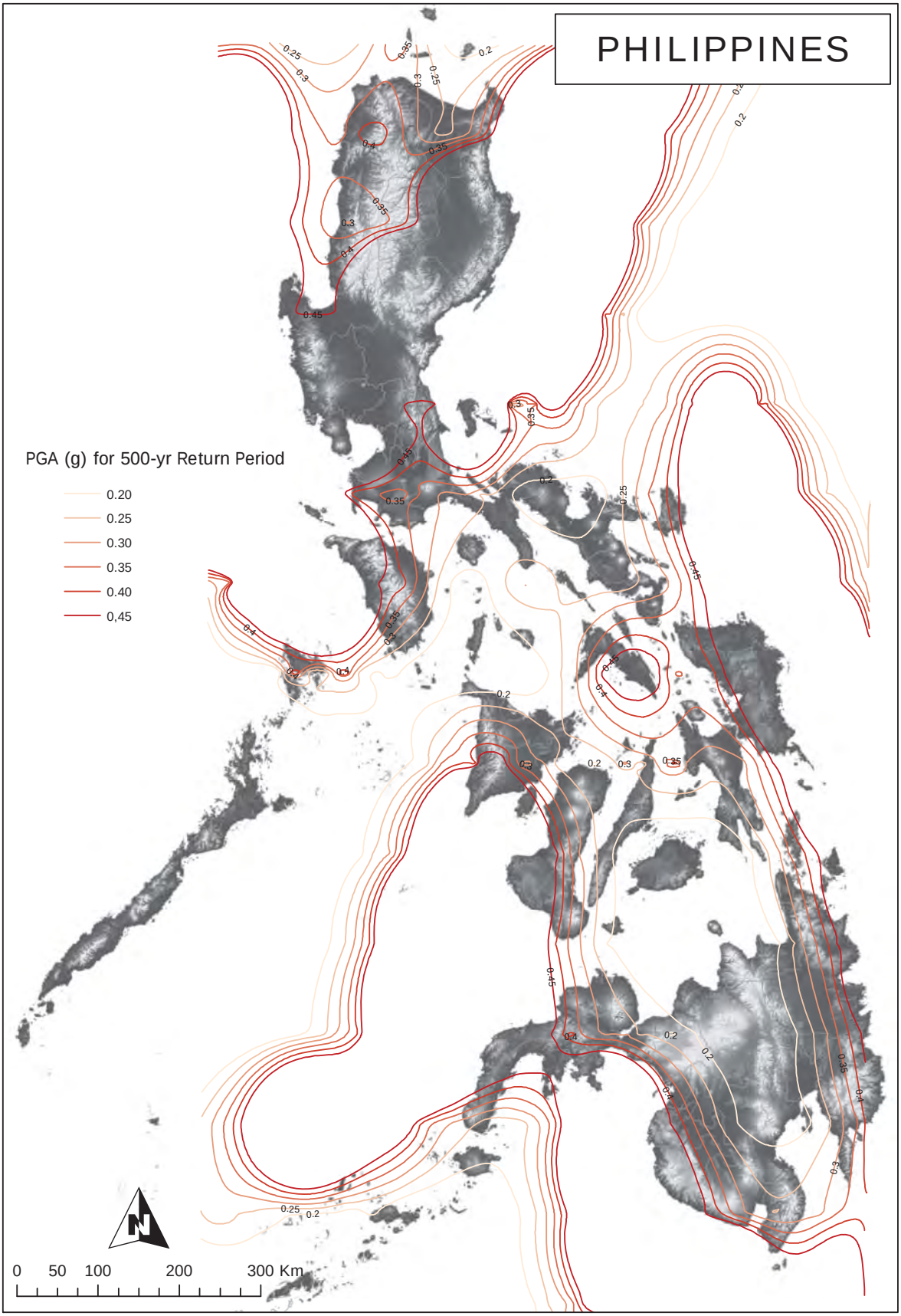

Figure 2A-70 Contour map of peak ground acceleration for 500-year return period

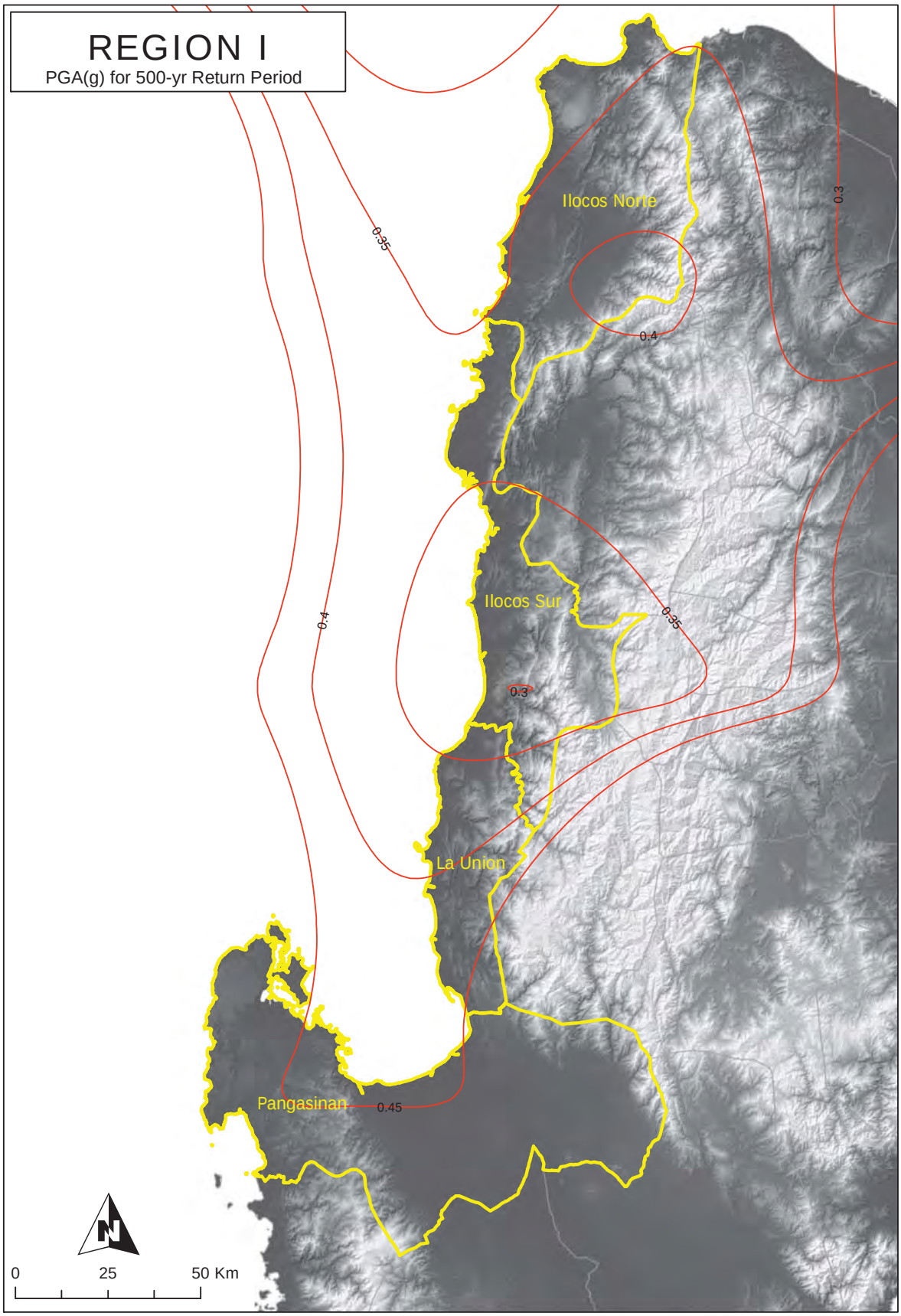

Figure 2A-71 Region I map of peak ground acceleration for 500-year return period

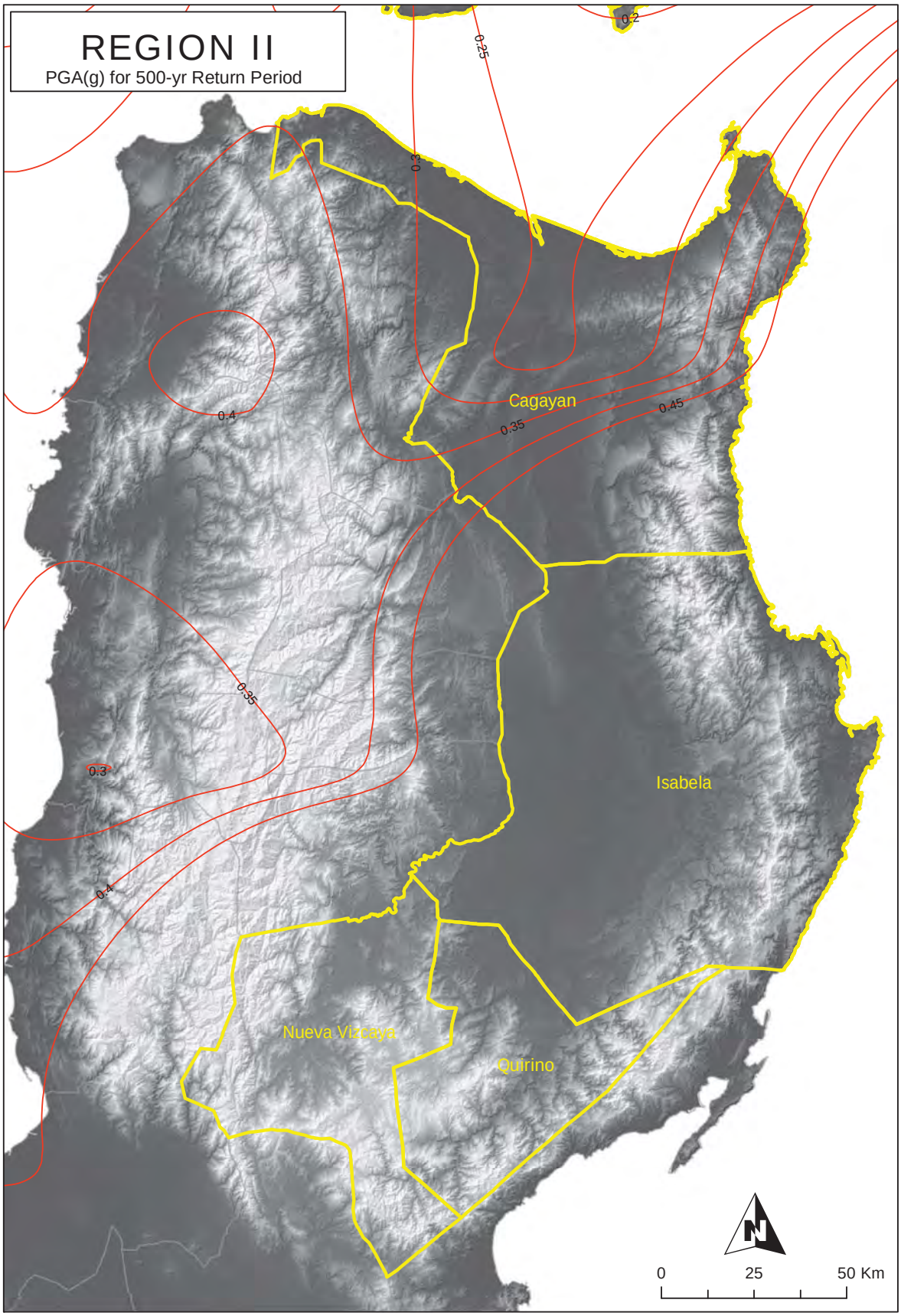

Figure 2A-72 Region II map of peak ground acceleration for 500-year return period

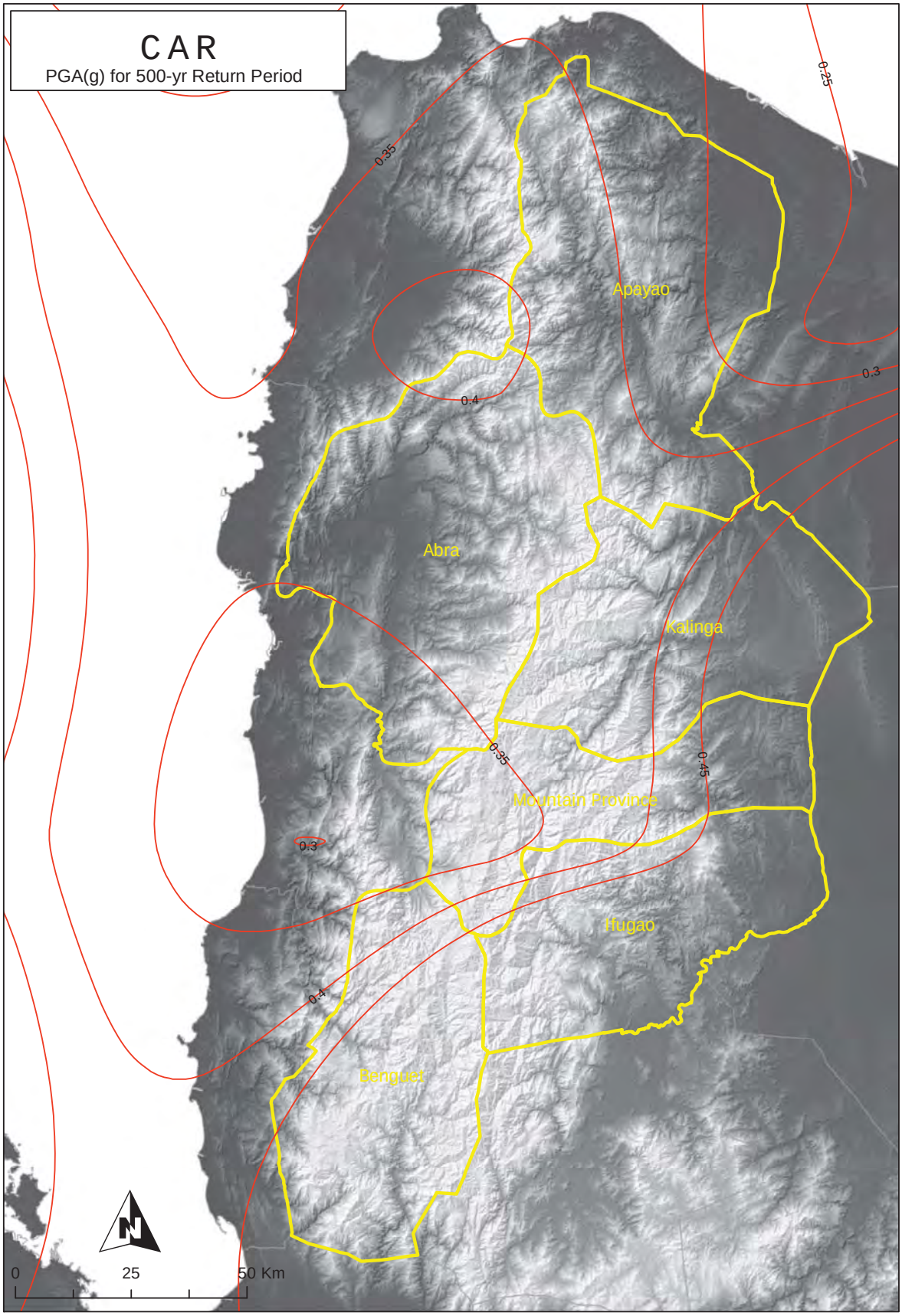

Figure 2A-73 CAR map of peak ground acceleration for 500-year return period

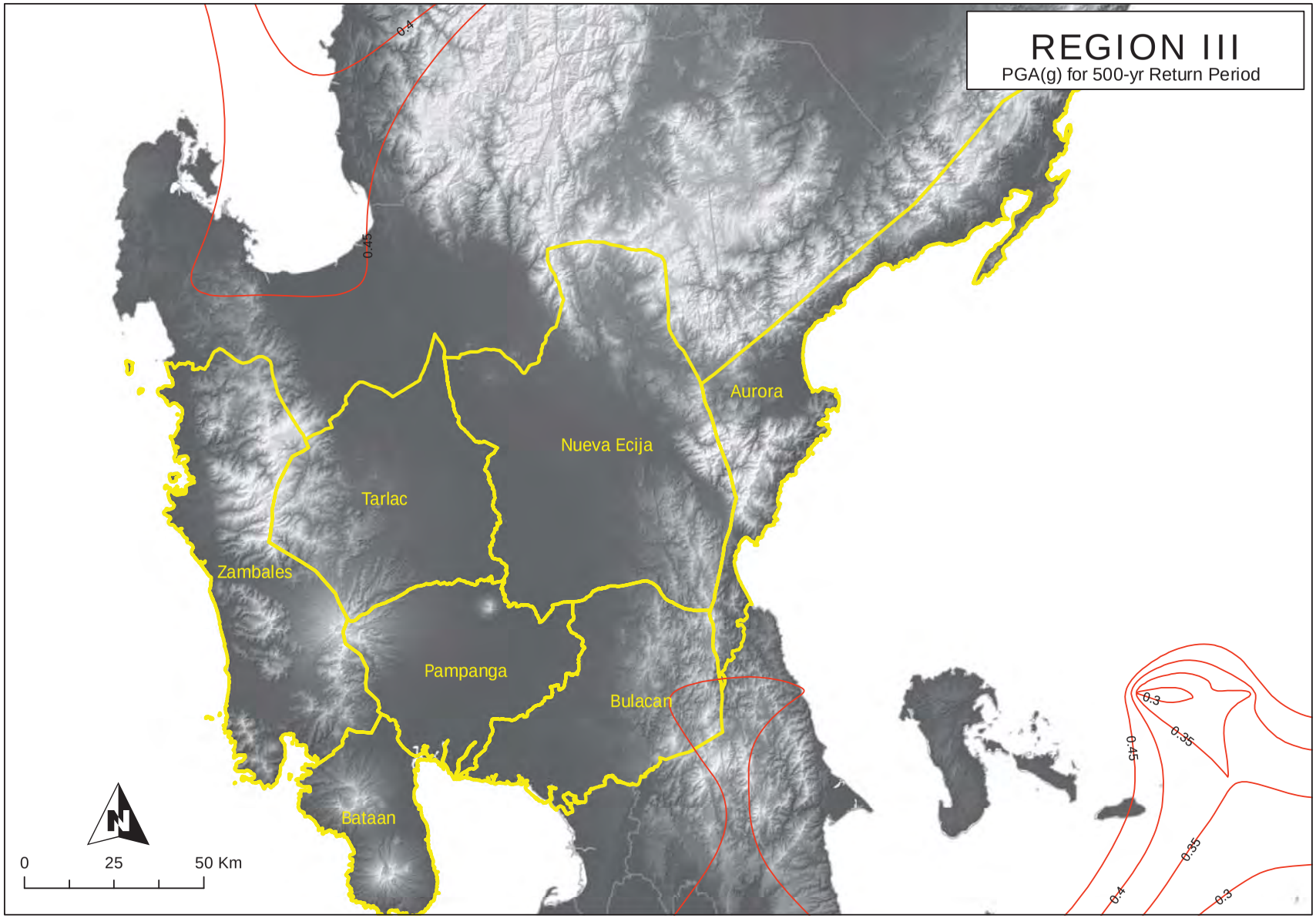

Figure 2A-74 Region III map of peak ground acceleration for 500-year return period

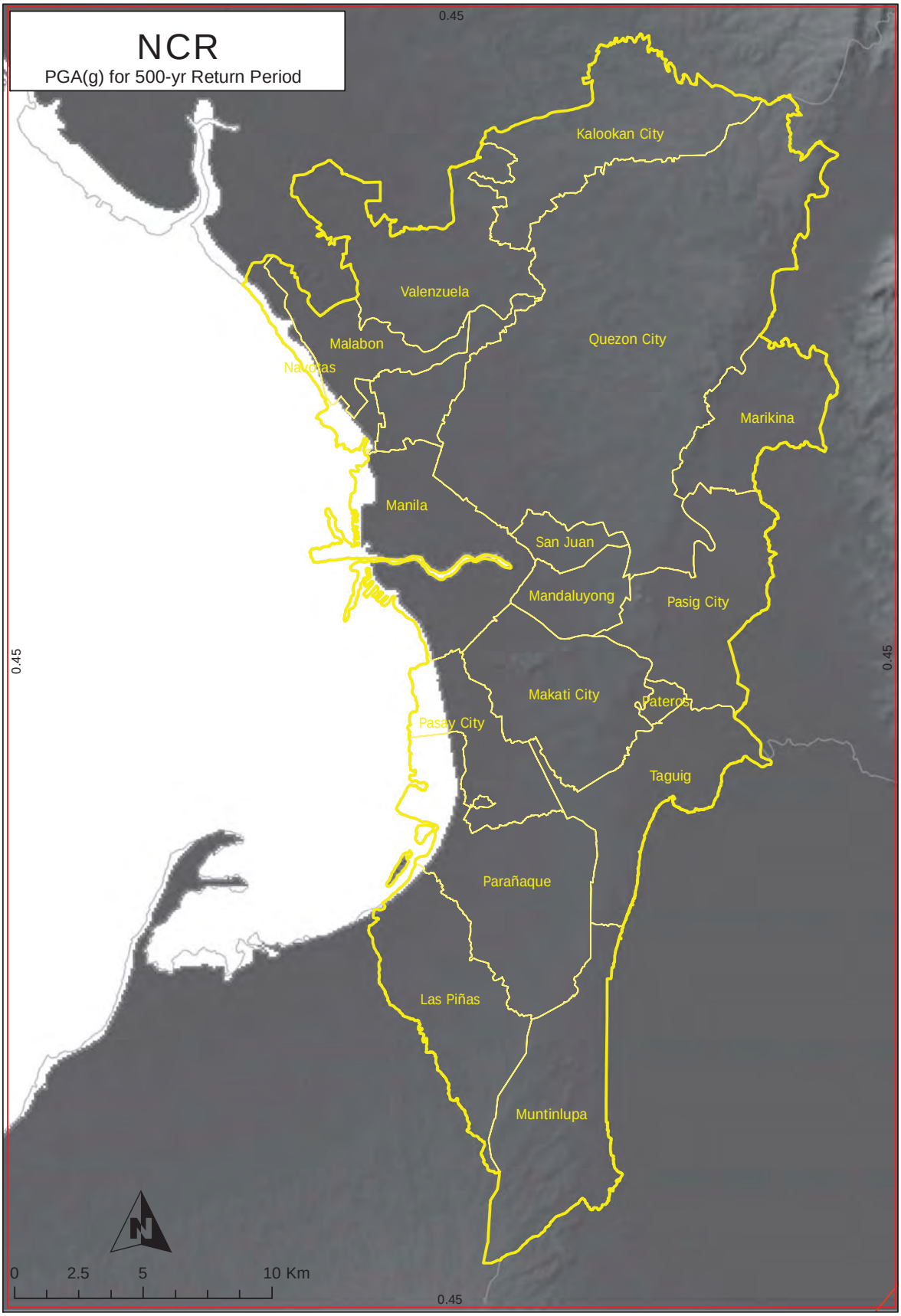

Figure 2A-75 NCR map of peak ground acceleration for 500-year return period

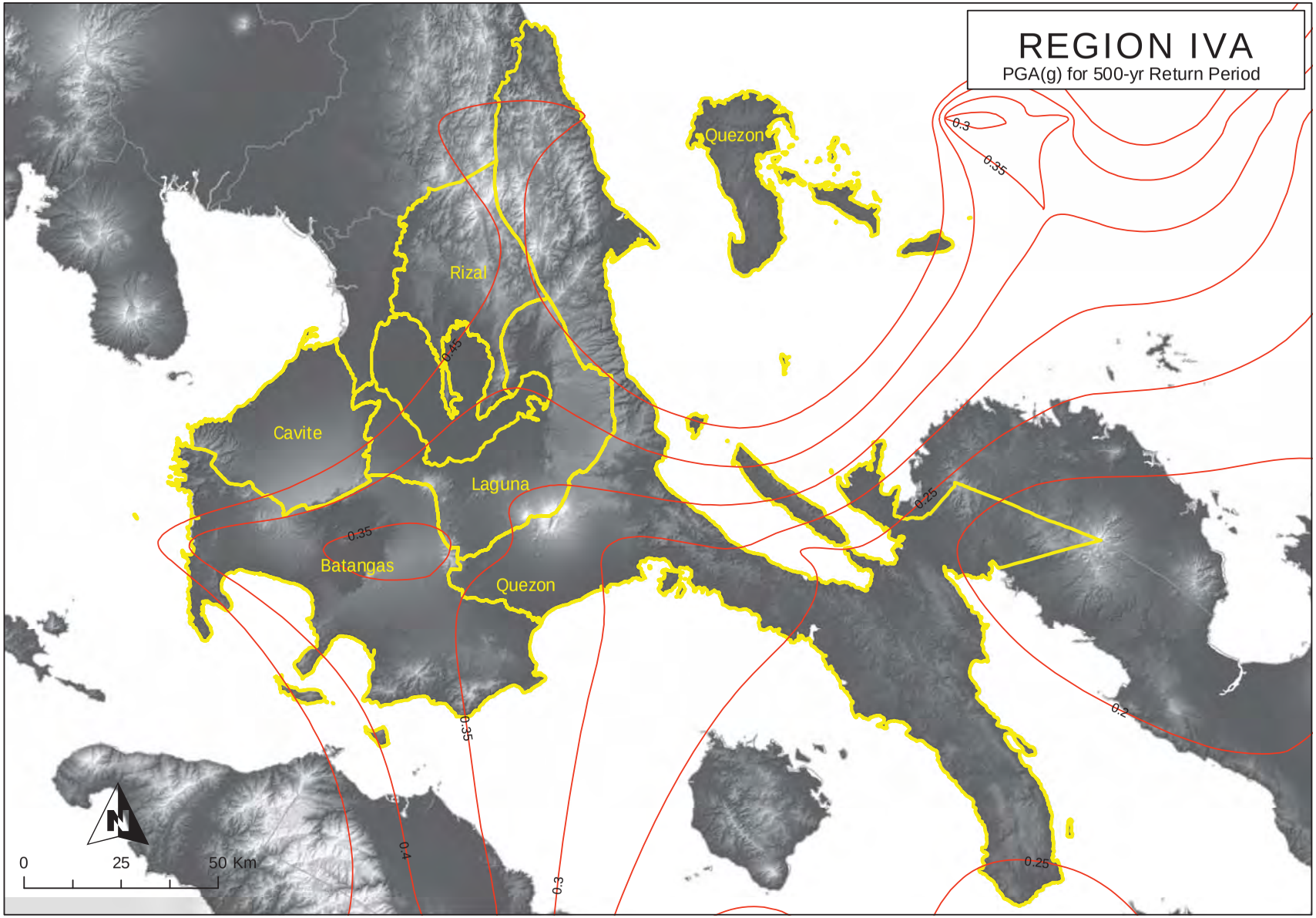

Figure 2A-76 Region IV-A map of peak ground acceleration for 500-year return period

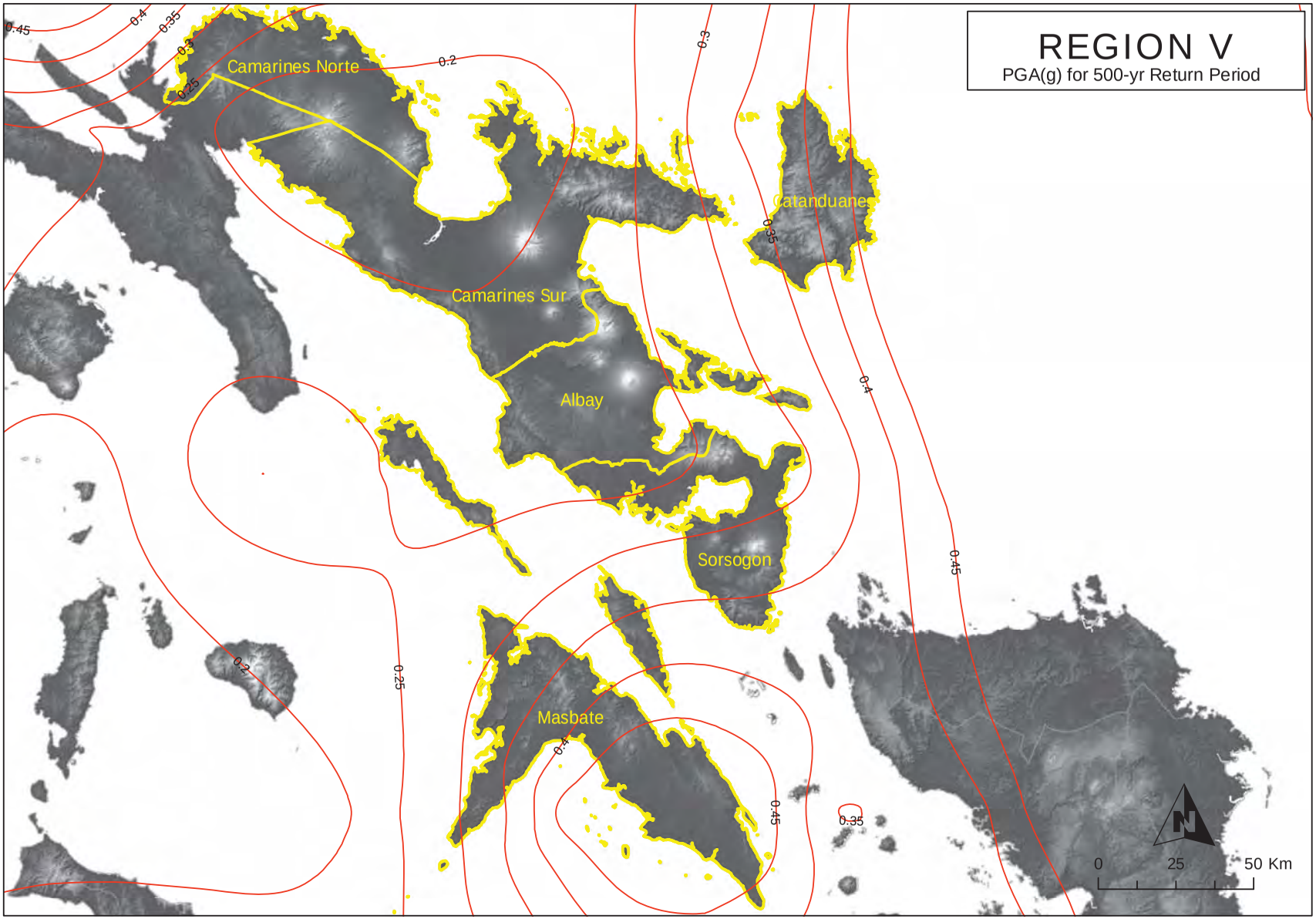

Figure 2A-77 Region V map of peak ground acceleration for 500-year return period

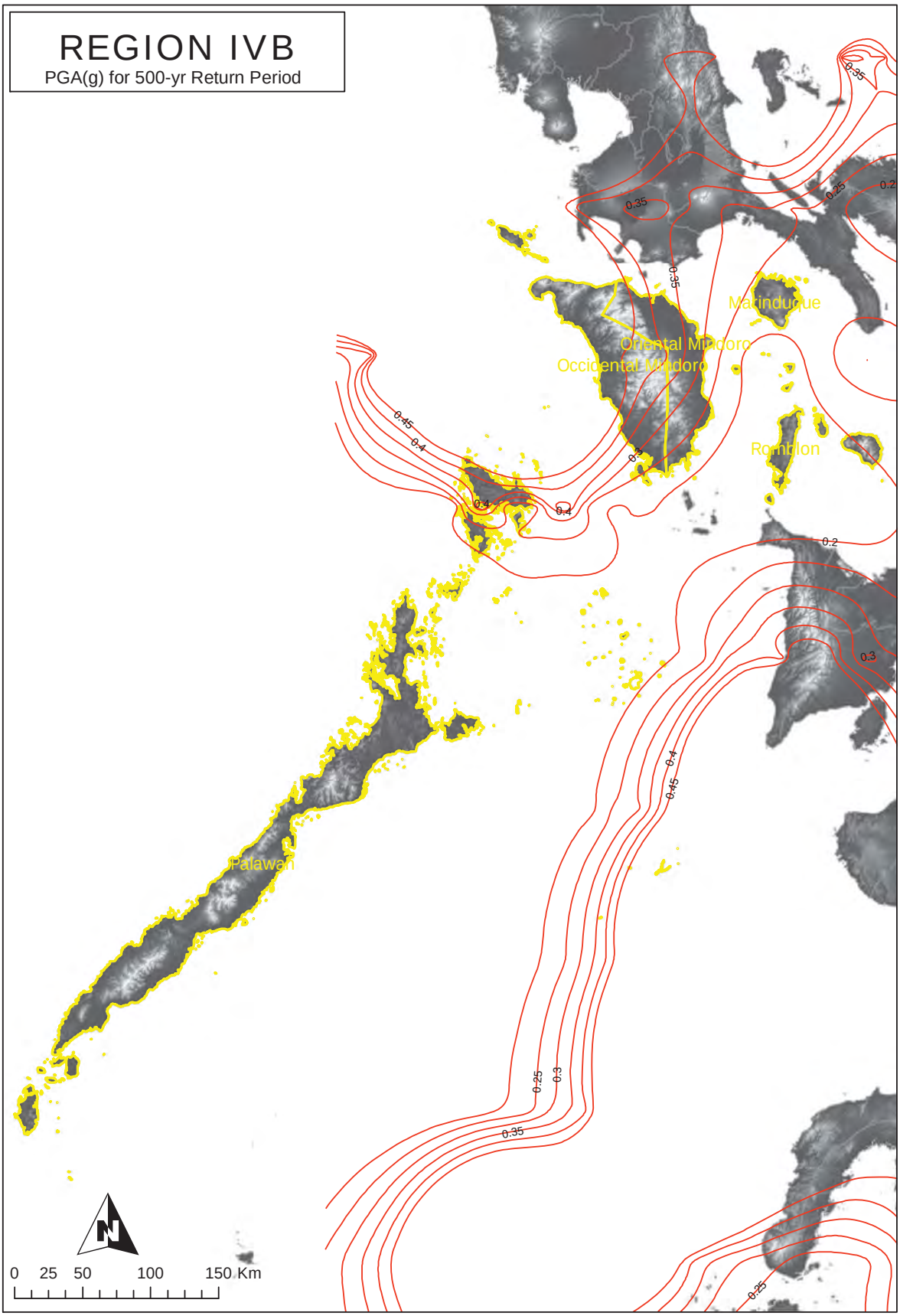

Figure 2A-78 Region IV-B map of peak ground acceleration for 500-year return period

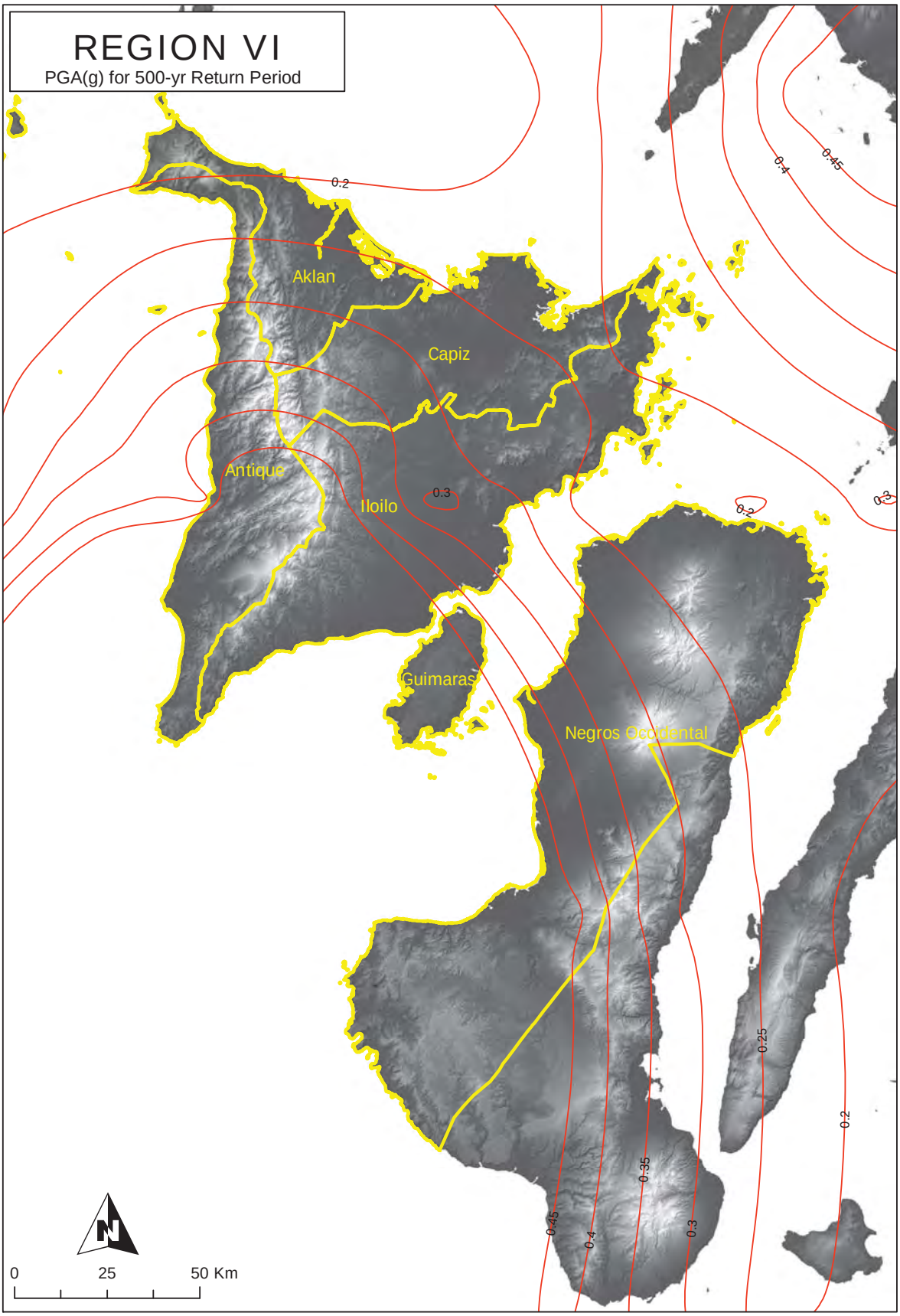

Figure 2A-79 Region VI map of peak ground acceleration for 500-year return period

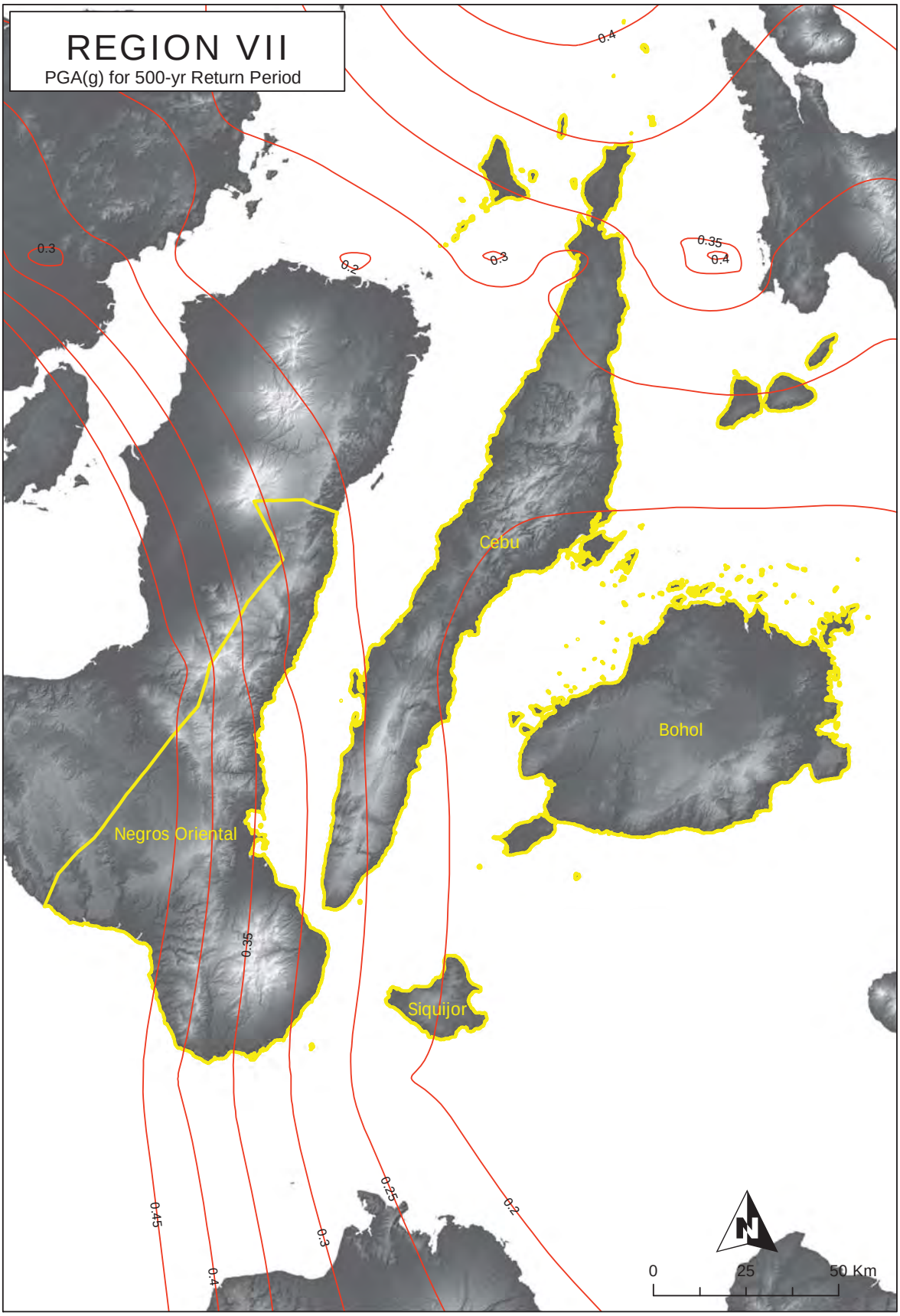

Figure 2A-80 Region VII map of peak ground acceleration for 500-year return period

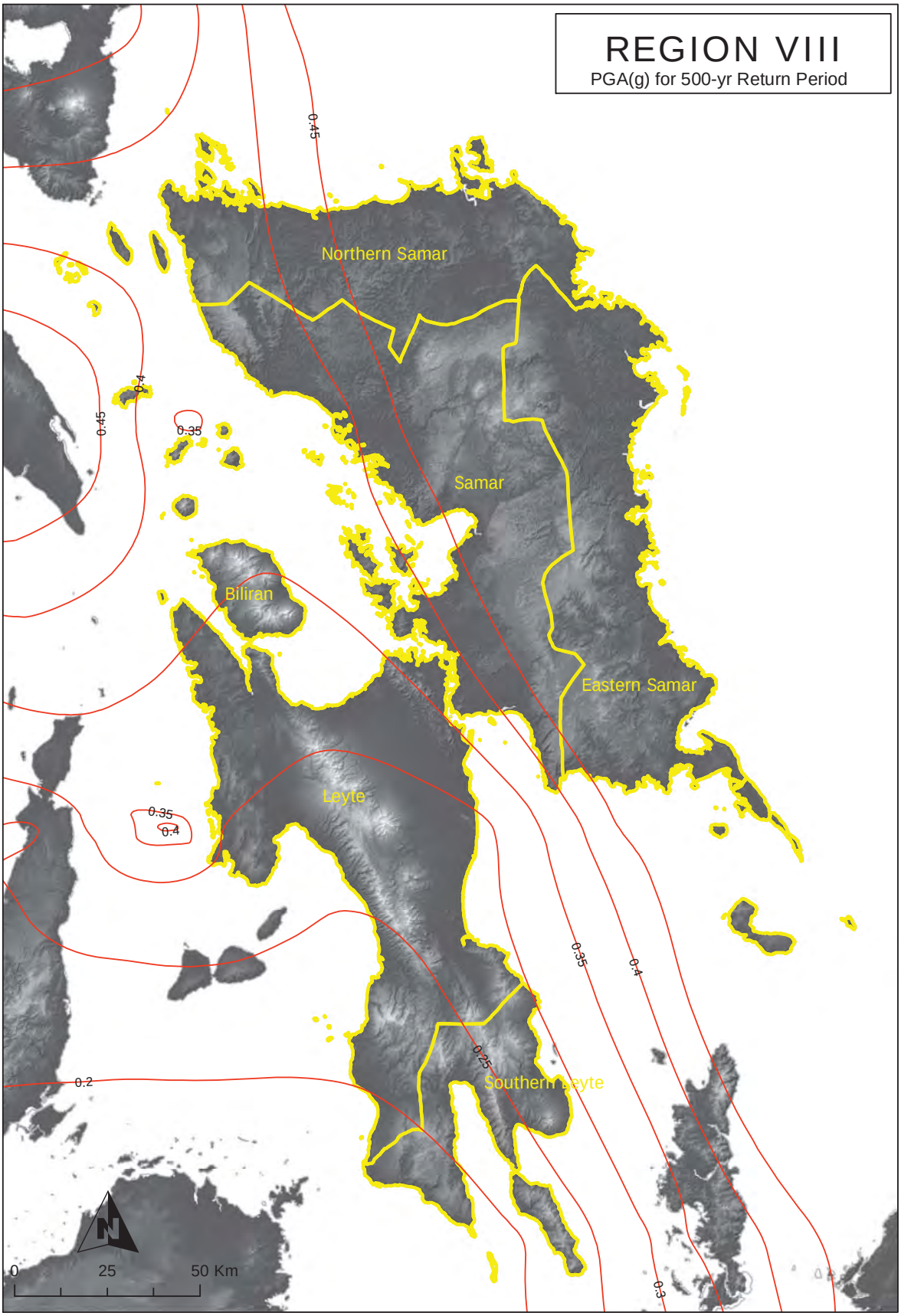

Figure 2A-81 Region VIII map of peak ground acceleration for 500-year return period

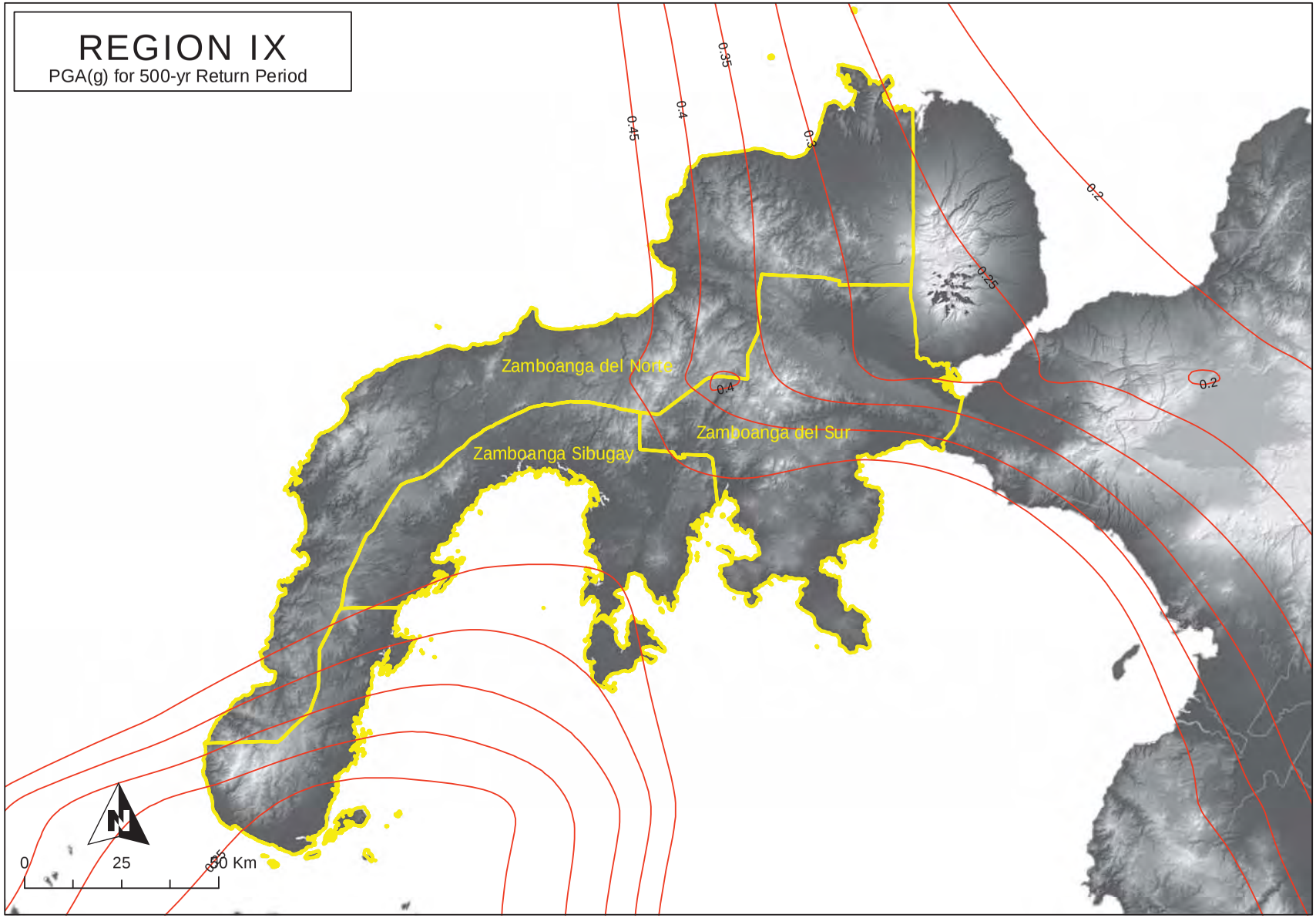

Figure 2A-82 Region IX map of peak ground acceleration for 500-year return period

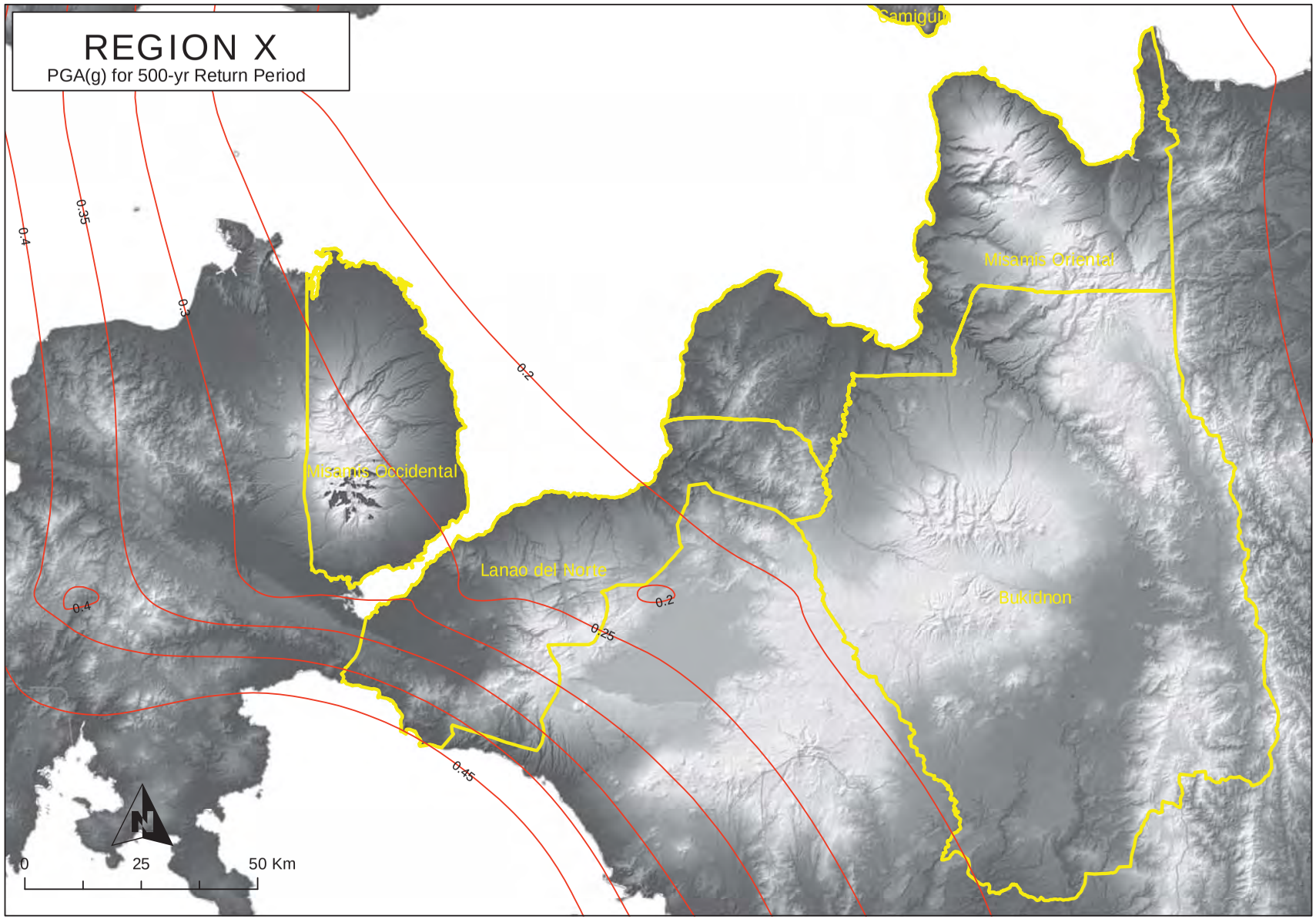

Figure 2A-83 Region X map of peak ground acceleration for 500-year return period

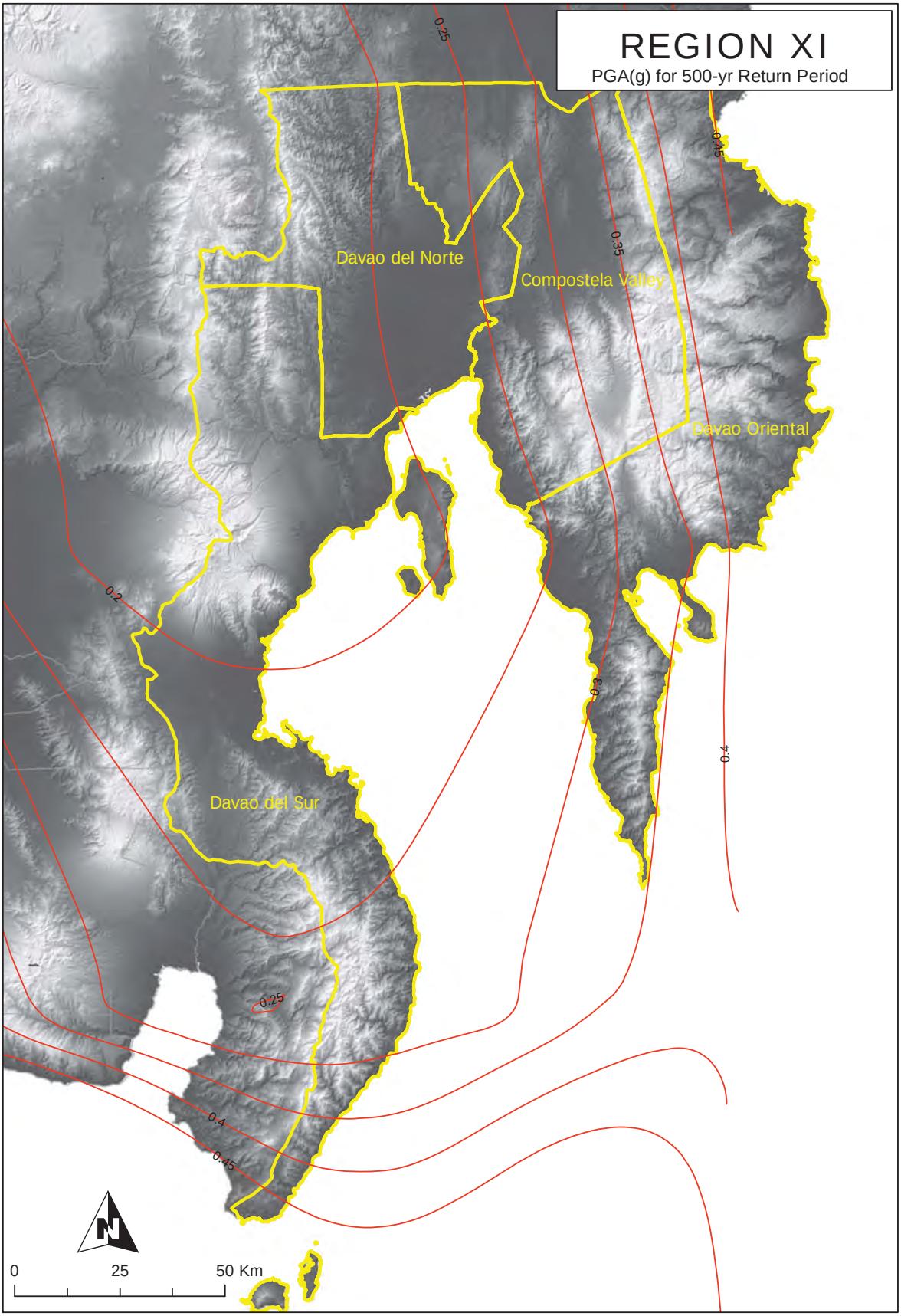

Figure 2A-84 Region XI map of peak ground acceleration for 500-year return period

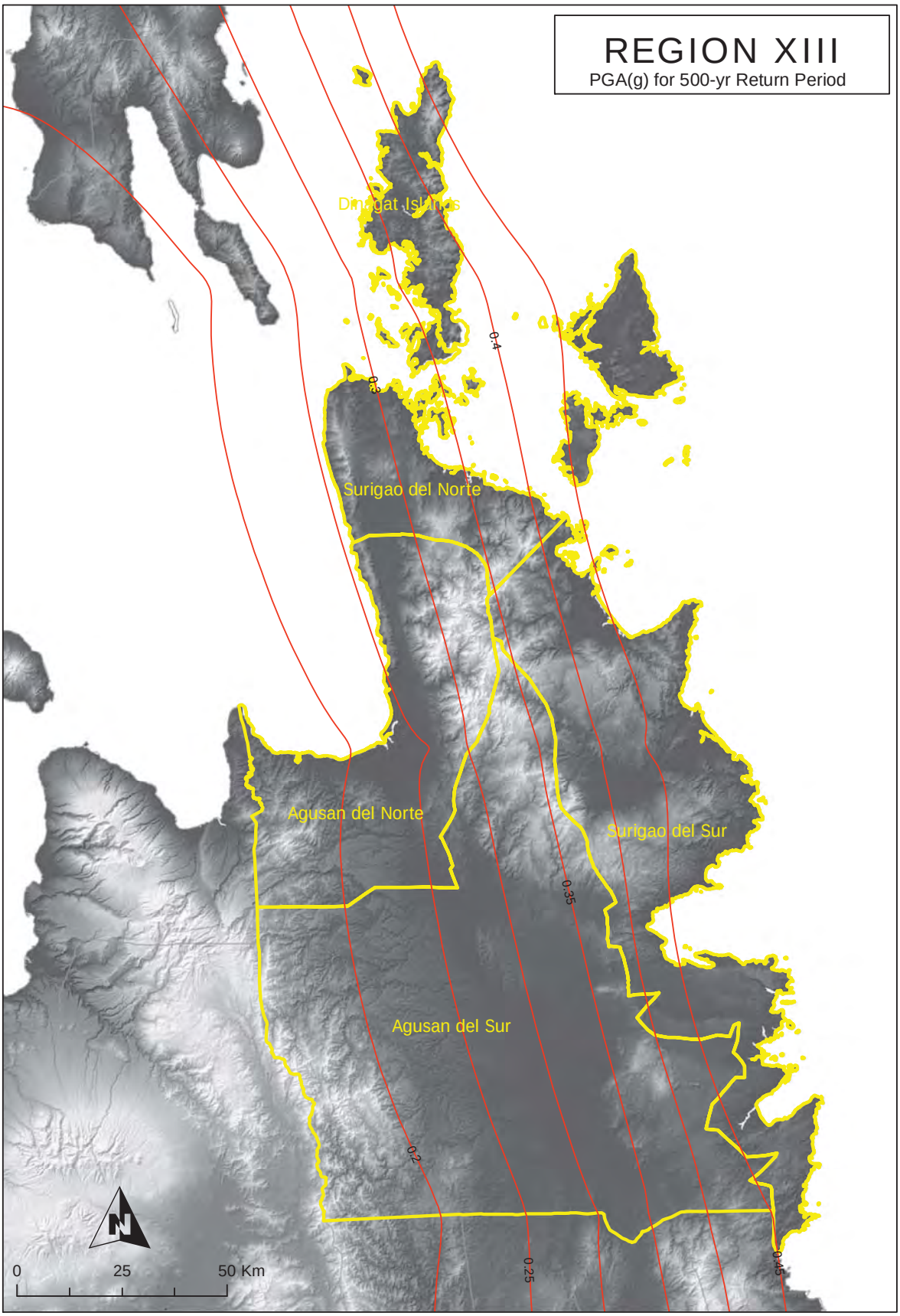

Figure 2A-85 Region XIII map of peak ground acceleration for 500-year return period

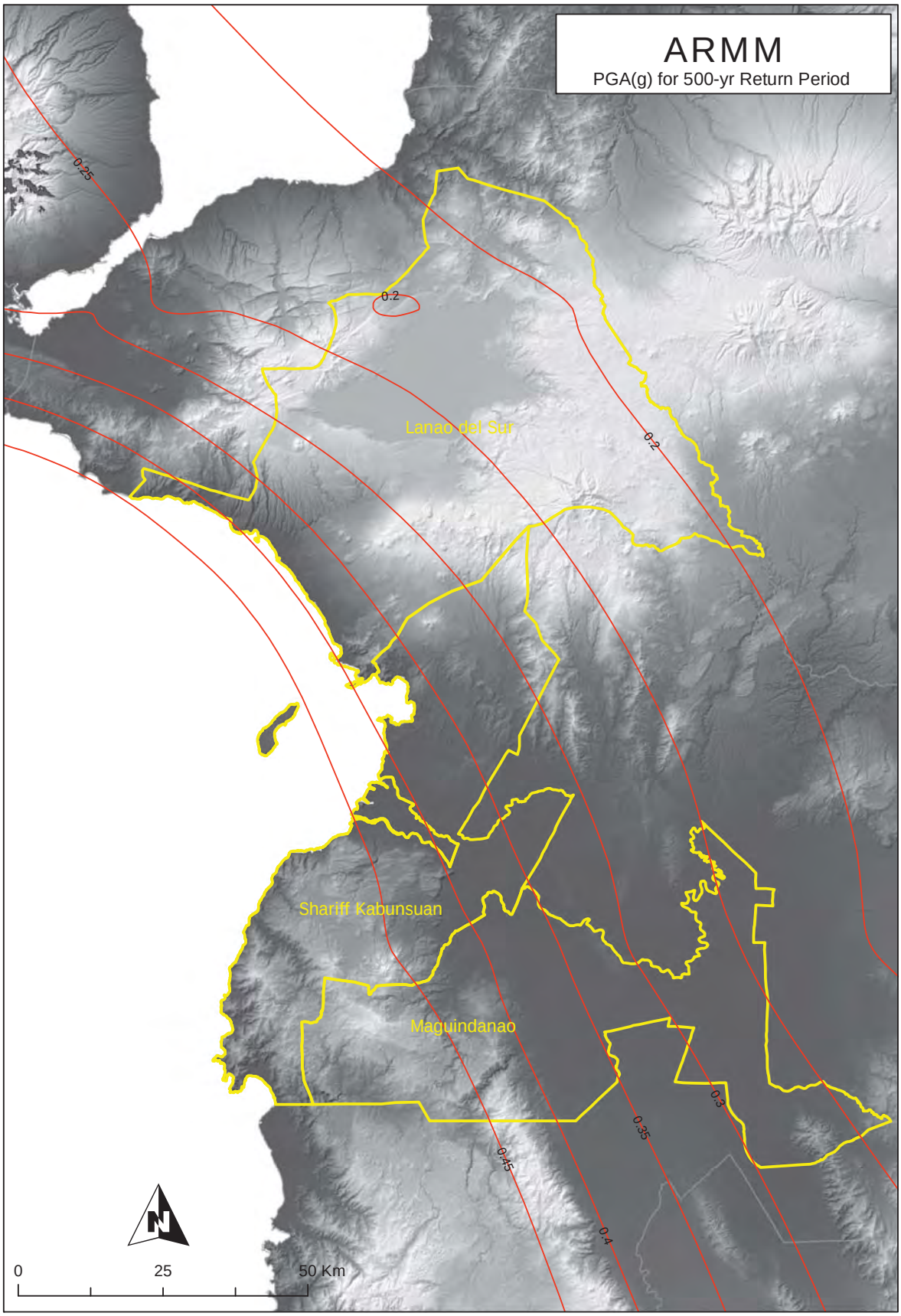

Figure 2A-86 ARMM map of peak ground acceleration for 500-year return period

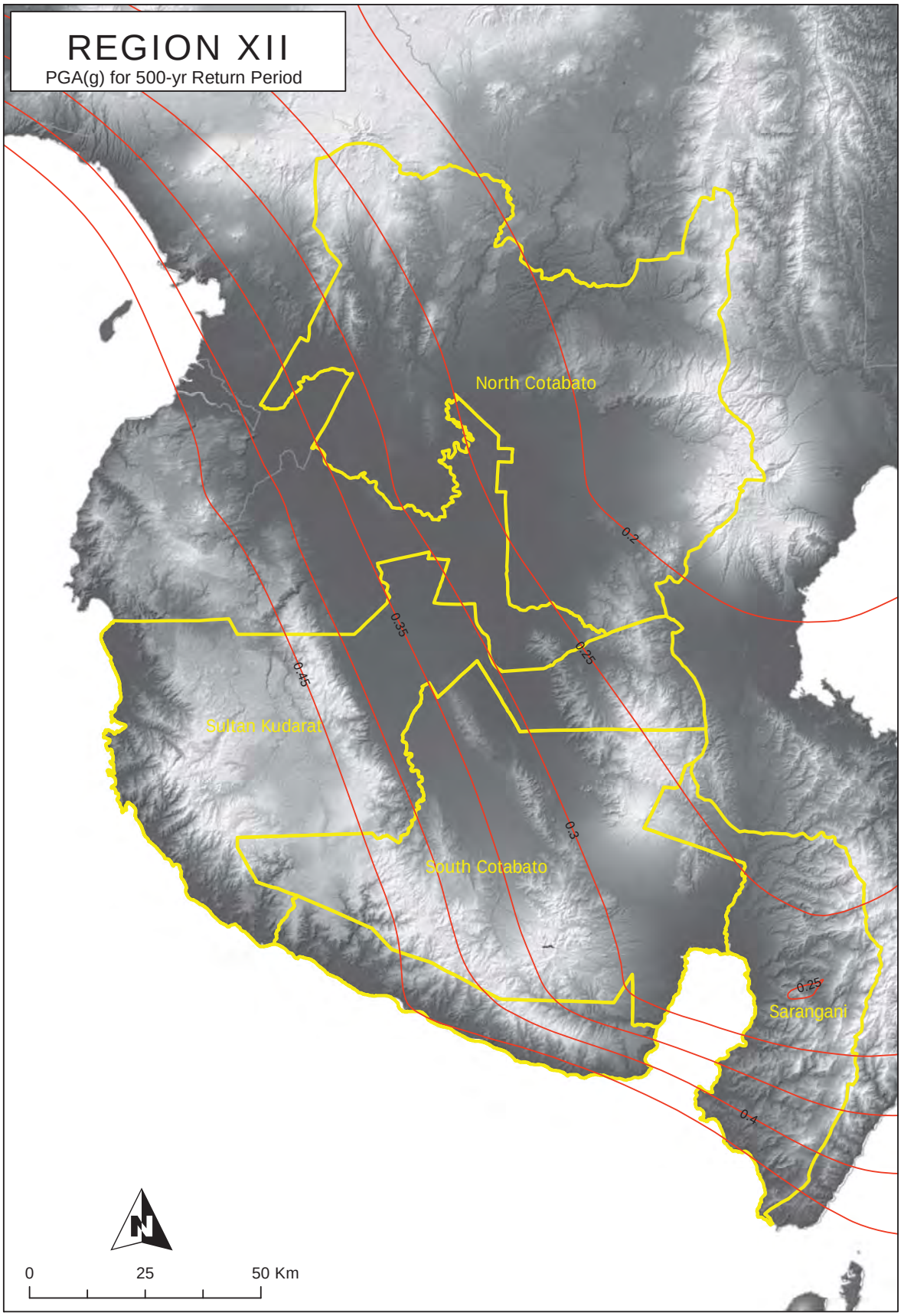

Figure 2A-87 Region XII map of peak ground acceleration for 500-year return period